Quantifying bed roughness of ice streams using palaeo-glacial landscapes

Volume 1 of 2

Francesca Anna Maria Falcini

Doctor of Philosophy

University of York

Environment and Geography

May 2019

Abstract

The roughness of the bed beneath ice is an important control on ice stream location and dynamics. Deglaciated terrain provides the opportunity to explore bed roughness in greater detail and over larger areas compared to glaciated terrain. This thesis examines three different aspects of palaeo-ice streams bed roughness. Firstly, this thesis explores methods used to measure bed roughness in glaciology. The choices made by researchers on transect orientation, window size, detrending and roughness methods have an impact on results. The Fast Fourier Transform analysis and Standard Deviation methods are both useful for calculating bed roughness in glaciology.

Secondly, this thesis directly compares the roughness of contemporary and palaeo-ice stream beds. The bed roughness of Minch Palaeo-Ice Stream (MPIS) is compared to the Institute and Möller Ice Streams (IMIS). The MPIS has a rough bed along major flow paths in the onshore onset zones. The results from the MPIS demonstrate that the presence of sediment does not necessarily correspond with fast flowing ice. The spacing of Radio Echo Sounding (RES) transects (10 x 30 km) used to measure bed roughness under contemporary-ice streams was too wide to capture bed roughness of MPIS glacial landforms.

Thirdly, this thesis investigates whether glacial landforms have unique bed roughness signatures. The results show that groups of glacial landforms have unique bed roughness signatures when anisotropy is taken into account. Bed roughness signatures of glacial landforms have the potential to be compared with known and unknown areas of glacial landforms at the bed of contemporary-ice streams.

Future studies should acquire RES transects where a rough bed or glacial landforms are inferred. 250 m transect spacing would be desirable but 1 km transect spacing is likely to be more practical because it would allow orthogonal and parallel transects to be acquired.

"I remembered the effect that the view of the tremendous and ever-moving glacier had produced upon my mind when I first saw it. It had filled me with a sublime ecstasy that gave wings to the soul and allowed it to soar from the obscure world to light and joy."

Mary Shelley, Frankenstein.

Contents

Acknowledgments

There are many people who have supported me throughout my time at York and without them the PhD experience would have been much more difficult. Firstly, I would like to thank my supervisors, Dave Rippin, Maarten Krabbendam and Katherine Selby, for their patience and helping me to become an independent researcher. Dave always challenged my ideas, which allowed me to ensure every detail was covered. Dave was particularly supportive when I had to take a leave of absence, for which I am very grateful. Maarten was always positive about my work, and although we didn't meet often, when we did he was like a ball of energy, coming up with ideas at an incredible speed. At times when I was in a negative frame of mind about the PhD, a meeting with Maarten would change that.

My fellow PhD students in York have been a constant throughout this project. There are too many of them to name but I must thank the 'Penthouse and friends' for being there through the highs and lows, and for always making me laugh. Thank you to my ice twin, Adrian Dye. Adrian was always a fantastic sounding board for bouncing ideas off and he took me on the best trip to date, when we went to Sweden for his fieldwork. I was also lucky enough to spend a month in Svalbard during the second year of my PhD, which I attended with my glaciology wife, Lauren Knight. We met other inspirational women in glaciology who have become great friends. Thank you to Arminel Lovell, Penny How and Lauren for supporting each other through academia. I would also like to thank UYSWC, the best water polo team I have been involved in. Getting in the pool and saving goals was often a welcome distraction.

Thank you to my family for always believing in me, and particularly my parents and sister for never asking when I was going to finish my PhD. Thank you to my Grandad Nilo for taking a genuine interest and understanding my work. One of the best moments was sending him my published paper and getting an email back with numerous thoughtful questions.

Lastly, thank you to Tom Sloan for always being there and reminding me that "Everything will be fine".

Declaration

This thesis has not previously been accepted for any degree and is not being concurrently submitted in candidature for any degree other than Doctor of Philosophy of the University of York. This thesis is the result of my own investigations, except where otherwise stated. All other sources are acknowledged by explicit references.

Chapter 1

Introduction

A clear understanding of ice dynamics, particularly at the ice-bed interface, is crucial in order to model accurately future ice-sheet behaviour (Stokes, 2018). As average global temperatures continue to increase, the impact of ice-sheet mass loss on sea-level rise will be significant (Alley et al., 2005; Bamber et al., 2009; Dutton et al., 2015). The estimated combined contribution to sea-level rise by the Antarctic and Greenland Ice Sheets between 2000/03 and 2009/11 was 0.82± 0.16 mm a^{-1} (Hanna et al., 2013), and ice-sheet melt is predicted to cause a global sea-level rise of 0.03 - 0.20 m by 2081 - 2100 (IPCC, 2013). Ice flows via internal deformation of the ice, basal sliding and deformation of subglacial substrate (Benn and Evans, 2010). Basal sliding and subglacial deformation are collectively termed basal motion. Basal motion has a strong influence on ice flow (Joughin et al., 2009; Durand et al., 2011; Bingham et al., 2017), and it is controlled by water pressure, basal shear and other bed properties that include roughness of the terrain beneath the ice (Pollard and Deconto, 2012). However, due to the inaccessibility of the bed beneath ice sheets, our understanding of basal sliding is lacking. Moreover, bed roughness is a parameter that has often been overlooked due to a lack of data (Taylor et al., 2004), or ignored altogether (cf. Bennett, 2003, p.321). Further insights into roughness will improve parametrisation of basal sliding and reduce uncertainty in ice-sheet models (Bingham et al., 2017; Stokes, 2018).

Roughness has many definitions, and has been used interchangeably with other terms that include rugosity, microrelief, ruggedness and microtopography (Helming et al., 1993; Washtell et al., 2009; Wolf et al., 2011; Brasington et al., 2012). Arguably, the cause of numerous definitions and terms is because roughness is used in multiple disciplines such as engineering, manufacturing, and bioengineering (Deligianni et al., 2001; Bigerelle et al.,

2003; Zhang et al., 2007). Defining an innate concept such as roughness seems simple, but in practice it is complex (see Chapter 2). For the purposes of this study, bed roughness is defined as 'the extent to which terrain varies vertically over a given horizontal distance' (Rippin et al., 2014, p. 141).

Bed roughness has been measured underneath the Antarctic and Greenland Ice Sheets, often with a focus on ice streams (e.g. Taylor et al., 2004; Siegert et al., 2005; Bingham et al., 2007; Rippin, 2013; Rippin et al., 2014) because the majority of ice mass loss from ice sheets is discharged through ice streams. These studies have suggested for the most part that the bed beneath ice streams is smooth, whilst the surrounding areas are rough. However, investigating the bed of an ice sheet is difficult and it can be argued that the link between bed roughness and ice velocity is complex. For example, a smooth bed is not always associated with fast ice flow and a rough bed is not always associated with slow flow (Rippin et al., 2011; Schroeder et al., 2014; Siegert et al., 2016). Bed roughness studies of contemporary ice sheets have used data acquired by Radio Echo Sounding (RES) techniques. RES or radar techniques use electromagnetic waves that pass through the ice, and the return signal from the electromagnetic waves provides information about the ice thickness and the properties of the bed, such as whether water is present (Plewes and Hubbard, 2001). RES is acquired along transects using either aircraft (e.g. Ross et al., 2012) or snowmobiles (e.g. Bingham et al., 2017). The spacing of data points (resolution) along RES transects can be high (e.g. one point every 10 m) (see Rippin et al., 2014), but the spacing between individual transects is often >10 km, specifically for the more common aeroplane transects (e.g. Siegert et al., 2004; Bingham et al., 2007; Rippin et al., 2014). Thus there are large areas of the bed beneath ice sheets where there are no bed roughness measurements.

Palaeo-glacial landscapes provide an opportunity to explore bed roughness in more detail and over larger spatial scales compared to contemporary glaciated beds because there is no ice cover and large areas are covered by high resolution Digital Terrain Models (DTMs; Bingham and Siegert, 2009; Gudlaugsson et al., 2013; Lindbäck and Pettersson, 2015). However, this opportunity is yet to be fully realised, with only a few studies carried out so far (e.g. Gudlaugsson et al., 2013; Lindbäck and Pettersson, 2015). Furthermore, there are many methods that can be used to measure bed roughness, and small changes in how they are applied can alter the results. For example, bed roughness is calculated along transects using moving windows, and changing the window size gives a different result for the same transect

(Prescott, 2013; Smith, 2014). The impact of transect spacing and method choices on bed roughness measurements requires investigation.

Glaciation leaves behind a clear mark on the landscape, which includes numerous types of glacial landforms. These features range from micro (0.01 m - 10 m), meso (1 m - 1 km) to macro (1km - 100 km) scale in size (Bennett and Glasser, 2009) and influence bed roughness at multiple scales. However bed roughness has mainly been calculated at large scales i.e. kilometre wavelength, although the roughness of the bed at the metre scale is important for understanding ice dynamics (Weertman, 1957; Kamb, 1970; Nye, 1970; Hubbard and Hubbard, 1998; Hubbard et al., 2000; Schoof, 2002).The relationship between landform genesis, growth and decay, and ice dynamics is poorly understood (Hillier et al., 2013; Stokes, 2018). This is because it is extremely difficult to record these processes beneath kilometres of ice present at the contemporary ice sheets of Antarctica and Greenland. To date, there are only a handful of studies that have identified landforms underneath contemporary ice sheets (King et al., 2007; Smith et al., 2007; King et al., 2009; Jezek et al., 2011; Schroeder et al., 2014; Bingham et al., 2017). Bed roughness provides a tool for identifying and describing the nature of the subglacial environment. Bed roughness measurements of glacial landforms from deglaciated terrain could be used to locate these features at the bed of contemporary ice sheets, allowing further links to be made between ice dynamics and glacial landforms. Despite this potential gain, bed roughness of glacial landforms has not been explored.

1.1 Research aims and objectives

The aim of this thesis is to investigate bed roughness underneath palaeo-ice streams. This knowledge will then be used as an analogue for contemporary-ice streams and to suggest best practice for acquiring bed roughness measurements from the major ice sheets. To achieve this aim, the thesis is split into three smaller projects, which comprise the following objectives:

1. *To compare different methods used in glaciology to measure bed roughness.* The choice of method and transect orientation in relation to ice flow can affect bed roughness results. Measuring roughness of deglaciated terrain allows for further interpretation of what the methods are measuring because the entire bed can be seen.

2. *To investigate how the roughness of contemporary-ice-stream and palaeo-ice stream-beds compare.* The bed roughness of a contemporary-ice stream has not been directly

compared to the bed roughness of a palaeo-ice stream before. By doing this, the bed roughness from palaeo-ice streams can be tested as an analogue for contemporary-ice streams. RES transects used to measure bed roughness for contemporary-ice streams are often widely spaced. The effect of this spacing on bed roughness results will be tested by using a palaeo-ice stream where the bed between transects can be seen.

3. *To test whether glacial landforms have unique bed roughness signatures.* If palaeo-glacial landforms have specific bed roughness signatures, the roughness data from the base of the Antarctic and Greenland Ice Sheets could be used to infer where these landforms are located. This could lead to new insights into the processes occurring at contemporary-ice stream-beds and they could better constrain reconstructions of palaeo-ice streams and ice-sheet models.

1.2 Study site

Excellent records of palaeo-ice streams can be found in the British and Irish Ice Sheet (BIIS), Laurentide Ice Sheet and Fennoscandian Ice Sheet (e.g. Hughes et al., 2014). This study will focus on the BIIS, and the Minch Palaeo-Ice Stream (MPIS) in particular, due to the accessibility of high resolution datasets such as NEXTmap (5 m resolution) (Intermap Technologies, 2009) and multibeam echosounder survey (MBES) bathymetry data (8 m resolution) (Bradwell and Stoker, 2015). The MPIS has one of the best records of a BIIS palaeo ice stream (Bradwell and Stoker, 2015), and is arguably one of the most studied in the UK.

1.2.1 The British and Irish Ice Sheet (BIIS)

The BIIS was present during multiple glaciations. During the Last Glacial Maximum (LGM) (∼21 ka BP Clark et al., 2012), the BIIS covered large parts of the UK and Ireland (Fig. 1.1), and extended as far south as the Isles of Scilly and out to the continental-shelf edge in the North Sea and Atlantic Ocean (Roberts et al., 2007; Livingstone et al., 2012; Clark et al., 2018). Several ice streams drained the BIIS at its maximum extent (Hughes et al., 2014), and it was estimated to have an areal extent of ∼840,000 km^2, with 300,000 km^2 of marine-based ice (Clark et al., 2012; Ó Cofaigh et al., 2019).The BIIS is thought to have reached its maximum extent around 27 ka BP (Bradwell, Stoker, Golledge, Wilson, Merritt, Long, Everest, Hestvik, Stevenson, Hubbard, Finlayson and Mathers, 2008; Clark et al., 2012,

2018). However, reported timings (from dated sediments) from the continental-shelf edge vary, suggesting that different parts of the BIIS reached their maximum extent at different times. For example, west of Scotland the maximum extent was 26.7 ka BP (Callard et al., 2018) whilst west of Ireland it was after 24.7 ka BP (Peters et al., 2015). Retreat of the BIIS also did not happen concurrently, with early deglaciation occurring on the continental shelf northwest of Ireland between 26.3 and 24.8 ka BP (Ó Cofaigh et al., 2019) compared to a later date of 20.9 ka cal BP from the continental shelf west of Ireland (Peters et al., 2016) and 23 ka BP from ice rafted debris deposits ranging from northwest of Scotland to southwest of Ireland (Scourse et al., 2009). The BIIS left behind a clear imprint on the landscape with a variety of glacial landforms that have been extensively mapped by various authors and combined into one map, BRITICE, which has over 170,000 glacial features (Fig. 1.2; Clark et al., 2018). Landforms mapped include: cirques, crag-and-tails, drumlins, eskers, ice-damned lakes, megagrooves, mega-scale glacial lineations (MSGLs), meltwater channels, moraines, ribbed moraines, roches moutonnées, trimlines, trough-mouth fans and whalebacks (Clark et al., 2018). These features vary in size, from meso scale (1 m - 1 km) such as whalebacks and roches moutonnées up to macro scale (1 km - 100 km) such as MSGLs and ice-damned lakes, and have been used to reconstruct a complex history of past ice dynamics (e.g. Livingstone et al., 2012; Hughes et al., 2014).

1.2.2 The Minch Palaeo-Ice Stream (MPIS)

The MPIS is situated in NW Scotland (Fig. 1.3), and was active during the Devensian (Weichselian) glacial period (110 - 11.7 ka BP), including the LGM (Bradwell, Stoker and Krabbendam, 2008; Bradwell and Stoker, 2015; Gandy et al., 2018). At the MPIS's maximum extent, several ice-stream tributaries flowed from the present day NW coast, between Kyle of Lochalsh and Loch Laxford, out to the Sula Sgeir Fan (Bradwell et al., 2007; Bradwell, 2013; Bradwell and Stoker, 2015; Krabbendam et al., 2016). The onset zone is situated in the NW Highlands of Scotland where the highest mountains are up to ∼1000 m above present-day sea level (a.s.l.). Here, ice-stream tributaries were topographically focused through gaps in the watershed at ∼300 m a.s.l. and flowed out into the deep basin which now contains the Minch Strait (Bradwell et al., 2007; Bradwell and Stoker, 2015, 2016; Krabbendam et al., 2016).The bedrock geology has a strong control on the MPIS bed topography where resistant Precambrian rocks make up present day land masses and bathymetric highs, whilst

the weaker Mesozoic rocks make up the bathymetric trough (Fig.1.4; Fyfe et al., 1993; Bradwell and Stoker, 2016). Up to 50 km wide, 200 km long, and with an estimated ice-flux discharge of 12-20 Gt a^{-1}, the MPIS is comparable with current ice streams in West Antarctica and Greenland (Bradwell et al., 2007; Bradwell and Stoker, 2015). The area drained by the MPIS was between 10,000 and 15,000 km^2 (Ballantyne and Small, 2018). Exact timings of maximum extent and retreat are uncertain, but the maximum extent was likely to have been between 26-28 ka BP (Chiverrell and Thomas, 2010; Clark et al., 2012; Praeg et al., 2015; Bradwell and Stoker, 2016); however, a stillstand during retreat occurred between ∼16-22 ka BP (Bradwell and Stoker, 2015). A model of MPIS retreat suggested that the ice stream was pinned on the northern tip of the Isle of Lewis where an ice shelf buttressed the ice stream, but when the ice became unpinned retreat accelerated due to a reverse bed slope (Gandy et al., 2018). Numerous bedform and landform types have been left behind by the MPIS, including megagrooves, crag and tails, whalebacks, roches moutonées and drumlins (Bradwell, Stoker and Krabbendam, 2008; Bradwell, 2013; Bradwell and Stoker, 2015; Krabbendam and Glasser, 2011; Krabbendam et al., 2016). Onshore, the MPIS bed is dominated by bedrock landforms (Krabbendam and Bradwell, 2010; Clark et al., 2018), with few soft-sediment covered landforms (Bradwell et al., 2007; Bradwell, Stoker and Krabbendam, 2008; Krabbendam and Glasser, 2011; Bradwell, 2013). In the Minch and further offshore on the Hebrides Shelf, the MPIS bed has more soft-sediment landforms, such as drumlinoid features, although streamlined bedrock (e.g. megagrooves), is also found, particularly in the inner Minch (Bradwell and Stoker, 2015, 2016; Ballantyne and Small, 2018). Increases in ice-flow speed are evident from changes to landform elongation ratios, which Bradwell and Stoker (2015) hypothesise is caused by the substrate beneath the ice transitioning from rough bedrock to smooth sediment.

1.3 Thesis structure

The three objectives outlined in Section 1.1 are investigated in Chapters 3, 4 and 5 respectively. These chapters have individual methods and discussion sections. The overall discussion and conclusions of the research are reported in Chapter 6. This thesis is split into two volumes; Volume 1 contains the text, references and appendices, and Volume 2 the figures and tables. This division was to enable easy cross-referencing between text and figures.

The focus of each chapter is now described to demonstrate how it relates to the overall aim of the research.

1.3.1 Literature review (Chapter 2)

This chapter contains a review of the literature regarding roughness and the glacial history of the British Isles. Firstly, the definition of roughness is explored to see how this varies within Earth Science disciplines. The way roughness has been measured to date is then reviewed because this affects the final results. The history of bed-roughness studies in glaciology is then investigated, where the focus has been on macro-scale bed roughness (1 km - 100 km) and contemporary-ice streams. Bed-roughness methods used outside of glaciology are then reviewed.

A history of glaciation in Great Britain and the island of Ireland is then included to provide context for the study sites. The evidence for palaeo-ice streams is discussed, including the Minch Palaeo-Ice Stream (MPIS), as these are thought to be a control on the behaviour of the British and Irish Ice Sheet (BIIS).

1.3.2 Investigating bed-roughness methods (Chapter 3)

Chapter 3 evaluates the different methods for establishing bed roughness. A major challenge to overcome with measuring bed roughness of contemporary-ice streams is that it is difficult to interpret results because the entire bed is not visible. This makes evaluating the effectiveness of bed-roughness methods challenging. To overcome this, the four main methods used in glaciology are applied to transects underneath a palaeo-ice stream (MPIS). Two different detrending methods are used to test how this pre-processing stage impacts bed-roughness measurements.

1.3.3 Quantifying bed roughness beneath contemporary and palaeo-ice streams (Chapter 4)

Building on the findings from Chapter 3, Chapter 4 compares bed roughness beneath a contemporary-ice stream and a palaeo-ice stream. This exercise has not been previously attempted, and is the first step needed to investigate whether palaeo-ice-stream beds provide a bed roughness analogue for contemporary-ice streams. An imitation of identically spaced RES transects used to calculate bed roughness on contemporary-ice streams is placed onto

the MPIS, in order to demonstrate data that are being missed between transects. Fast Fourier Transform (FFT) analysis and standard deviation methods are both used to calculate bed roughness to evaluate their suitability for use in future studies. The orientation of transects used to calculate bed roughness in relation to ice flow has been shown to be important by previous studies (e.g. Gudlaugsson et al., 2013; Prescott, 2013; Rippin et al., 2014), and this is also investigated. This chapter provides the foundations for putting together best practice for future RES surveys and has been published in the Journal of Glaciology (Falcini et al., 2018).

1.3.4 Do glacial landforms have bed-roughness signatures? (Chapter 5)

One of the benefits of using deglaciated terrain to explore bed roughness is that smaller scales of bed roughness can be investigated, which cannot currently be done for contemporary-ice streams. The opportunity to explore whether different glacial landforms have a unique range of bed-roughness values (bed-roughness signatures) is one that has not been investigated to date. If areas of homogeneous glacial landforms (e.g. areas of drumlins only), have a unique bed-roughness signature, this information could be used to locate areas of these landforms underneath ice sheets. This would provide more knowledge about contemporary-ice-stream beds, enabling the link between ice dynamics and types of landforms (King et al., 2007) to be better understood, which may have implications for ice-sheet modelling. Six sites from across the BIIS are chosen, comprising of homogeneous glacial landforms, and other sites that had mixed glacial landforms (heterogeneous). Different transect spacing and window sizes are chosen to test how this impacted bed-roughness signatures. Transects were aligned parallel and orthogonal to palaeo-ice flow, which allowed anisotropy of bed roughness to be calculated. As the orientation of transects has been shown to impact bed-roughness results, anisotropy is investigated as a key metric in establishing bed-roughness signatures of glacial landforms.

1.3.5 Discussion and conclusions (Chapter 6)

Chapter 6 gives a discussion of the key themes and shows how the aim and objectives put forward in Chapter 1 are met. Recommendations for future RES surveys over contemporary ice are made and a framework for the approach and methods that future studies on bed roughness of deglaciated terrain could follow are set out. Recommendations for future

research focus on bed roughness of deglaciated terrain are also made.

Chapter 2

Literature review

2.1 Roughness

2.1.1 Defining roughness

Roughness is a multidisciplinary term which is applied in engineering (Kubiak et al., 2011), bioengineering (Deligianni et al., 2001), mechanical engineering (Suresh et al., 2002) and geomorphometry (Amaral, 2002) to name but a few. Consequently, roughness has different definitions, leading to an understanding that is often vague and ambiguous (Smith, 2014). Throughout the Earth Sciences multiple processes produce or are affected by roughness. For example, roughness is a key parameter in understanding processes such as sand dune initiation (e.g. Jerolmack et al., 2012), ice movement over a surface (e.g. Schoof, 2002), and fluvial hydraulics (e.g. Lawless and Robert, 2001). The concept of whether a surface is rough or smooth is relatively intuitive but subjective (Smith, 2014). There is no one definition of roughness, with some authors arguing that such a definition may not be possible because different roughness methods require different parameters such as amplitude or frequency (Hobson, 1967; Grohmann et al., 2011). Surface roughness is the most widely used term across the Earth Sciences; however other terms have been applied such as rugosity (Jenness, 2004; Wilson et al., 2007; Brasington et al., 2012), microrelief (Stone and Dugundji, 1965; Potter et al., 1990; Helming et al., 1993), ruggedness (Beasom et al., 1983; Riley et al., 1999; Washtell et al., 2009) and microtopography (Moser et al., 2007; Wolf et al., 2011). Cowan (1956) defined total roughness as the sum of multiple inputs from different spatial scales, whilst Lane (2005) argued that this is more complicated in reality, and as spatial

scale changes, so does the roughness definition. A distinction between relief and roughness, where relief is the range of elevation and roughness is the variability of those elevations, is made by Moser et al. (2007) and Wolf et al. (2011). Grohmann et al. (2011) state that in geomorphometry, surface roughness is the variability of a topographic surface at a specified landform scale. In glaciology the terms bed or basal roughness are used to describe roughness at the base of a glacier or ice sheet (e.g. Bingham and Siegert, 2009; Winsborrow et al., 2010; Schroeder et al., 2014). Bed roughness is defined as 'the extent to which terrain varies vertically over a given horizontal distance' (Rippin et al., 2014, p. 141). More simply, Taylor et al. (2004) define it as the extent of surface irregularity. This study will use the term bed roughness because the focus here is on measuring the roughness of palaeo-ice streams beds. The definition used in this study for bed roughness is 'the extent to which terrain varies vertically over a given horizontal distance' (Rippin et al., 2014, p. 141) because the majority of the data used is in the form of transects. A moving window (given horizontal distance) is applied to calculate bed roughness along transects. This is achieved by using the elevation changes either side of the central point within the moving window.

2.1.2 Bed roughness in glaciology

In glaciology the focus has often been on the relationship between macro-scale (1-100 km) bed roughness and ice streams (e.g. Siegert et al., 2004; Taylor et al., 2004; Siegert et al., 2005; Rippin et al., 2006; Bingham et al., 2007; Bingham and Siegert, 2009; Li et al., 2010; Rippin et al., 2011; Rippin, 2013; Rippin et al., 2014; Schroeder et al., 2014). There are a number of factors that cause a rough bed beneath an ice sheet, including ice-flow direction, bedrock geology (lithology, faults and fractures), the absence or presence of sediment, and ice dynamics (Fig. 2.1) (Taylor et al., 2004; Siegert et al., 2005; Bingham and Siegert, 2009). Roughness, combined with lubrication of the bed, controls the amount of basal stress applied at the ice-bed interface i.e. resistance to ice flow (Bennett, 2003; Siegert et al., 2004; Rippin et al., 2006, 2011). Rougher beds will reduce the speed of ice flow by generating increased drag as the ice is forced to flow around bedrock obstacles e.g., a sticky spot (Alley, 1993; Benn and Evans, 2010). Furthermore, bedrock bumps often have either a thin layer of till or no till, creating an increase in friction (Winsborrow et al., 2010).

Bed roughness has been measured using Radio Echo Sounding (RES) data from underneath the Antarctic and Greenland Ice Sheets (e.g. Layberry and Bamber, 2001; Taylor

et al., 2004; Siegert et al., 2005; Rippin, 2013; Bingham et al., 2017). However, the inaccessibility of the bed beneath contemporary ice sheets has hampered research (Krabbendam and Bradwell, 2014) and caused bed roughness to be previously overlooked (Bennett, 2003; Rippin, 2013). Further still, the investigation of bed roughness of palaeo-ice-stream beds is still very much in its infancy. Palaeo-ice-stream beds have the potential to produce unique bed-roughness signatures for individual landform types, e.g., drumlins. In other words, if we compare the bed-roughness values of a swarm of drumlins to a field of megagrooves, will there be a difference? If different types of glacial landforms have a unique bed-roughness signature, this could be used to infer the presence of landforms underneath contemporary ice sheets (Bingham and Siegert, 2009). Many authors express the potential of these palaeo-glacial landforms as analogues for landforms underneath contemporary ice sheets (e.g. Stokes and Clark, 2001; Taylor et al., 2004; Bennett and Glasser, 2009; Bingham and Siegert, 2009) but only a handful of studies have looked at the bed roughness of previously glaciated landscapes (e.g. Hubbard and Hubbard, 1998; Hubbard et al., 2000; Gudlaugsson et al., 2013; Krabbendam and Bradwell, 2014) despite its non-reliance on the location of RES tracks (Fig. 2.2b) (Bingham and Siegert, 2009) and the substantial amount of high resolution Digital Elevation Models (DEMs) available (e.g. Golledge and Stoker, 2006; Eyles, 2012; Bradwell, 2013; Evans et al., 2014; Margold et al., 2015).

2.1.2.1 Contemporary-ice streams

Bed roughness and its relationship to ice dynamics were first acknowledged by Shabtaie and Bentley (1987), who mapped ice-stream margins on the Siple Coast, West Antarctica, using RES. Shabtaie and Bentley (1987) observed subglacial topographical control on the Whillans Ice Stream (previously referred to as Ice Stream B) and qualitatively described an area where rugged bed topography occurred underneath a zone of isolated crevassing. They also identified that Kamb Ice Stream (previously referred to as Ice Stream C) had a smoother bed compared to other neighbouring Siple Coast Ice Streams. Up until the late 1990s, little attention was given to measuring bed roughness, mainly due to the limited availability of widespread RES data (Rippin, 2013). Layberry and Bamber (2001) were the first to quantify bed roughness underneath the Greenland Ice Sheet, finding that the central region was smooth in comparison to the rougher margins. This is supported by the findings from Rippin (2013), who also suggested that there is a strong geological control on bed

roughness, and subsequently ice flow. For example, the east coast is rougher compared to the west coast, due to the mountainous terrain, which exerts a topographical control on fast ice flow. Furthermore, a north-south trending fault approximately defines the boundary between the rough and smooth beds (Rippin, 2013).

Siegert et al. (2004) and Taylor et al. (2004) were the first to measure bed roughness underneath contemporary ice streams by applying a Fast Fourier transform (FFT) to a 70km moving window along individual RES tracks, collected from the Siple Coast (Fig. 2.2). Siegert et al. (2004) found that the bed of ice streams had low roughness values i.e. smooth, which became progressively smoother downstream. The bed surrounding the majority of the ice streams was found to be rougher, interpreted as a topographic control on ice-stream location. However, the smooth bed either side of Kamb Ice Stream suggests that internal ice dynamics rather than topography control its location. Similar results were found for other ice streams in Antarctica. For example, the bed was found to be relatively smooth beneath the northernmost tributary of Slessor Glacier (Rippin et al., 2006), Institute and Möller Ice Streams (Bingham et al., 2007; Rippin et al., 2014), Foundation and Support Force Ice Streams (Bingham et al., 2007), Pine Island Glacier (Rippin et al., 2011) and West Ragnhild Glacier (Callens et al., 2014); whilst conversely being relatively rougher in the surrounding areas where ice flow is significantly slower (Table 2.1).

Earlier studies suggested that marine sediments beneath ice streams were the reason behind such a smooth bed (e.g. Siegert et al., 2004; Rippin et al., 2006; Bingham et al., 2007). Marine sediments were found at the base of boreholes drilled on the Siple Coast ice streams (Engelhardt and Kamb, 1998). To map the likely coverage of these marine sediments, isostatically adjusted subglacial topography was used to infer the location of a palaeo-shoreline, below which marine sediments could have been deposited during periods without ice cover (Studinger et al., 2001). These areas of inferred marine sedimentation corresponded with areas of the bed measured as smooth underneath the Siple Coast ice streams (Siegert et al., 2004), and this interpretation was applied in other studies (e.g. Bingham et al., 2007).

However, later research has shown that this may be an oversimplification and has demonstrated that there can be a combination of roughness values underneath fast flowing ice streams and outlet glaciers (Table 2; e.g. Rippin et al., 2006, 2011; Rippin, 2013). Schroeder et al. (2014) for example, found that the lower trunk of the fast flowing Thwaites Glacier

is underlain by a very rough bed due to outcropping bedrock, whilst the upper trunk is underlain by smooth deformable sediment (Fig. 2.3). This finding was supported by Muto et al. (2019), who also found rougher topography perpendicular to ice-flow direction compared to parallel to ice flow. Using an enhanced two parameter FFT method developed by Li et al. (2010), and importantly focussing on the difference between bed roughness parallel and orthogonal to ice flow, Rippin et al. (2014) found that whilst some locations with high ice velocities were underlain by sediments, others were underlain by a streamlined topography, and that rougher locations with decreased ice velocities indicated historic erosion had occurred (Institute and Möller Ice Streams, West Antarctica). Further analysis of Institute and Möller Ice Streams by Bingham et al. (2015) found a relationship between high/low bed-roughness values and continuous/disrupted internal ice layering, whilst Rose et al. (2015) found that smooth, flat areas of the bed are not always related to areas of current or former fast ice flow. Siegert et al. (2016) showed that Ellsworth Trough tributary, a fast flowing tributary of Institute Ice Stream, had a rough bed, likely to be caused by the strong topographical control on this trough (Ross et al., 2012). In northern Greenland, rougher areas of the bed are often associated with complex topography but can also be found over flatter regions (Jordan et al., 2017). In East Antarctica, a smooth bed was found in the Bailey Trough Region but a rough bed exists underneath the fastest flowing ice in the neighbouring Slessor Glacier, suggested to be caused by crystalline bedrock (Diez et al., 2018).

RES data are acquired along transects, typically using aircraft, and whilst the data resolution can be high along transect ∼10 m, the spacing between transects can be more than 10 km (e.g. Rippin et al., 2014). Bingham et al. (2017) acquired high resolution RES data using snowmobiles (transects spaced 500 m apart) to investigate the bed of Pine Island Glacier in West Antarctica. They found the rate at which ice thinning moves upstream was different between the glacier's tributaries. The tributary with a rougher bed had a 2 to 3 times slower upstream migration of ice thinning compared to the smoother tributaries. Furthermore, Davies (2018) found that bed-roughness values from Pine Island Glacier did not decrease with distance downstream and suggested that other factors were causing a high driving stress that allowed fast ice flow to effectively overcome a rough bed, such as topographic control from a subglacial trough, or the presence of sediment (Brisbourne et al., 2017).

In summary of the above, previous studies initially showed that there is a link between

slow flowing ice and a rough bed, and fast flowing ice and a smooth bed, e.g., the Siple Coast Ice Streams. More recently, it has been demonstrated that this link is more complex, with areas of fast flow occurring over rough beds, e.g., Thwaites Glacier. Interpretation of areas that have a rough bed underneath fast flowing ice is often difficult because the entire bed cannot be seen (due to widely spaced RES transects). For example, if there are no boreholes in these areas, it is not known whether till is present at the bed, and if the spacing of RES tracks is wide i.e. km scale, it is hard to identify whether glacial landforms are present at the bed. There is a need for further research on the bed roughness of contemporary ice streams, particularly to increase the coverage, resolution and understanding. The interpretation of bed-roughness results could be aided by the use of studies on palaeo-ice streams. This is reviewed in the next section.

2.1.2.2 Palaeo-ice streams

In comparison to bed-roughness studies from contemporary settings, measurements of bed roughness from deglaciated terrains are fewer in number. However, deglaciated terrain has the potential to give more detailed bed-roughness measurements than from contemporary ice beds due to the availability of high resolution DTMs, acquired over the last decades. The interpretation of bed-roughness results from deglaciated terrain can be directly compared to features on the bed such as glacial landforms and geology. One of the first papers to quantify roughness of deglaciated terrain was by Hubbard et al. (2000), who studied the roughness of exposed bedrock in a recently deglaciated area in front of Glacier de Tsanfleuron, Switzerland. They found that for horizontal scales from 1 mm to 40 m, roughness values were lower parallel to former ice-flow direction compared to roughness values orthogonal to former ice flow. However, bed roughness of the entire Laurentide Ice Sheet was calculated by Winsborrow (2007) using a low resolution DTM (1 km), who argued that there was no difference between palaeo-ice-stream bed roughness and the surrounding slow ice flow areas. This conclusion is likely to have been influenced by the scale of bed-roughness measurements in her study, where bed roughness was calculated using 11 x 11 km windows across a 1 km resolution DEM. Ebert (2015) found that bed roughness on Baffin Island, once covered by the Laurentide Ice Sheet, matched reasonably well with qualitative maps of glacial erosion.

Another study looked at macro-scale bed roughness of palaeo-ice streams, focussing on the British and Irish Ice Sheet, and found that roughness parameters differed between an

area of the Tweed Palaeo-Ice Stream and the non-glacially modified Cheviots (Prescott, 2013). Prescott (2013) also showed that changing the orientation of a transect by 22.5° changes the bed-roughness results, and that transects orientated parallel to palaeo-ice flow are smoother compared to those orientated orthogonal to palaeo-ice flow. Other studies have found that bed roughness under contemporary-ice streams is smoother parallel to ice flow vs orthogonal to ice flow (e.g. Rippin et al., 2014; Bingham et al., 2017) and this demonstrates that directionality of roughness in relation to ice flow is important. The importance of transect orientation was also shown by Gudlaugsson et al. (2013), who calculated the bed roughness of the Barents Sea Ice Sheet, and found higher roughness values orthogonal to past ice flow than parallel to past ice flow. Gudlaugsson et al. (2013) showed that the bed roughness of a palaeo-ice stream was similar to bed-roughness measurements from Antarctic ice streams, and this was an important step towards using bed roughness of palaeo-ice streams as analogues for contemporary-ice streams.

A novel study by Lindbäck and Pettersson (2015) measured the bed roughness beneath an area of the Greenland Ice Sheet and its associated proglacial area, demonstrating a correlation between low bed-roughness values, fast ice flow and subglacial troughs. They also found lower roughness values parallel to ice flow compared to orthogonal to flow, and showed that there was a strong geological control on bed roughness. Importantly, this study was able to show that bed topography underneath the ice resembled the proglacial area, and they were able to use the geological mapping of the proglacial area to infer that subglacial troughs are preglacial in origin. Using the full extent of a high resolution DEM (0.5 m), Tegowski et al. (2016) measured the bed roughness of Hansbreen Glacier's proglacial area, and were able to distinguish the roughness values of different landforms. However, as the bed roughness was measured using a 2D approach rather than the 1D transect approach, the difference of roughness values in relation to ice flow could not be assessed. A 1D approach measures bed roughness along transects whereas a 2D approach measures bed roughness of a central pixel within a moving window. Spagnolo et al. (2017) measured the bed roughness of palaeo MSGLs (mega scale glacial lineations) in Antarctica, and argued that MSGLs have a unique spectral signature (or roughness signature) and were shown to have low roughness values along flow compared to other subglacial topographies.

In summary of the above, studies on palaeo-ice-stream bed roughness have demonstrated similarities with results from contemporary-ice-stream studies, such as the importance of

transect orientation in relation to ice flow. Similar bed-roughness measurements have been found with Antarctic ice streams (e.g. Gudlaugsson et al., 2013), which suggests that the bed roughness of palaeo-ice streams could be used as analogues for the bed roughness of contemporary ice streams. However, it can be seen that there is currently a lack of bed-roughness studies on palaeo-ice streams in comparison to contemporary-ice streams, and much more work is needed to explore how bed-roughness measurements relate to properties of an ice-stream bed, e.g., absence/presence of till, bedrock and glacial landforms, and how bed-roughness measurements are affected by RES track spacing.

2.1.2.3 Causality

An issue that has arisen from the measurement of bed roughness at the base of fast flowing ice can be summed up as a classic causality conundrum. Did an initial smooth bed promote fast flow of ice, or did the ice streams smooth their beds and create a positive feedback mechanism whereby fast flow smoothes the bed further, in turn increasing ice velocity (Siegert et al., 2005)? It can be argued that until this problem is addressed, bed roughness at the bed of ice streams will continue to be overlooked as a controlling factor on ice-stream location (e.g. Bennett, 2003; Winsborrow et al., 2010). Rippin et al. (2011) argue that assuming such a causal relationship is an oversimplification. A smooth bed reduces the basal drag, meaning that a lower driving stress is needed to equal the balance flux, but it does not necessarily equate to fast flow, demonstrated by the Byrd Subglacial Basin (Fig. 2.4). They acknowledge that locating areas where smoothing of the ice-stream bed is currently taking place would be key to solving this problem.

2.1.3 Measuring roughness

There are many methods that can be applied to measure roughness. Making the correct choice of method can initially seem like a difficult task. However, there are suggestions from the literature that make this choice easier. This section will review how to choose a method, and review the methods that have been used in glaciology and other disciplines.

The first step in choosing a method to measure roughness is to establish what is being measured. This is because there are different roughness metrics such as amplitude or frequency of surface bumps (Fig. 2.5) (Smith, 2014). Choosing the correct method should be theoretically driven and/or take into account the process or landform of interest (Smith

et al., 2011). Scale plays a major role in measuring roughness (Andrle and Abrahams, 1989; Skidmore and Saleh, 1997; Borselli, 1999). Two scales exist at either end of the roughness window (Fig. 2.6); the measurement scale, below which roughness cannot be measured due to instrument resolution (e.g. satellite imagery), and the partition scale, which is defined by the user and is the appropriate size to capture the landform of interest (Smith, 2014). Fig. 2.7 shows examples of how the DEM resolution (measurement scale) and moving-window size (partition scale) affect the roughness measurements. The smallest moving-window size in Fig. 2.7 (3x3) measures the steep slope as rough at the beginning and end of the slope but smooth in the middle, which is not shown by the larger windows. Grohmann et al. (2011) applied different techniques for measuring roughness such as standard deviation of elevation, and vector dispersion, at multiple resolutions to measure the roughness of landforms in the Midland Valley, Scotland. They found that neither the measurement scale nor the partition scale affected certain methods such as the area ratio method, whilst other methods were affected, such as standard deviation of residual topography, which produced roughness values for individual landforms rather than regional relief. It is clear from this study that the choice of method depends on the application and data available.

In glaciology a change in the partition scale is likely to be needed when measuring the roughness of roches moutonnées (1-700 m long) vs. MSGLs (>1 km long) (Benn and Evans, 2010). Thus there is unlikely to be one window size that is appropriate for measuring bed roughness across all glacial landscapes. In numerous studies the reasoning behind the selection of the partition scale is often not stated (e.g. Rippin et al., 2006; Siegert et al., 2016; Diez et al., 2018) thus producing results to which it is difficult to assign significance (Lane, 2005), and making it impossible to compare results between studies. As the sampling window size is so important to roughness results, authors often employ different window sizes to evaluate this effect (e.g. Frankel and Dolan, 2007; Haubrock et al., 2009; Sankey et al., 2010; Eitel et al., 2011; Grohmann et al., 2011). To aid the clarity needed in roughness analysis methods, Smith (2014) recommend a five step process that authors could apply to their method justification (Fig. 2.8).

2.1.3.1 Detrending

Before bed roughness can be measured, DEMs need to be detrended. The detrending process removes large scale features such as valleys and hills, which would otherwise dominate the

bed-roughness measurements (Taylor et al., 2004; Prescott, 2013; Lindbäck and Pettersson, 2015). For example, consider a topographically confined palaeo-ice stream that has left behind numerous landforms. The bed roughness scale of interest is the landforms rather than the larger scale valley, because subglacial obstacles up to 1 m high and long have been theoretically shown to produce basal drag (Weertman, 1957; Kamb, 1970; Nye, 1970; Hubbard and Hubbard, 1998; Hubbard et al., 2000; Schoof, 2002). Without detrending, these scales would be obscured in the results because roughness methods would measure the large scale features. There are many methods to detrend data (e.g. Shepherd et al., 2001; Glenn et al., 2006; Bryant et al., 2007; Hillier and Smith, 2008; Rodríguez-Caballero et al., 2012). Taylor et al. (2004) used a least-square linear regression to detrend data along 2D transects underneath the Siple Coast Ice Streams, Antarctica, whilst Rippin et al. (2014) subtracted the mean bed topography along 2D transects beneath the Institute and Möller Ice Streams, Antarctica. However, it can be argued that subtracting the mean does not remove all large scale topography, particularly if there is one large surface feature which increases the mean. Using the method deployed by Taylor et al. (2004), Prescott (2013) found that varying the detrending window length along 2D transects affected the profile shape of bed-roughness results, where as the detrending window increased, the range of bed-roughness values increased. A method employed by Spagnolo et al. (2012) to correctly measure drumlin relief can also be used to detrend a drumlin swarm. Here, the drumlins are effectively sliced off the landscape, removing the underlying topography. The advantage of this method is that it just leaves the landforms behind which would allow bed-roughness signatures to be produced.

2.1.4 Bed-roughness methods used in glaciology

2.1.4.1 FFT analysis / spectral analysis

In glaciology, taking into account the effect of subglacial bed roughness is key to understanding ice motion, and Weertman (1957) first addressed this in his model of glacier sliding by using the amplitude (i.e. vertical change) and spatial frequency (i.e. horizontal change) of bed roughness over a hypothetical homogeneous bed (Li et al., 2010). Kamb (1970) and Nye (1970) expanded Weertman's theory by introducing Fourier transformations of bed elevation profiles, which allowed heterogeneous bed surfaces to be considered because a Fourier transform can transform any surface (Li et al., 2010). Fourier transform and fast Fourier

transform (FFT) produce the same output, but the calculation is quicker when using FFT (Cochran et al., 1967). The majority of bed-roughness studies in glaciology have used a method that applies FFT analysis to RES data beneath current ice streams (e.g. Siegert et al., 2004; Taylor et al., 2004; Siegert et al., 2005; Bingham et al., 2007; Bingham and Siegert, 2009; Li et al., 2010; Rippin et al., 2011; Rippin, 2013; Rippin et al., 2014; Schroeder et al., 2014) and transects across DEMs of areas beneath former ice streams (Gudlaugsson et al., 2013; Ebert, 2015; Lindbäck and Pettersson, 2015). FFT analysis can calculate amplitude and spatial frequency for a variety of wavelengths by converting a surface into a sum of multiple episodically occurring wavy surfaces (Li et al., 2010). However, FFT analysis is too complicated to measure spatial changes of bed roughness using one parameter. This was overcome by Hubbard et al. (2000) and Taylor et al. (2004) by defining the 'total roughness' parameter as the 'integral of a spectrum within a specified wavelength interval' (Li et al., 2010, p. 832). Essentially the 'total roughness' parameter is a measure of how the bed elevation amplitude varies. FFT analysis and spectral analysis have been used interchangeably in the literature to describe this method (e.g. Prescott, 2013; Rippin et al., 2014; Spagnolo et al., 2017). FFT analysis is used to calculate the spectral power density of all bed obstacle amplitudes contained within one transect or one moving window. Spectral power density is a measure of amplitude versus frequency i.e. the amplitude of each bed obstacle. As well as the 'total roughness' parameter, another parameter has been defined to measure bed obstacle frequency (Li et al., 2010; Rippin et al., 2014), which together with the 'total roughness parameter', enabled researchers to differentiate between discrete subglacial environments such as marine deposits vs. an erosional continental setting (Rippin et al., 2014).

The findings using this method to measure bed roughness underneath contemporary ice streams have been outlined in Section 2.1.2.1 and Table 2.1. FFT analysis has been used at a variety of scales, which is often dictated by the resolution of the raw data. For example, Gudlaugsson et al. (2013) used FFT to calculate bed roughness of the former Barents Sea Ice Sheet. They followed the two parameter method developed by Li et al. (2010) and applied it to high resolution (12 m) multibeam bathymetry data (25 m between tracks and window length of 384 m) and single beam bathymetry data (600 m resolution and window length of 1600 m). Findings from this study show that changing the moving window over which FFT is calculated changes the bed-roughness results. The bed-roughness results are scaled with the length of the moving window. Lindbäck and Pettersson (2015) calculated bed roughness

of the subglacial and proglacial area in West Greenland. They applied FFT to RES data with a 30 m resolution along transects and 2.5 km spacing between transects (960 m window length) and DEM data (30 m resolution), where they produced artificial profiles with the same spacing as the RES data. Low bed-roughness values were found along flow, compared to high bed-roughness values perpendicular to flow, and low bed roughness was correlated with fast ice flow. These are just a few examples, but they show that there is a wide range of window sizes used to calculate bed roughness using FFT analysis. Unfortunately the results from these studies cannot be compared because this difference in window size means that the scale of roughness being measured is different between studies. This is true for a large majority of studies measuring bed roughness of contemporary-ice streams (see table 2.2 for further examples of window size).

FFT analysis is the most widely used method to measure bed roughness in glaciology, and has been improved to measure frequency of bed obstacles as well as amplitude. However, there are certain assumptions that are made when using the FFT method. For example, data along RES transects are assumed to be equally spaced. This is not the case as bed returns can be lost (Bingham and Siegert, 2009), and interpolation between points along a RES track has been used to maintain this assumption (Taylor et al., 2004; Rippin et al., 2014). Bed-roughness measurements using FFT along 1D transects are sensitive to their location and interpolation between transects can miss data that would otherwise be seen by finer spacing of transects, or 2D methods. Prescott (2013) argued that because FFT measures multiple parameters, interpretation of the results is complex as it is not possible to say which parameter caused the spatial variation in bed roughness. This is often due to the results being presented using the integrated 'total roughness' parameter, which can obscure information regarding any relationship between vertical bed roughness and the horizontal length prescribed by the window size (Jordan et al., 2017). Adding to this, different topographies can produce the same bed-roughness measurements using the 'total roughness' parameter (Fig. 2.9) (Li et al., 2010). These issues should be taken into account when interpreting bed-roughness measurements, particularly from underneath contemporary-ice streams where large parts of the bed cannot be seen.

2.1.4.2 Standard deviation

The standard deviation of bed topography method is widely used as a simple roughness measurement amongst earth scientists (Smith, 2014) and has been used as an alternative to FFT analysis on RES data underneath contemporary ice streams (e.g. Rippin et al., 2006, 2014). Standard deviation measures how spread out the values are. A higher standard deviation implies a bigger range between the high and low elevations, thus a rougher bed. Standard deviation can be referred to as root mean square (RMS) height (Shepard et al., 2001). The main advantage of standard deviation is that it is a simple calculation which can be quickly applied to produce bed-roughness measurements of palaeo-ice streams from DEMs in either 1D or 2D. It has been applied to measure amplitude as a representation of roughness (Grohmann et al., 2011) and also combined with others in a so called hybrid parameter (Kean and Smith, 2006; Prescott, 2013; Smith, 2014).

Bed roughness underneath the Greenland Ice Sheet was measured using standard deviation by Layberry and Bamber (2001). Standard deviation was measured along transects (1D) that had an along-track resolution of 130 m, using a window of 15 km. Rippin et al. (2006) used standard deviation of bed elevation data beneath the tributaries of Slessor Glacier, East Antarctica, as a measure of bed roughness. Standard deviation was calculated in 5x5 km windows using a RES dataset that had an along transect resolution of 60-75 m, and a transect spacing of 40 km. Rippin et al. (2014) demonstrated that standard deviation calculations of 1D bed roughness produced the same trends of roughness variation as FFT, although they were less pronounced. They used RES data which enabled bed-roughness measurements using windows 320 m long with a transect spacing of 30 km (Vaughan et al., 2006; Ross et al., 2012). Winsborrow (2007) was the first to calculate 2D bed roughness in glaciology. This was done with a 1 km horizontal resolution DTM, using an 11 by 11 km moving window to calculate standard deviation of bed roughness on Laurentide palaeo-ice streams. However, detrending was not used in these calculations. There are limitations with the standard deviation method, which include a sensitivity to the largest changes in amplitude (Sedlaček et al., 2009). Furthermore, the standard deviation method suffers from the same issue as FFT analysis, where different topographies can give the same value (Li et al., 2009).

2.1.4.3 Topographic Position Index

Topographic Position Index (TPI) measures how the elevation of a cell in a DTM differs from the mean elevation of multiple cells that surround it i.e. calculated within a window (Ebert, 2015). A higher value indicates a rougher topography because the cell elevation deviates more from the mean elevation (Tagil and Jenness, 2008). It was devised as a measure of terrain ruggedness (Jenness, 2004) and is calculated as:

$$TPI = \frac{smoothedDEM - minimumDEM}{maximumDEM - minimumDEM} \tag{2.1}$$

Ebert (2015) used TPI alongside FFT when investigating the impact of ice-sheet erosion on Baffin Island. This is the only time this method has been used in glaciology. She found that areas with a higher density of high TPI values corresponded with intense ice-sheet erosional impact, and that TPI and FFT showed similar patterns. The TPI method did have an issue with the edges of the DEMs because they can be seen in the roughness results. De Reu et al. (2013) argued that TPI was able to classify landforms in homogeneous landscapes but not heterogeneous ones.

2.1.4.4 Hurst exponent

The Hurst exponent (H) is a scaling parameter, and is used to measure the rate at which elevation increases vertically in relation to the horizontal length scale (Shepard et al., 2001; Jordan et al., 2017). Low values (H $\approx$0) suggest that the topography quickly becomes smooth as the horizontal scale increases (called stationary) (Fig. 2.10). Shepard et al. (2001) provide the excellent example of a flat lawn. If you consider the roughness at millimetre to centimetre scale, individual blades of grass create a rough topography, but at larger scales ($>$ a few metres) the surface of a lawn is relatively smooth. Where vertical scale increases with the square root of the horizontal scale, H $\approx$0.5, and is called Brownian. High values (H $\approx$1) indicate that the topography maintains its roughness as the scale increases i.e. the horizontal and vertical scales increase at the same rate (Shepard and Campbell, 1999). This is called self-similar. Natural topography often shows a scaling behaviour called self-affine, where the elevation increases in the vertical direction at a fixed, slower rate compared to the horizontal scale (Shepard et al., 2001; Jordan et al., 2017). Hubbard et al. (2000), Macgregor et al. (2013) and Jordan et al. (2017) showed that subglacial topography is self-affine for length

scales of $\sim 10^{-3}$ to $\sim 10^{2}$ m.

2.1.5 Methods used in other disciplines

Outside glaciology, numerous methods to calculate roughness exist. These will now be reviewed together in sections relating to the parameter that they measure such as amplitude, shape etc. An in depth review of each individual method has already been completed by Prescott (2013).

2.1.5.1 Amplitude parameters

There are five different methods that have been used to calculate amplitude as a measure of roughness: *mean height, standard deviation, highest peak/lowest trough, mean peak/trough* and *range* (Table 2.2). *Standard deviation* has already been reviewed in Section 5.2.2. A key difference outside of glaciology is that detrending does not seem to be a prerequisite when applying these methods. However, as discussed in Section 2.1.3.1, detrending is an important component of bed-roughness measurements. The method of *mean height* measures the average amplitude along a transect or in a moving window, and is one of the most widely used methods in many scientific disciplines (Kupko et al., 2007). For example, in engineering and manufacturing this method is used to assess the quality of parts (Bigerelle et al., 2003; Zhang et al., 2007). Yet this method has been criticised. One of the problems with this method is the same as that of FFT and SD, where different profile shapes can produce the same roughness value (Feng et al., 2003). Thus, a profile across a landscape that has a few high mountains would not be distinguished from a profile across the landscape that has numerous small hills. A further criticism is that the *mean height* method cannot differentiate between an area dominated by crests or troughs (Prescott, 2013).

The *highest peak* or *lowest trough* can be used as a measure of roughness, and is calculated relative to the *mean height* (Gadelmawla et al., 2002). Assessing the size of peaks is important when researching frictional resistance and surface wear (Najjar et al., 2003). This method could be used to measure the maximum bed obstacle to ice flow. It can be measured as one value along a profile, or in a moving window. If measured using a moving window, some of the highest peaks or lowest troughs may be missed if the window edge is positioned on them (Fig. 2.10). Prescott (2013) argued that when using this method it cannot be ascertained as to whether the highest peak or lowest trough is representative or anomalous. One way

to address this has been to calculate the mean peak or mean trough height i.e. the average peak or trough size. The mean peak or mean trough height is calculated over a user defined number of sampling windows, usually five (Hall et al., 1997; Gadelmawla et al., 2002). When measuring the amplitude along a profile it can be argued that it is insufficient to just look at peaks, or just troughs (Prescott, 2013).

The *range* of values along a profile can be used as a measure of roughness. It can be calculated as highest peak added to the lowest tough, or the highest peak minus the lowest trough (Gadelmawla et al., 2002). However, roughness measurements using range have been identified as unrepresentative (Hall et al., 1997; Kupko et al., 2007) and can be skewed by anomalous values (Gadelmawla et al., 2002). Again, this method cannot distinguish between peaks and toughs, as a high range could be caused by either (Shaw, 2007; Prescott, 2013).

2.1.5.2 Spacing parameters

Three different methods can be used to calculate roughness in terms of the spacing between peaks; *number of peaks* or *number of troughs, average wavelength* and *surface aspect ratio* (Table 5). The *number of peaks or troughs* is calculated for each window along a transect (Najjar et al., 2003; Shaw, 2007). This shows the density of peaks and troughs, which would be useful in identifying certain landform groups such as megagrooves. A problem with this method would be comparing results that use different window sizes because a bigger window size is more likely to have more peaks or troughs (Prescott, 2013). Several profile shapes could produce the same peak count, but to distinguish between these the average wavelength could be used. *Average wavelength* calculates the mean distance between peaks or valleys (Mendeleev, 2003). Prescott (2013) asserted that the same criticisms of the mean height method can be applied to the average wavelength method as it gives no information on distribution on values around the mean. *Surface aspect ratio* measures whether a surface pattern exists or not using autocorrelation, and is particularly used in engineering (Suh and Polycarpou, 2003; Suh et al., 2003). Assemblages of certain landforms have a clear visual pattern which has been shown in satellite imagery such as drumlins, rogen moraines and megagrooves (Benn and Evans, 2010; Bennett and Glasser, 2009; Hughes et al., 2010; Krabbendam et al., 2016). Prescott (2013) argued that this method could be used to identify patterns created by glaciation, but noted that this method does not provide orientation or dimension information of the surface roughness measurements.

2.1.5.3 Shape parameters

Four different methods can be used to describe the shape of 1D profiles or 2D data as a measure of roughness; *skewness, slope, kurtosis,* and *sinuosity* (Table 2.2). *Skewness* is a measure of the distribution of values in relation to the average (Gadelmawla et al., 2002; Boscher et al., 2014). Importantly it can show whether a profile is mostly composed of peaks or of troughs (Sedlaček et al., 2009), which may be useful for distinguishing between glacial landforms dominated by grooves, e.g., megagrooves, or peaks, e.g., drumlins. However it does not give any information on the size and density of peaks or troughs (Prescott, 2013). *Kurtosis* calculates the 'peakedness' of peaks or troughs (Hall et al., 1997). A profile composed of multiple large peaks and troughs will have a kurtosis value below 3 whilst one with fewer large peaks and troughs will have a kurtosis value above 3 (Gadelmawla et al., 2002; Sedlaček et al., 2009; Zou et al., 2016). This is a useful method as it provides information of peak amplitude and distribution (Prescott, 2013). However, it can be argued that it is not a very detailed method as a profile is either peaky or not peaky. *Slope* variation along a profile can be used as a measure of roughness, and is calculated by the gradient of a surface (Prescott, 2013). Steeper slopes along a profile indicate higher peaks. Grohmann et al. (2011) tested multiple methods to measure surface roughness on a DEM of the Midland Valley, Scotland. They found that standard deviation of slope was the best method of surface roughness calculations as it performed well at multiple scales and could pick up small scale relief. However, it can be argued that it does not provide any information on frequency or wavelength.

2.2 Glaciation of the British Isles

The glaciation of Britain has been the subject of much discussion and has many unresolved issues; from the timing and extent of British and Irish Ice Sheet (BIIS) coalescence with the Fennoscandian Ice Sheet (FIS) (Merritt et al., 2017; Roberts et al., 2018) to whether nunataks existed during the Last Glacial Maximum (LGM) (McCarroll, 2016; Clark et al., 2018). Understanding the factors that cause ice sheet disintegration are vital in enabling researchers to effectively model the dynamics of current ice sheets in Greenland and Antarctica (Shepherd and Wingham, 2007). With sections of the BIIS being marine based, and the role of ice streams in controlling ice dynamics, it has been posited as an analogue for the West Antarctic

Ice Sheet (Bradwell, Stoker and Krabbendam, 2008). The quality and spatial extent of geomorphological studies focused on glaciology in Britain and the surrounding sea basins are significantly varied when compared to records from other Quaternary ice sheets, e.g., the Laurentide Ice Sheet (Evans et al., 2005; Golledge and Stoker, 2006). One of the largest problems has been a poor chronological record for constraining the timing of advance and retreat. For example, the LGM limits for the BIIS in the 1990s had a few radiocarbon dates from the 1960s and 1970s (Chiverrell and Thomas, 2010), but since 2000 this has increased by adding new sites, using cosmogenic nuclide dating (Ballantyne, 2010; Smedley et al., 2017) and optically stimulated luminescence dating (Telfer et al., 2009; Roberts et al., 2018). With the advent of satellite imagery, evidence of glaciation in Britain has been improved (Evans et al., 2005; Hughes et al., 2014; Clark et al., 2018) whilst investigations into the offshore record have increased (Chiverrell and Thomas, 2010; Clark et al., 2018). The BIIS has also been modelled numerically (e.g. Boulton and Hagdorn, 2006; Hubbard et al., 2009) and can be compared to empirical reconstructions (e.g. Clark et al., 2012; Hughes et al., 2014) that incorporate chronological and geomorphological evidence. However, a detailed understanding of how and when the BIIS retreated has been difficult to fully realise, with studies either producing a rough overall picture of the ice sheet (e.g. Boulton et al., 1985; Sejrup et al., 2005) or an in depth interpretation of regional processes (Charlesworth, 1924; Merritt et al., 1995; Bradwell, Stoker, Golledge, Wilson, Merritt, Long, Everest, Hestvik, Stevenson, Hubbard, Finlayson and Mathers, 2008; Clark et al., 2012; Fabel et al., 2012).

2.2.1 Pre-Devensian glaciations

Before ca 1.1 Ma BP ice was only found in the upland areas of Britain (Lee et al., 2012). Evidence from cores in the North Atlantic containing Ice Rafted Debris (IRD) suggests that the first continental scale BIIS was formed ca 2.7-2.4 Ma BP (Jansen et al., 2000; Kleiven et al., 2002; Hall et al., 2018). With an extremely limited terrestrial record due to erosion and overprinting by subsequent glaciations, and non-existent provenance data, the size and location of such early BIIS is hard to ascertain (Thierens et al., 2012). The terrestrial record for the mid-Pleistocene glaciation is more substantial with the Ancestral Thames deposits recording at least two large scale glaciations; the Saalian glaciation during Marine Isotope Stage (MIS) 6 and Anglian glaciation during MIS 12. During the Anglian glaciation (ca 0.48 – 0.3 Ma), ice reached its most southerly extent in Britain (Fig. 2.12). The initiation of

these glaciations and the LGM is linked to the change from an obliquity to an eccentricity influenced climate at ca 1.1 – 0.7 Ma (Lee et al., 2012).

2.2.2 The Last Glacial Maximum

Conception of the LGM in Britain has changed significantly from the early interpretations of Boulton et al. (1985). The most recent delineation of the BIIS has doubled in size to 0.72 million km^2 and changed from a mainly terrestrial-based to a marine and terrestrial-based ice sheet (Clark et al., 2012). The work of early researchers was hampered by the paucity of chronological evidence, bathymetry data, and misinterpreting one till deposit to mean one glaciation, when it is now known that multiple tills can be deposited during a single glaciation (Chiverrell and Thomas, 2010). Stretching to the Isles of Scilly (Hiemstra et al., 2006; Roberts et al., 2007), the last BIIS inundated Ireland (Peters et al., 2015) and reached parts of the continental-shelf edge in the present day North Sea and Atlantic Ocean (Fig. 1.1 b) (Sejrup et al., 2005; Lee et al., 2012; Livingstone et al., 2012; Peters et al., 2016; Callard et al., 2018; Ó Cofaigh et al., 2019).

The timing of the LGM globally is thought to have occurred ∼27 ka BP (Clark et al., 2012). However, individual areas of ice sheets did not peak at the same time (Clark et al., 2009) and for the BIIS, the LGM is thought to have taken place between 27 – 21 ka BP (Chiverrell and Thomas, 2010).

A paradigm shift occurred where the understanding of the LGM in Britain moved from a conceptual model of fixed ice-dispersal centres to a model of migrating ice divides influenced by competing ice streams; a 'binge-purge' model (Benn and Evans, 2010; Hubbard et al., 2009; Hughes et al., 2014; Livingstone et al., 2012). This has been supported by findings from numerical and empirical models. A numerical model found a self-regulating binge-purge system occurred where a cold based thick ice sheet builds (binge) and ice streaming then enables the ice sheet to thin and expand (purge) (Hubbard et al., 2009). The modelled ice streams are very dynamic, competing for ice from dispersal centres to facilitate streaming behaviour. The locations of modelled ice streams agree with recent empirical evidence of overprinting flowsets (Fig. 2.13 d) and regional studies of geomorphological evidence (e.g. Merritt et al., 1995; Everest et al., 2005; Golledge and Stoker, 2006; Bradwell et al., 2007; Graham et al., 2007; Roberts et al., 2007; Livingstone et al., 2010; Yorke et al., 2012). A recent empirical model using flowsets (Fig. 2.13) found that the BIIS initiated as an

integrated ice sheet with an ice divide running N-S (Hughes et al., 2014). Ice streaming caused thinning and a change to a complex polycentric topographically controlled ice sheet (binge-purge). Flowsets were divided into two categories; isochronous and time-transgressive, and of the 11 flowsets identified as ice streams, 8 were isochronous. As the time-transgressive flowsets were used to model retreat from the LGM, it can be argued that this model suggests the majority of ice streams in the BIIS were active before deglaciation (Hughes et al., 2014).

2.2.3 Palaeo-ice streams

During the last glaciation, ice streams were important controls on ice dynamics and behaviour of the BIIS. Ice streams and outlet glaciers account for up to 90% of the ice discharge from the Antarctic Ice Sheet (Bamber et al., 2000), but accessing the bed is difficult and thus researchers have turned to palaeo-ice streams as analogues to increase understanding of active ice streams (Stokes and Clark, 2001; Benn and Evans, 2010). Stokes and Clark (1999) posited geomorphological criteria that need to be met in order to classify areas of past ice sheets as palaeo-ice streams (Table 2.3). Of course it can be difficult to satisfy all of these requirements due to certain factors such as evidence being under the sea and lack of bathymetric data, e.g., Irish Sea Ice Stream (ISIS).

The most commonly cited requirement associated with whether BIIS landsystems are ice streams or not is the elongation ratio of landforms such as drumlins or mega-scale glacial lineations (MSGLs) (e.g. Everest et al., 2005; Golledge and Stoker, 2006; Graham et al., 2007; Bradwell et al., 2007; Roberts et al., 2007; Livingstone et al., 2010; Yorke et al., 2012). Approximately 11 palaeo-ice streams have been identified in and around Britain; 6 terrestrial and 5 marine (Fig. 2.13 d). Others have been mooted but not studied such as Firth of Forth (Golledge and Stoker, 2006), whilst ice streams in Wales have been identified by Jansson and Glasser (2005) but have been left out by other authors (e.g. Hughes et al., 2014) (Table 2.4). The majority of palaeo-ice streams identified are located in Scotland and the North of England (Fig. 2.13 d). The latter of the two has a very complex yet poorly understood geomorphological record with overprinting of flowsets, where the Tweed, Tyne Gap and Stainmore Ice Streams competed and interacted with the ISIS and ice from the North Sea (Evans et al., 2009; Livingstone et al., 2010; Yorke et al., 2012). The Tweed Ice Stream (TIS) was initially investigated by Clapperton (1971) who identified long landforms which have elongation ratios of 23:1. Five out of eight criteria in Table 2.3 are satisfied by the

TIS, which deformed the substrate at the bed where a high porewater pressure enabled high velocities for streaming (Everest et al., 2005) (Table 2.4). Timing of the TIS is unknown, but Yorke et al. (2012) argue that the TIS caused the Tyne Gap Ice Stream (TGIS) to deflect southeast. The TGIS was a major conduit for ice flowing from Scotland and the Lake District, and it experienced several flow changes during the last BIIS, the last of which switching from east to west flow as it was drawn down by the ISIS. It was a topographically constrained ice stream with low bedform elongation ratios, and it meets some of the criteria in Table 2.3. The majority of lineations are bedrock moulded which suggest a limited amount of substrate to facilitate fast flow (Livingstone et al., 2010, 2012; Yorke et al., 2012).

The marine record arguably holds some of the most convincing evidence for palaeo-ice streams. MSGLs (Fig. 2.14) from the Minch Ice Stream (MIS) (Fig. 2.13 d) were found with elongation ratios of 70:1 using sidescan sonar and multibeam echo-sounding data (Bradwell et al., 2007). However, obtaining evidence has been problematic. In the North Sea, for example, there is a limited core record that has poor chronological constraints (Graham et al., 2007). The ISIS is inferred to have existed from terrestrial evidence in the Isles of Scilly (Hiemstra et al., 2006; Smedley et al., 2017), in Northern England (onset zone flowsets) (Hughes et al., 2014), East coast of Ireland (Small et al., 2018) and in the Isle of Man, which was possibly a sticky spot located in the convergent zone of the ice stream (Roberts et al., 2007). Combined with the marine evidence of a tidewater margin in the southern Celtic Sea, it is argued that the ISIS did exist even though geomorphological evidence for the main flow trunk has not yet been discovered (Roberts et al., 2007). Using 3D reflection seismic data, Graham et al. (2007) mapped the Witch Ground Ice Stream (Fig. 2.13 d) and found iceberg plough marks dating between 22 – 10 ka BP 15-20 m below the seabed surface, overlying MSGL. In the Inner Hebrides, Dove et al. (2015) recorded landforms composed of sediment and or bedrock (Fig. 2.15), which included drumlins overprinted by recessional moraines and convergence zones.

Only a handful of studies have used a combination of marine and terrestrial evidence; Bradwell et al. (2007) found MSGL on the Scottish mainland as well as in the Minch, and Bradwell and Stoker (2015) mapped an increase in elongation ratios offshore in the Minch, which implies an increase in ice-flow velocity. Golledge and Stoker (2006) focused on the Strathmore Ice Stream (SIS), finding terrestrial landforms with elongation ratios of up to 38:1 with offshore evidence of lineations and a lateral moraine. They argue that ice-

flow mechanisms varied either being associated with meltwater or deformation of substrate (Smith, 1997), and areas free of streamlining may be caused by multiple scenarios, such as bed roughness. The SIS satisfies 5/6 of the 8 criteria for palaeo-ice streams (Table 2.4) Golledge and Stoker (2006).

2.2.4 Glaciation of the British Isles - Concluding remarks

Much has changed over the last decade regarding our understanding of the BIIS. A conceptual model of fixed ice dispersal centres has given way to one of a dynamic ice sheet where shifting ice divides and ice streams play a key role in growth and demise. Uncertainty still exists however, with a clear example of this being a question mark over the origin of the Witch Ground Ice Stream. The trunk of the ISIS remains unmapped, and a clear understanding of timings is yet to be forthcoming. Palaeo-ice streams have a large part to play in solving uncertainties regarding the BIIS and more work is needed to confirm the number of ice streams that existed and understand what caused the high velocities that left behind a clear impression on the landscape. This work will aid research being undertaken on current ice streams, and allow a better understanding of current ice-sheet behaviour in Antarctica and Greenland.

Chapter 3

Investigating methods for quantifying bed roughness

3.1 Introduction

Currently there is no standard method for quantifying bed roughness in glaciology, or in other disciplines (Sections 2.1.4 & 2.1.5). Different studies have used different methods, and it is often not clear why methods have been chosen over others. Method choice is made difficult by the large number available. For example, Prescott (2013) tested 20 roughness methods that could be used in glaciology, and a further 9 were not tested. The use of different methods makes comparisons between studies difficult. If a single method was used by multiple studies, it would help to create a better understanding of bed roughness between sites and in glaciology. However, this may not be possible, and as our understanding of bed roughness increases, it might be that multiple methods reported together will provide a more robust approach.

A prerequisite of calculating bed roughness is to detrend the data. As detailed in Section 2.1.3.1, there are many detrending methods that can be used (e.g. Shepherd et al., 2001; Glenn et al., 2006; Bryant et al., 2007; Hillier and Smith, 2008; Rodríguez-Caballero et al., 2012), but detrending methods can affect the profile shape of bed-roughness results (Prescott, 2013).

One factor contributing to method selection is that past bed-roughness studies underneath contemporary ice sheets have come up against data resolution issues. The along transect resolution can be high (∼4-6 m) (Bingham et al., 2017), yet the spacing between

transects is often tens of kilometres (e.g. Siegert et al., 2005; Rippin et al., 2014). This wide transect spacing makes it difficult to analyse roughness of the entire bed, particularly as glacial landforms are often tens of metres in length, width and height. Bed-roughness measurements have been limited to window sizes (length scales) that are larger than the along transect resolution (typically 30 m), which cannot capture smaller scale landforms. Therefore the importance of roughness at smaller scales, particularly when metre-scale information is needed to understand basal ice sliding, is unclear (Jordan et al., 2017). Ultimately, this problem will not be solved until higher resolution data from contemporary ice streams and glaciers are acquired, like in the studies of King et al. (2009, 2016) and Bingham et al. (2017). However, data from deglaciated terrain are now available at a resolution where they can be used to measure roughness at the metre-scale. Therefore, a grid of transects that has the same resolution as a DTM can be set up to measure roughness at a higher resolution than has been achieved under contemporary ice streams so far. This will provide a more detailed picture of bed roughness. In glaciology, four different methods have been used to measure bed roughness: Fast Fourier Transform analysis, Standard Deviation, Hurst Exponent, and Topographic Position Index (e.g. Taylor et al., 2004; Rippin et al., 2014; Ebert, 2015; Jordan et al., 2017). A more detailed description of how they have been used, and a current understanding of advantages and disadvantages, is given in Chapter 2, Section 2.1.4. Each method is briefly described below.

1. Fast Fourier Transform (FFT) analysis transforms bed elevations into wavelength spectra (Gudlaugsson et al., 2013), producing a power spectrum (Bingham and Siegert, 2009), which is a measure of the intensity (power) of different wavelength obstacles along a transect.

2. Standard deviation (SD) is a measure of amplitude variation. Applied to elevation data, a higher standard deviation implies a larger range between the high and low elevations, and thus a rougher bed (Prescott, 2013).

3. The Topographic Position Index (TPI) measures how much one pixel of a DEM differs compared to the mean elevation within a specific area of the DEM surrounding that pixel. The higher the value, the more the pixel differs from the mean elevation, thus the rougher the terrain (Ebert, 2015).

4. The Hurst exponent is a measure of the rate at which elevation increases vertically in

relation to the horizontal length scale (Jordan et al., 2017).

3.2 Aim and objectives

The overall aim of this chapter is to assess how detrending affects bed roughness, compare different methods used in glaciology to measure bed roughness, and explore how using the highest resolution data available affects roughness results. Several objectives have been identified.

1. Create one transect parallel to palaeo ice flow along a flow line of a palaeo ice stream: here the Minch Palaeo Ice Stream (MPIS) is used as the study area (see Section 1.2). The chosen flow line should include both onshore and offshore data i.e. the onset zone and main ice-stream trunk, as it is likely that ice speed increased from the onset zone into the trunk. Create orthogonal transects that cross this flow line to assess whether transect orientation in relation to ice flow affects roughness values.

2. Use the parallel and orthogonal to ice-flow transects (flow line transects) to test the effect of detrending and window size on roughness results.

3. Test the methods identified above that have been used to measure bed roughness in glaciology (see Section 2.1.4) on the flow line transects (1D).

4. Use the full resolution of the NEXTMap DTM to calculate roughness for a small area (2D) to test how using higher resolution data affects roughness results.

3.3 Data and methods

3.3.1 Data

NEXTMap DTM (Intermap Technologies, 2009) was chosen as the base data set. Although there are some areas in the UK covered by higher resolution LiDAR data the MPIS is not one of them. NEXTMap has complete coverage and a comparatively high resolution compared to a large amount of Radio Echo Sounding (RES) data from underneath contemporary ice streams. NEXTMap DTM has a 5 m horizontal resolution and a 1 m vertical resolution (Bradwell, 2013). NEXTMap DTM tiles were downloaded from the Centre for Environmental Data Analysis (CEDA) Archive (Intermap Technologies, 2009). In addition, offshore

Bathymetric Multi Beam Echosounder Survey data (MBES) are used (Bradwell and Stoker, 2015). This provides coverage of the main MPIS ice-stream trunk. The MBES data subset has a resolution of 4 m and includes the Little Minch and the southern area of the Minch (Fig. 3.1). The surveys around NW Scotland were completed by the Maritime & Coastguard Agency (MCA) between 2006 and 2012. For more detail on acquisition and processing of MBES data see Bradwell and Stoker (2015) or the Reports of Survey, which can be requested from MCA, the UK Hydrographic Office, the British Geological Survey or the Natural Environment Research Council. Geomorphological mapping of the offshore data was undertaken by Bradwell and Stoker (2015, ; Fig. 3), who identified drumlins, streamlined bedrock and glacial lineations.

3.3.2 Methods

3.3.2.1 Transects

To test the different roughness methods, transects parallel and orthogonal to palaeo ice flow were constructed (Fig. 3.1). The location of the parallel to palaeo ice-flow transect was decided by using the inferred MPIS flow lines from Bradwell et al. (2007). Six flow lines begin on the West coast of Scotland, but only three of these cross the bathymetry data from the Minch. Of the three flow lines, the one that was chosen crossed a similar size area of both the onshore and offshore data. As the parallel to palaeo ice-flow transect is located on the narrow Isles of Raasay and Rona, the orthogonal transect is substantially smaller. Therefore, to increase the amount of data, three orthogonal transects were created for the onshore data, and placed at the widest locations on this part of the island. The offshore orthogonal to palaeo ice-flow transect was located where it crosses numerous types of glacial landforms as observed in Bradwell and Stoker (2015). The transects were split into onshore and offshore, because there is a gap between the NEXTMap and bathymetry data (Fig. 3.1). Points were constructed at the full resolution of each data set; 5 m onshore and 4 m offshore, and the x, y and z coordinates were extracted from NEXTMap DTM and MBES bathymetry.

3.3.2.2 Detrending

Before bed roughness can be calculated, the elevation data must be detrended to remove large wavelengths caused by mountains and valleys, which would otherwise dominate roughness measurements (Shepard et al., 2001; Smith, 2014). Smaller obstacle scales than this are

of interest to glaciologists such as scales which affect drag (∼0.5 - 1 m) (Weertman, 1957; Schoof, 2002) and the scales of glacial landforms (0.01 m - 100 km) (Bennett and Glasser, 2009). Detrending is an important part of the final bed roughness calculation, because it determines the scale of data used to measure roughness. Altering the window size used to detrend elevation data has been shown to change the bed-roughness results along a transect (Prescott, 2013). To remove this issue, a different detrending method is tested and compared to the previously used method. Past studies have calculated the mean in moving windows along a transect and subtracted this from the original elevation data (e.g. Rippin et al., 2014; Diez et al., 2018). This method will be referred to as the *mean detrending method*. The alternative method is to calculate the difference between a specified number of points along a transect. For example, if the number of points specified was 3, then the difference would be calculated between the 1st and 4th value along a transect, then the 2nd and 5th value, and so on. The advantage is that the alternative method does not require a moving window, which removes one of numerous variables that affects the final bed-roughness results (Prescott, 2013; Smith, 2014). The alternative method will be referred to as the *difference detrending method*.

The offshore orthogonal to palaeo-ice-flow transect (Section 3.3.2.1: Fig. 3.1b) was chosen to test the two detrending methods because it crosses numerous glacial landforms of different scales. These landforms are of interest as they provide resistance to ice flow. Thus, finding the roughness scale that picks them up is important. Five window sizes were chosen to test how this affected the roughness measurements calculated from both detrending methods. These range from 100 m to 1 km, and increased incrementally by 200 m. Glacial landforms can vary in size from metres to kilometres (Bennett and Glasser, 2009), so these window sizes aim to capture this range in scale. For the difference detrending method, the elevation data for the transect were detrended in R using the difference function (where difference = 2). For the mean detrending method, the mean was calculated in R within a moving window. A data point is located in the middle of the window, and the value for that point is calculated using the elevation data within the window. This is done for every point along the transect. The resulting mean elevation transect is taken away from the original elevation data to produce the detrended output.

3.3.2.3 Bed-roughness calculations - standard deviation (SD)

Using the detrended transects, standard deviation (SD) was calculated along transect using a moving window. A higher standard deviation shows there is a larger range between the high and low elevations, and therefore a rougher bed. SD was calculated for five window sizes of 100 m to 1 km, increasing incrementally by 200 m, for the offshore orthogonal transect. This allows the effect of the detrending window on roughness to be investigated. The 100 m window was chosen to be used as the comparison for the other methods (20 points onshore, 25 points offshore), and subsequently calculated for all transects (Fig. 3.1). Where the transects crossed lakes and coastline, bed-roughness values were removed in ArcMap to prevent bias towards smooth surfaces (Gudlaugsson et al., 2013) using the Ordnance Survey Meridian 2 lake regions shapefile (Survey, 2017). To visualise the bed-roughness calculations spatially, the bed-roughness results were interpolated using the Topo to Raster tool in Arcmap, with a 100 m output cell size. A buffer of 500 m was applied either side of the transects. The SD results are not normalised, but shown as absolute values in metres. However, when presented alongside the results from the other methods, the SD results were normalised, to enable a comparison. Following the post processing stages of interpolation, buffering, and smoothing, the data were normalised using a linear transformation. The data were re-scaled to range between 0 and 1.

3.3.2.4 Bed-roughness calculations - Fast Fourier Transform (FFT) Analysis

Fast Fourier Transform (FFT) analysis was undertaken for the along-flowline transects (Fig. 3.1), for both detrending methods. The same lake removal (including where transects crossed the sea) interpolation, and normalising was used (Section 3.3.2.3). For FFT analysis to work, the transects require continuous along-track data. Thus for gaps of >100 m long (10 points), the transects were 'cut' (Rippin et al., 2014). This was only required for the onshore transects where a lake functions like a data gap. FFT analysis was not applied across these gaps. FFT analysis transforms bed elevations into wavelength spectra (Gudlaugsson et al., 2013), producing a power spectrum (Bingham and Siegert, 2009), which is a measure of the intensity (power) of different wavelength obstacles along a transect. FFT analysis was performed along transects using a window size of 100 m. The total roughness parameter was then defined by calculating the integral of the power spectra for every window. This

parameter is a measure of the bed amplitude, or vertical irregularity (Li et al., 2010).

3.3.2.5 Bed-roughness calculations - Topographic Position Index (TPI)

Topographic Position Index (TPI) was calculated for all the along flowline transects (Fig. 3.1). It is calculated using the raw elevation data from the NEXTMap DTM using the following equation from Ebert (2015):

$$TPI = \frac{smoothedDEM - minimumDEM}{maximumDEM - minimumDEM} \tag{3.1}$$

The same window size that had been used for SD and FFT analysis was applied (100 m). The same lake removal (including where transects crossed the sea) interpolation, and normalising was used (Section 3.3.2.3).

3.3.2.6 Bed-roughness calculations - Hurst exponent

The Hurst exponent (H) was calculated for all transects. This was done using a variogram, with bins every 4 m offshore and 5 m onshore. The variogram is a plot of the logarithm of elevation variance vs the logarithm of distance along transect (McClean and Evans, 2000). The variogram slope is 2H. The first 100 values on a logarithm scale of the variogram were used to calculate the variogram slope, from which H can be calculated. Values of H range between 0 and 1. Low values of H suggest that the topography quickly becomes smooth as the horizontal scale increases. High values of H indicate that the topography maintains its roughness as the scale increases i.e. the horizontal and vertical scales increase at the same rate. This is called self-similar. Natural topography shows a scaling behaviour called self-affine, where the elevation increases in the vertical direction at a fixed, slower rate compared to the horizontal scale (Shepard et al., 2001; Jordan et al., 2017).

3.3.2.7 Pixel-scale transects

Within the Minch bathymetry raster alone there are 1,495,108,455 pixels. This constitutes a very large dataset. Thus for this chapter, an area the size of 1x1 km was chosen to test the calculation of roughness at the pixel-scale (2D). The 1x1 km area is made up of 200 columns and 200 rows (5m pixel resolution), and has 40,000 pixels. The 1x1 km area is located on the Ullapool megagrooves, as this is an area of fast ice flow within the MPIS (Bradwell,

Stoker and Krabbendam, 2008) and these landforms are anisotropic (Krabbendam et al., 2016; Newton et al., 2018). Therefore, it would be expected that the roughness values would be different for parallel and orthogonal to palaeo ice-flow directions. The palaeo ice-flow direction is approximately east to west. This makes extracting the data easier, because the raster pixels are aligned in columns running north to south and rows running east to west.

The Create Fishnet tool was used in ArcMap to produce a grid of points for the 1x1 km area, with a point every 5 m. The xy coordinates and elevation data from the NEXTMap DTM were added to each point. The shapefile was then split into transects for each row and column in R by using the xy coordinates (each horizontal transect has the same eastings and each vertical transect has the same northings). The horizontal transects are approximately parallel to palaeo-ice flow and the vertical transects are approximately orthogonal to palaeo-ice flow. Each transect was detrended using the mean detrending method, with a 100 m window. Roughness was calculated using SD, with a 100 m window. The transects were then combined to create a raster using the roughness data to allow for easy data visualisation. This was done separately for the parallel and orthogonal to flow transects.

3.4 Results and discussions

The results are split into two main sections: detrending and roughness methods comparison. After each section there is a discussion, which feeds into a wider overall discussion at the end of the chapter.

3.4.1 Detrending comparison

3.4.1.1 How does the window size affect mean detrending?

An increase in the window size reduces the amount of detail in the mean detrending profile (Fig. 3.2 - 3.6). The transects detrended using a 100 m window pick out the drumlins more effectively for the first part of the transect (Fig. 3.2a) compared to the second part (Fig. 3.2.1c). Using the 100 m window, smaller scale features than the drumlins and bedrock areas are included in the detrended profiles (Fig. 3.2a, c), and some drumlins are split across multiple peaks, e.g., the drumlin between 21000 and 22000 m along track (Fig. 3.2c). As the window sizes increase, these smaller scale features disappear from the detrended profiles, and from the 500 m to 1 km window size, the drumlin between 21000 and 22000 m becomes

a more defined single peak (Fig. 3.3c – 3.6c). The 700 m and 1 km windows produce a mean detrended profile similar to what would be expected when eyeballing the data. As the window sizes increase, the range of the detrended profile values increases i.e. the peaks and troughs become bigger (Fig. 3.2a & c – 3.6a & c), and the mean detrended profiles for the first section of the transect lose more data at the beginning of the transect (Fig. 3.2a – 3.6a).

3.4.1.2 The difference between the two detrending methods

From the smallest to the largest window, the drumlins in section one of the transect are clearly shown in the mean detrended profile (Fig. 3.2 a – 3.6 a). The difference detrending only picks out the drumlin between 1000 and 2000 m along the transect (Fig. 3.2 b – 3.6 b). However, this profile is the same for all subsequent roughness measurements as a window was not used to produce the detrended data. For the second section of the transect, the drumlins are not as easily distinguishable from the mean detrended data, and areas of bedrock produce similar detrended values (Fig. 3.2 c – 3.6 c). The differenced detrended data pick up some of the isolated elongated drumlins such as the drumlins located between 22000 and 23000 m, and after 25000 m, along the transect (Fig. 3.2 d – 3.6 d). The highest detrended values are found over the continuous bedrock area between 24000 and 25000 m along the transect (Fig. 3.2 d – 3.6 d). As the window size increases, the range of roughness measurements from both detrending methods increases (Fig. 3.2 - 3.6). Using the 1km window, roughness measurements have a similar pattern for the first section of the profile but the roughness values from the mean detrending method are higher (Fig. 3.6a & b). The roughness measurements calculated from the difference detrending method strongly picks out the middle drumlin in the first section of the transect for all windows (Fig. 3.2b – 3.6b). In the second section of the transect, the roughness values calculated from the difference detrending method are highest for the bedrock areas (Fig. 3.2d – 3.2d). The roughness values calculated from mean detrending for the first section of the transect pick out the three drumlins for the 100 m and 300 m windows (Fig. 3.2a – 3.3a). For the bigger windows, the drumlins become less clear (Fig. 3.2a – 3.6a). The second section of the transect has no clear pattern from roughness measurements calculated using mean detrending between the drumlins and areas of bedrock Fig. 3.2c – 3.6c).

3.4.2 Detrending discussion

3.4.2.1 How does window size affect detrending?

Window size is an important variable when using the mean detrending method. Before roughness is calculated, the detrending window size will change the scale of features in the detrended data (Fig. 3.2 - 3.6). This was shown by Prescott (2013) in relation to RES data from Antarctica. Here, data from the deglaciated Minch allow a more detailed inspection of the effects of the detrending window size because more information is available for the interpretation i.e. there is no ice covering the bed. Even within the same class of landforms, different window sizes were able to capture some but not all of the landforms (Fig. 3.2a & c – 3.6a & c). This is caused by the difference in landform size. For example, the drumlin located between 21000 and 22000 m was split between multiple peaks using 100 m window in the detrended transect (Fig. 3.2c) but from the 500 m to 1 km window sizes, it became a defined single peak (Fig. 3.4c – 3.6c). The transects detrended using the 100 m window pick out the drumlins more effectively for the first part of the detrended transect (Fig. 3.2a) compared to the second part (Fig. 3.2c). This could be due to the complexity of the second section of the transect. Rather than just three isolated drumlins, the second section has drumlins located next to each other, as would be expected (Maclachlan and Eyles, 2013), and exposed bedrock either side of drumlins. The subsequent roughness calculations from the 100 m window mean detrended data (Fig. 3.2c) are the only ones that are able to distinguish between drumlins and bedrock (excluding the drumlin between 22000 – 23000 m). Some of these are bedrock cored drumlins (Bradwell and Stoker, 2015), which is likely to be a factor in the roughness measurements when compared to the surrounding bedrock. However, it can be argued that prior knowledge of the landscape is needed to make this interpretation. All subglacial landforms will have a size range. Subglacial landforms range from 10 - 10^5 (Clark, 1993; Bennett and Glasser, 2009). Within this, drumlins are 10^2 – 10^3 m long, whilst megagrooves or MSGL are 10^2 – 10^5 m long (Clark, 1993). This is just one metric of size; there is also a range of widths and heights. Therefore, no one window size will be able to capture all individual landforms. The smaller window sizes (i.e. <500 m) will capture the smaller drumlins for example, but split larger ones. However, the bigger windows will merge roughness values for multiple landforms. The downside of this is that other features could be merged to contribute to the roughness value, for example, a drumlin

is merged with a flat hill (Fig. 3.6a). Thus choosing the correct window size for a data set comes down to what scale of feature is to be measured. Is the roughness of individual landforms or the roughness of many landforms more important?

3.4.2.2 How do the two detrending methods vary?

The two detrending methods produce different results, although to what extent depends on the window size and section of track. Using the 100 m window, the mean detrending method picks out all three drumlins in the first section of the transect, whilst the difference detrending method only picks out one (Fig. 3.2a & c). For the second section of the transect, the pattern of roughness produced by both detrending methods is more similar (Fig. 3.2b & d). The difference detrending method picks out the bedrock more clearly than the mean detrending method (Figs. 3.2 - 3.6). This is due to the nature of the bedrock; it has steep slopes and has lots of 'short sharp' peaks and troughs. The advantage of the difference detrending method is that it removes window size as a variable during the roughness measurement process. This detrending method, when combined with SD, is useful at picking out very rough areas, i.e. those where there are sharp changes in slope. It shows the shape of the topography rather than amplitude. It was able to distinguish between the bedrock areas compared to the drumlins, which the mean detrending could not. However, the mean detrending was able to pick out the individual drumlins more clearly, and when combined with SD as a roughness measurement, it used the amplitude of features instead of shape. Both detrending methods are useful when measuring glacial bed roughness, and arguably would be useful together. Yet, the results from both of these methods still need a prior knowledge of the landscape to be able to distinguish between different landforms/area types.

3.4.2.3 Is there a best window size?

For the mean detrending method, a larger window size >500 m could be more appropriate as it picks out the landforms of interest for these transects, and removes the smaller scale features. However, caution should be taken, as these larger window sizes also pick out some of the troughs in the original elevation data, e.g., at 23000 m along the transect (Figs. 3.2c – 3.6c). For roughness measurements, a smaller window may be more appropriate i.e. 100 m – 300 m to capture individual landforms. These tend to become obscured at the larger window sizes, particularly for the second section of the transect. For example, it is impossible

to distinguish between bedrock and drumlins (Fig. 3.6c). The larger windows will be able to capture a wider range of landforms, as the upper limit of feature size that can be used to measure roughness is dictated by the window size (Prescott, 2013). However, this will merge landforms, which makes interpretation of what is causing roughness difficult. It should also be noted that as window size increases, the length of the transect reduces regardless of detrending method; for example, the first drumlin is lost from the analysis (Fig. 3.6 a & b). There is unlikely to be a 'one size fits all' window, capable of capturing all individual glacial landforms.

3.4.3 Methods comparison results

3.4.3.1 Standard deviation – mean detrended transects

Bed-roughness measurements are higher onshore compared to offshore, for both transect directions (Fig. 3.7.1). For the onshore transects, the parallel to palaeo-ice flow transects have mean roughness values of 1.9 m compared to 2.3 m for the orthogonal transects (Table 3.1). The onshore orthogonal transects have a higher maximum roughness value of 8.1 m compared to 5.6 m for the parallel transect and they have a larger range of roughness values (Table 3.1). The offshore transects are smoother than the onshore ones (Fig. 3.7.1) with means of 0.1 and 0.3 m compared to 1.9 and 2.3 m respectively (Table 3.1). In terms of anisotropy, the offshore transects also show the same pattern as the onshore transects (Fig. 3.7.1), with the orthogonal transects having higher roughness values (mean of 0.3 m) compared to the parallel transects (mean of 0.1 m) (Table 3.1).

Offshore, the highest roughness measurements are found orthogonal to palaeo-ice flow over an area of exposed bedrock (>2 m) (Fig. 3.1a), although not all of the bedrock has high roughness values (0.2 m) (Fig. 3.7.1a). The drumlins located in section 1 of the offshore orthogonal transects (orange line, Fig. 3.1b) have roughness values around 1 m. The drumlins located in section 2 of the offshore orthogonal transects (blue line, Fig. 3.1b) have roughness values from 0.4-0.6 m. Offshore, the one area of exposed bedrock is rough parallel to palaeo ice flow (0.8 m). The roughest area is where the parallel transect crosses the edge of what looks like a bedrock overdeepening (0.9 m) (Fig. 3.7.1a).

Onshore, orthogonal to palaeo-ice flow, the highest roughness measurements are located where transects pass over fault lines (up to 7 m). Lower roughness values are found in the middle transect, and the western part of the bottom transect (Fig. 3.7.1c). Parallel to

palaeo-ice flow, the highest roughness values are also associated with fault lines (up to 5.5 m) (Fig. 3.7.1b).

3.4.3.2 Standard deviation – difference detrended transects

Bed-roughness measurements are again higher onshore compared to offshore, for both transect directions (Fig. 3.7.2). For the onshore transects, the parallel to palaeo-ice-flow transects have mean roughness values of 0.7 m compared to 0.9 m for the orthogonal transects (Table 3.2). The onshore orthogonal transects have a higher maximum roughness value of 4.6 m compared to 2.3 m for the parallel transect and they have a larger range of roughness vales (Table 3.2). The offshore transects are once again smoother than the onshore ones (Fig. 3.7.2) with means of 0.1 m compared to 0.7 and 0.9 m respectively (Table 3.2). The difference detrended transects differ from the mean detrended transects in two ways. The overall roughness values are lower; means of 0.1 – 0.9 m for the difference detrended transects compared to means of 0.1 – 2.3 m for the mean detrended transects. Secondly, there is little difference between the overall roughness values of the difference detrended offshore transects (both have a mean of 0.1 m) (Table 3.2). The highest roughness measurements for the offshore orthogonal to palaeo-ice-flow transect occur over an area of exposed bedrock (0.7 m). Similarly to the mean detrended SD roughness values, not all of the bedrock is rough (0.07 m). The drumlins located in section 1 of the offshore orthogonal transects (orange line, Fig. 3.1b) have roughness values from 0.09-0.3 m. The drumlins located in section 2 of the offshore orthogonal transects (blue line, Fig. 3.1b) have roughness values from 0.03-0.07 m. Offshore, parallel to palaeo ice flow, the one area of exposed bedrock is again rough (0.6 m). As with the mean detrending SD results, the roughest area is where the parallel transect crosses the edge of what appears to be a bedrock overdeepening (0.9 m) (Fig. 3.7.1b).

Onshore, the roughness measurements are again, not as high as the mean-detrended SD results. The highest and lowest orthogonal roughness measurements (0.7 m and 0.3 m respectively) occur in the same area as those from the mean-detrended SD results (bottom transect; Fig. 3.7.2c). The highest roughness values parallel to palaeo-ice flow occur where fault lines are crossed by the transect (2.3 m). Overall, there are fewer rough values for the difference detrending compared to the mean detrending SD results.

3.4.3.3 FFT analysis – mean detrended transects

Bed-roughness measurements are higher for orthogonal transects both onshore and offshore (Fig. 3.8.1); producing means for parallel transects of 63.7 and 0.9, and orthogonal transects 115.5 and 10.8 (Table 3). The roughness values are higher for the onshore transects compared to the offshore transects (Fig. 3.8.1), with means of 63.7 and 115.5, and 0.9 and 10.8 respectively. Offshore, the highest roughness values occur over an area of exposed bedrock (up to 187) (Fig. 3.8.1). However, there are some lower values over this bedrock (down to 1) (Fig. 3.8.1). The drumlins located in section 1 of the offshore orthogonal transects (orange line, Fig. 3.1b) have roughness values from 0.1-36. The drumlins located in section 2 (blue line, Fig. 3.1b) have roughness values from 0.5-13. Parallel to palaeo ice flow, an area of exposed bedrock has values of 20. The highest roughness values are where the parallel transect crosses the edge what looks like a bedrock overdeepening (38) (Fig. 3.8.1a). Onshore, the highest roughness values for the orthogonal transects occur on the top and bottom transects, 937-1253 and 765-929 respectively (Fig. 3.8.1c). The lowest roughness values are found at the western end of the middle transect (0.2-1) (Fig. 3.8.1c). The highest roughness values parallel to palaeo-ice flow are 521-931 and are found in multiple locations (Fig. 3.8.1b). The lowest roughness values are 0.001-0.5 and found close to where the transect crosses waterbodies.

3.4.3.4 FFT analysis – difference detrended transects

Bed-roughness measurements are higher for the onshore transects compared to the offshore ones (Fig. 3.8.2). Offshore mean values are 1.1 and 1.02, in comparison to 31.4 and 65.5 for the onshore mean values (Table 3.4). Onshore, the orthogonal to palaeo-ice-flow transects have higher roughness values compared to the parallel ones (Fig. 3.8.2b & c) with means of 65.5 compared to 31.4 respectively. However, offshore, the orthogonal to palaeo-ice-flow transects have lower roughness values compared to the parallel transects, with means of 1.02 compared to 1.1 respectively, and maximum values of 28.8 and 41.2 respectively (Table 3.4).

Offshore, the highest roughness values occur over areas of exposed bedrock (12-28). Yet within the bedrock, values go down to 0.3. The drumlins located in section 1 of the offshore orthogonal transects (orange line, Fig. 3.1b) have roughness values from 0.3-5. The drumlins located in section 2 (blue line, Fig. 3.1b) have roughness values from 0.07-0.6. Parallel to

palaeo ice flow, the area of exposed bedrock has values of 11-16. The highest roughness values are where the parallel transect crosses the edge of what looks like a bedrock overdeepening (up to 41).

Onshore, the highest roughness values orthogonal to palaeo-ice flow are found in the most southerly transect (810-947) (Fig. 3.8.2c). The lowest roughness values orthogonal to palaeo-ice flow are found on the western half of the bottom transect (0.2-0.5) (Fig. 3.8.2c). The highest roughness values parallel to palaeo-ice flow occur over a fault line (193-233) (Fig. 3.8.2b). The lowest roughness values parallel to palaeo-ice flow occur close to waterbodies (0.13-0.7).

There are differences between the results from the mean detrending and difference detrending using FFT analysis. Offshore, the orthogonal to palaeo-ice-flow transect has higher roughness values when mean detrending is used, whilst this is not the case for differenced detrending (Tables 3.3 & 3.4). The roughness values have a larger range for the mean detrended transects (Tables 3.3 & 3.4). Some areas are picked out as rough by the mean detrended transects and not by the difference detrended transects. For example, the most northerly onshore orthogonal transect (Fig. 3.8.1c & 3.8.2c).

3.4.3.5 Topographic Position Index (TPI)

There is not much difference between the onshore and offshore roughness results, or between parallel and orthogonal to palaeo-ice-flow transects. Onshore means are 0.49 and 0.52 for parallel and orthogonal to palaeo-ice flow respectively (Table 3.5). Offshore means are 0.49 and 0.47 for parallel and orthogonal to palaeo-ice flow respectively (Table 3.5).

Offshore, the highest roughness results orthogonal to palaeo-ice flow (0.7-0.8), occur in numerous locations, with only one of these on the exposed bedrock, and includes a drumlin in section 1 (orange line, Fig. 3.1b) (Fig. 3.9a). The lowest roughness measurements occur in the bedrock area (0.1-0.2) (Fig. 3.9a). The drumlins located in section 1 of the offshore orthogonal transects (orange line, Fig. 3.1b) have roughness values from 0.4-0.7. The drumlins located in section 2 (blue line, Fig. 3.1b) have roughness values from 0.4-0.6. The highest roughness results parallel to palaeo-ice flow (0.7-0.8), also occur in numerous locations, as do the lowest values (0.2-0.3) (Fig. 3.9a). Roughness values for the exposed bedrock and bedrock overdeepening are 0.6.

Onshore, the highest roughness results orthogonal to palaeo-ice flow also occur in numer-

ous locations (0.7-0.8), including areas where other methods had their lowest values, e.g., the western end of the middle transect (Fig. 3.9c). The lowest roughness values are also in multiple locations (0.2-0.3) (Fig. 3.9c). Parallel to palaeo-ice flow, the highest values again occur in numerous locations (0.8-1). The lowest values occur close to waterbodies (0.05-0.1) (Fig. 3.9b).

3.4.3.6 Hurst exponent

All transects have a similar Hurst exponent. Both onshore transects and the offshore orthogonal transect have a Hurst exponent of 0.7 (Table 3.6). The offshore parallel transect has a Hurst exponent of 0.8 (Table 3.6).

3.4.4 Methods comparison discussion

3.4.4.1 How do the detrending methods vary between SD and FFT?

Generally, both detrending methods picked up the same broad bed-roughness trends: orthogonal to palaeo-ice flow, roughness values are higher, and onshore roughness was higher than offshore roughness. However, there are clear differences between the two detrending methods. For the SD and FFT analysis methods, the roughness values are collectively lower for the difference detrended transects compared to the mean detrended transects. This is due to the way the data are collected from the detrending methods. Taking the mean elevation away from the original will give larger values compared to calculating the difference along transect. The mean values for the offshore transects are the same when difference detrending is used (Table 3.2) or slightly lower (Table 3.4). This suggests that the shape of the transects is similar. The sediment cover offshore (Bradwell and Stoker, 2015), which is not found for the onshore transects, could be a reason for this. The sediment cover will have subdued any sharp slopes. The highest roughness values are also found offshore using the difference detrended method on the parallel transect (Table 3.2 & 3.4). These are located where the transect crosses what appears to be a bedrock overdeepening (Fig. 3.10). This is an area where the vertical elevation values change quickly moving along the transect. Thus, this one location could be the reason why overall, the parallel roughness values have the same or slightly smaller mean compared to the orthogonal offshore transect.

3.4.4.2 Hurst Exponent

These values are between Brownian and self-similar (Table 3.6). Brownian describes terrain where H = 0.5 and elevation increases vertically with the square root of the horizontal window size. Self-similar describes terrain where H = 1 and elevation increases vertically at the same rate as the window size increases (Shepard and Campbell, 1999). This means that the values of these transects have "persistent trends", where subsequent elevation values often follow a trend of increasing or decreasing (Shepard and Campbell, 1999; Jordan et al., 2017). It is unexpected that all transects would have a similar H value, as previous studies have found that subglacial terrain has a self-affine scaling behaviour (Jordan et al., 2017) i.e. there would be a range of H values. This may be due to Jordan et al. (2017) deriving H from the root mean square height, which in itself is a measure of roughness. Here, H was derived from the fractal dimension (D). As there were no clear trends from this method, it is not considered further.

3.4.4.3 Similarities and differences between the methods

To compare the results of all the methods, the data have been normalised so that the roughness values are all on the same scale. The results from the TPI method are very different from the others (Fig. 3.9). The values are much higher throughout all of the transects, and there are no clear patterns relating roughness to the landscape. The TPI method does not show a difference between the orthogonal and parallel transects, or a difference between the onshore and offshore data. The TPI method has been used once previously to assess the erosional impacts of the Laurentide Ice Sheet on Baffin Island (Ebert, 2015). Here, the author also used FFT analysis and suggested that both methods were in agreement (Fig. 3.11). However, it is difficult to tell from the paper whether this is the case as no values are reported (the values are on a scale from low to high) and it is not clear whether values from both methods are on the same scale. Ebert (2015) applied TPI over a whole DTM, therefore the data she shows are not directionally dependent, as are the data used in this study. This could be a reason for the differing results. However, from the data and methods used here, it is suggested that TPI is not a useful method to measure bed roughness along transects because it shows no discernible patterns that relate to the landscape.

There are some similarities and differences to the bed-roughness values from SD and

FFT analysis (Figs. 3.7 & 3.8). Both SD and FFT analysis show that bedrock offshore has lower roughness values than onshore i.e. it is smoother. This is likely to be due to two reasons: sediment deposition and more erosion at the bed. Onshore, there is very minimal till deposition from the MPIS whereas offshore there is much more (Fyfe et al., 1993). Surrounding the exposed bedrock area offshore, there are numerous landforms composed of sediment, e.g., drumlins (Bradwell and Stoker, 2015, 2016). The sediment is visible in between peaks of exposed bedrock. Thus, the deposited sediment will reduce the amplitude of the bedrock compared to that onshore. Additionally, the offshore bedrock is in the trunk of the MPIS, whilst the onshore bedrock is in the onset zone. A large amount of glacial modification of the landscape can cause smoothing of bedrock (Bradwell, 2013; Krabbendam and Bradwell, 2014). The strongly streamlined landforms offshore indicate intense erosional sculpting by fast flowing ice (Bradwell and Stoker, 2016).

Onshore, the same area is measured as being the smoothest by both SD and FFT analysis methods (Figs. 3.7 & 3.8); the western end of the southernmost orthogonal transect. This is caused by a change in geology from the hard, Lewisian Gneiss (r value $\sim$55) to the softer Torridonian Sandstone (r value $\sim$47) (Fig. 3.12) (Krabbendam and Glasser, 2011). The Torridonian Sandstone is more susceptible to erosion by glacial abrasion compared to the Lewisian Gneiss (Bradwell, 2013), and in this case, glacial abrasion is likely to be just as quantitatively efficient as plucking (Krabbendam and Glasser, 2011). Thus, the amplitude of bedrock features is lower compared to the Lewisian Gneiss.

Some of the roughness trends differ between the SD and FFT analysis results. Onshore, the SD results show higher roughness values compared to the FFT analysis (Figs. 3.7 & 3.8). Both methods use the amplitude of features to provide roughness measurements (Rippin et al., 2014). However, FFT analysis is influenced by the frequency of features (Bingham and Siegert, 2009). A landscape with a similar frequency of undulations that also has large amplitude changes between undulations will be smoother when measured by FFT analysis compared to SD. Onshore the area is made up of visible bedrock with numerous ridges and lakes, a cnoc and lochan landscape (Bennett and Glasser, 2009). Cnoc and lochan landscapes are largely influenced by the bedrock geology, and the roughness is inherited from the pre-glacial weathering front (Krabbendam and Bradwell, 2014). As both SD and FFT analysis give different roughness results, this could be useful for identify a cnoc and lochan landscape in other locations.

Onshore, at the northern end of the parallel to palaeo-ice-flow transect, the transect crosses the sea numerous times. These values are removed, and the transect has fewer values at this location. This could be the reason for lower roughness measurements in this location from both methods.

3.4.4.4 Is there a best method?

The TPI method did not show any clear patterns that related to the landscape, and it is not clear that this is a useful method for measuring bed roughness in glaciology. The SD and FFT analysis methods were more useful methods for calculating bed roughness but both have advantages and disadvantages. SD does not require the continuous data that FFT analysis needs (Taylor et al., 2004; Bingham and Siegert, 2009; Rippin et al., 2014) and thus the data for SD do not have to be resampled or interpolated along transects (Cooper et al., 2019). SD results have a unit (metres) whilst FFT analysis provides a dimensionless number (Siegert et al., 2005; Cooper et al., 2019). Furthermore, Cooper et al. (2019) argued that SD enables shorter length-scales to be measured than FFT analysis does, which allows the difference between parallel and orthogonal to ice flow roughness (anisotropy) to be calculated. The complicated nature of FFT analysis may reduce the ability of glaciologists to communicate the importance of bed roughness. However, FFT analysis can provide more information on bed roughness than SD if other parameters are also used. As well as total bed roughness, the slope and wavelength can also be calculated using FFT analysis (Li et al., 2010; Wright et al., 2012; Rippin et al., 2014). Both FFT analysis and SD are useful methods for calculating bed roughness as they generally provide similar results, but deciding which method to use in future studies will be determined by data availability and the roughness parameters that are going to be investigated.

3.4.5 Pixel-scale transects

Roughness is higher orthogonal (up to 4 m) rather than parallel (up to 2.2 m) to palaeo-ice flow (Fig. 3.13). The megagrooves are clearly outlined in the orthogonal to palaeo-ice flow raster (Fig. 3.13b). Here, the trough of the megagroove is picked out as smooth, whilst the crests either side of the trough are rough. The parallel to palaeo-ice flow does not pick out the megagrooves (Fig. 3.13c). Instead, it shows a terrain of small round hummocks.

3.4.6 Pixel-scale transects discussion

The directional differences in bed roughness, previously referred to as directionality (Rippin et al., 2014) or anisotropy (Jordan et al., 2017) are very clear (Fig. 3.13). Previous studies have found that roughness values are higher orthogonal to ice flow compared to parallel to ice flow (Hubbard et al., 2000; Gudlaugsson et al., 2013; Prescott, 2013; Rippin et al., 2014; Lindbäck and Pettersson, 2015). These studies were limited to either a few transects, or had gaps in between transects. This study shows directional dependent 2D roughness data for the first time. Thus, it goes further than showing rougher values orthogonal compared to parallel to palaeo-ice flow. Fig. 3.13. shows that the roughness values orthogonal to palaeo-ice flow can be linked to the landforms, and in turn, demonstrate how ice flow organises the landscape. This area of the MPIS bed is dominated by megagrooves (Bradwell, Stoker and Krabbendam, 2008). Orthogonal to palaeo-ice flow i.e. across the megagrooves, the bed is rougher compared to the parallel to flow. This makes sense, as simplistically, the shape of megagrooves can be described as corrugated. The MPIS has preferentially eroded bedding of the metasandstone to form megagrooves (Krabbendam and Glasser, 2011). In this instance, ice flow has streamlined the landscape, making it smoother parallel rather than orthogonal to palaeo-ice flow.

Parallel to palaeo-ice flow the bed is smoother, although there are what appear to be bumps in the landscape (Fig. 3.14b). The landscape can be rough at smaller scales and smooth at larger scales. Shepard et al. (2001) use the example of a flat lawn to illustrate this point. At small scales the grass is rough, but at a larger scale, the lawn is smooth. At the larger scale, i.e. before the 1x1 km area is detrended, the landscape appears smoother parallel to palaeo-ice flow than it does once it has been detrended. However this is not the only factor in the appearance of these bumps; only the bed roughness of the horizontal transects is being calculated, rather than a combination with the orthogonal transects. These bumps are likely to be superimposed on the megagroove landscape, and may be caused by the bedrock.

One problem with using the data at the pixel-scale is the accuracy of the DTM. On the parallel to palaeo-ice flow detrended raster, it picks up some artefacts. These areas appear to be pixelated and not smooth compared to the rest of the raster (Fig. 3.14b). In some parts of the roughness raster, these artefacts can be seen as thin lines. Although it does not affect the general trend of the data overall, it should be noted. It is important to note that

data of this resolution cannot be acquired from underneath ice sheets because of the nature of RES. RES collects data in a cone, similar to a ship using sonar. Therefore for subglacial landforms, such as megagrooves or MSGL, RES can pick up multiple landform crests parallel to ice flow (Bingham et al., 2017). RES is acquired at a high resolution using orthogonal transects (500 m between transects) (King et al., 2009; Bingham et al., 2017).

3.5 Concluding remarks

The choices made by a researcher on data resolution, window size, detrending and roughness methods can significantly affect the results of a study. Window size affects which landforms are measured as rough. Landforms are on a size continuum, therefore no one window size will capture the roughness of all landforms. Mean detrending picked up drumlins, whereas difference detrending showed where areas of exposed bedrock were located. Both detrending methods are useful when measuring glacial bed roughness, potentially being more robust when used together. Importantly the results from both of these detrending methods and the roughness methods applied to detrended data, still need a prior knowledge of the landscape to be able to distinguish between different landforms/area types. For roughness measurements a smaller window would be needed (100 m – 300 m) to show individual landforms. A larger window (>500 m) can measure a wider range of landforms, but this will merge landforms, making interpretation of what is causing roughness difficult.

The TPI method was not useful as there was no trend that could be related to the landscape. Unexpectedly, the Hurst exponent did not find much difference between the transects, which could be due to the way it was calculated. FFT analysis and SD showed similarities and differences between the roughness results. Both methods had lower roughness values offshore compared to onshore. Sediment deposition and increased erosion rates are likely to be the cause. Onshore the same area was measured as smooth by both methods due to a change in bedrock geology. Yet, onshore SD measured higher roughness compared to FFT analysis for the cnoc and lochan landscape. FFT analysis and SD both have advantages and disadvantages. FFT analysis can provide more information than SD. However, SD can be used on a wider range of data and does not need a large amount of data preprocessing. FFT analysis and SD are useful methods for calculating bed roughness as they give similar results. SD is more flexible in terms of the data that can be used. Thus, both methods can

be used by future studies but the method choice will be determined by the data available and which roughness parameters are going to be investigated.

Directional dependent pixel scale roughness data were shown for the first time. The orthogonal to palaeo-ice-flow direction clearly showed the megagrooves, whilst parallel to palaeo-ice flow showed bumps that are likely to be superimposed on the megagrooves. It can be seen from this small area that roughness values can be linked to glacial landforms and emphasises the importance of directionality when measuring bed roughness.

Chapter 4

Quantifying bed roughness beneath contemporary and palaeo-ice streams

This chapter has been published in the Journal of Glaciology (see Falcini et al., 2018) and there is a copy of this article in the thesis appendix. For consistency, the reference style has been changed from the published version to match the format of the rest of the thesis. The table and figures have been taken out of the published text and placed in volume two. The figure and table numbers have been changed from the published version to match the thesis format. I declare that the work submitted is my own. The contribution of the co-authors was as follows: David Rippin, Maarten Krabbendam and Katherine Selby: Supervision, review and editing.

4.1 Introduction

This paper aims to measure the bed roughness of contemporary subglacial and deglaciated terrains at analogous length scales. We define bed roughness as the vertical variation of terrain over a given horizontal distance (Siegert et al., 2005; Rippin et al., 2011). Accurate quantification of bed roughness beneath ice sheets is important because it is a primary control on basal drag and therefore ice flow velocity (Siegert et al., 2005; Bingham et al., 2017). Subglacial obstacles of ∼0.5 to 1 m in both amplitude and horizontal wavelength have been shown theoretically to exert critical basal drag (Weertman, 1957; Kamb, 1970;

Nye, 1970; Hubbard and Hubbard, 1998; Hubbard et al., 2000; Schoof, 2002); however, these obstacle dimensions lie below the resolution achievable by radio-echo sounding (RES) across ice sheets. Several authors have nevertheless explored the relationship of higher amplitude (several 100 m) and longer wavelength (100s of m to several km) bed roughness and ice dynamics across ice sheets using available RES data. These analyses have suggested that beds beneath contemporary ice streams are relatively smooth, with roughness values decreasing downstream, whilst in surrounding areas of slower ice flow, the beds are relatively rougher (Siegert et al., 2004; Rippin et al., 2006, 2011; Callens et al., 2014). As a consequence, basal roughness is regarded as one of the controls on ice-stream location, in particular for ice streams not topographically controlled by deep valleys (Siegert et al., 2004; Bingham and Siegert, 2009; Winsborrow et al., 2010; Rippin, 2013).

While a relationship between bed roughness and ice dynamics is intuitive, quantifying such a relationship has proved elusive and several studies have produced findings that should be explored further. For example, it has been observed that fast flowing ice can also occur over a rough, hard bed (Schroeder et al., 2014). The reasons for a smooth bed underneath fast flowing ice can be varied, e.g., the existence of fine-grained sediments vs. streamlined topography (Li et al., 2010; Rippin et al., 2014). Ice-stream beds can be smooth along ice flow (parallel) and rough across flow (orthogonal) (King et al., 2009; Bingham et al., 2017), showing that the direction of bed roughness measurements is extremely important. Palaeo-ice-stream beds show the same pattern (Gudlaugsson et al., 2013; Lindbäck and Pettersson, 2015). Geology can have a strong control on the roughness underneath fast flowing ice as shown in previously glaciated gneiss terrains (Krabbendam and Bradwell, 2014). An increase in landform elongation ratios in a palaeo-ice stream has been related to the change from a rough to smooth bed (Bradwell and Stoker, 2015). The points raised by these studies demonstrate that bed roughness and its relationship to ice dynamics is complex. By using Digital Terrain Models (DTMs) from now-exposed palaeo-ice streams to calculate bed roughness, we propose that it may be possible to explore these complexities in more detail because the bed of a palaeo-ice stream can be directly observed over its entirety at much higher spatial resolutions than contemporary ice-stream beds.

The bed roughness of contemporary ice sheets has been calculated along 1D topographic profiles (from RES tracks) predominantly using two different approaches, frequency domain methods e.g. Fast Fourier Transform (FFT) analysis (Taylor et al., 2004; Siegert et al., 2005;

Bingham et al., 2007; Li et al., 2010; Rippin, 2013) and space domain methods e.g. Standard Deviation (SD) (Layberry and Bamber, 2001; Rippin et al., 2014). Radar specularity has also been used to infer bed roughness (e.g. Schroeder et al., 2014).The scale of bed roughness measurements has mostly been controlled by the spacing between flight tracks, and the along track resolution, which is a function of the radar system used. Ice sheet scale studies have typically used track spacing of several kilometres with an along track resolution of a few metres (Siegert et al., 2004; Rippin et al., 2006; Bingham et al., 2007). Higher resolution radar imaging by King et al. (2009, 2016) and Bingham et al. (2017) has shown topographic detail that cannot be captured by the larger scale studies, and is similar to the detail available on deglaciated terrains from DTMs and bathymetric data unconstrained by ice cover (e.g. Bradwell and Stoker, 2015; Margold et al., 2015; Perkins and Brennand, 2014). Using DTMs also allows bed roughness to be measured in 2D and at much smaller scales. The resolution of DTMs is becoming finer, with pixels down to a few metres or less (e.g. LiDAR; Salcher et al., 2010; Putkinen et al., 2017). Analysis of DTMs from deglaciated areas provides an opportunity to show what is being missed when bed roughness measurements are interpolated across widely spaced RES transects. Bed roughness calculations made on this terrain can also be much more easily linked to the geomorphological and geological character of the bed, because individual landforms and geological variation can be observed directly. In this study, we compare the bed roughness of the deglaciated, Devensian, Minch Palaeo-Ice Stream and surrounding areas in NW Scotland, with the contemporary Institute and Möller Ice Streams in West Antarctica. The bed roughness of both ice streams is quantified along transects with the same grid spacing, but for the palaeo-ice stream is also calculated between transects. We test how several parameters influence the measurement and interpretation of bed roughness. Firstly, we gauge whether the method used to measure bed roughness, FFT analysis or SD, produces different results. Secondly, we explore whether RES track spacing is sufficient to capture bed roughness trends. Thirdly, we compare bed-roughness results from transects that have the same grid spacing as RES data with results calculated down to the DTM pixel resolution. Finally, we show how the orientation of transects in relation to ice-flow direction influences bed-roughness results.

4.2 Data and methods

4.2.1 Study sites and data

The Minch Palaeo-Ice Stream (MPIS) drained the NW sector of the British and Irish Ice Sheet during the Devensian (Weichselian) glacial period (116 – 11.5 ka BP), and has a well-documented glacial landform and sediment record Bradwell, Stoker and Krabbendam (2008); Bradwell and Stoker (2015, Fig. 4.1). Its onset zone lies in the mountainous NW Highlands of mainland Scotland, with peaks up to c. 1000 m above present-day sea level (m a.s.l.). At its maximum extent, several ice-stream tributaries flowed from breaches (at c. 300 m a.s.l.) in the present-day watershed in the NW Highlands mainland out to the shelf edge, at c. 200 m below present-day sea level (Bradwell et al., 2007; Bradwell and Stoker, 2015, 2016; Krabbendam et al., 2016). MPIS likely reached its maximum extent at c. 26 – 28 ka (Chiverrell and Thomas, 2010; Clark et al., 2012; Praeg et al., 2015; Bradwell and Stoker, 2016).

Institute and Möller Ice Streams (IMIS) drain the West Antarctic Ice Sheet into Ronne Ice Shelf (Fig. 4.1). Ice surface velocities are up to 400 m a^{-1} (Rignot et al., 2011). The inferred occurrence of sediments at the bed of Institute Ice Stream has been interpreted to be associated with a smooth bed (Bingham et al., 2007; Siegert et al., 2016). The Ellsworth Trough Tributary, a tributary of Institute Ice Stream, is topographically controlled (Ross et al., 2012).

We compare MPIS with IMIS due to their relatively comparable scale. IMIS ice thickness varies between c. 50 – 3000 m (Fretwell et al., 2013). A maximum ice thickness of 750 – 1000 m has been modelled for MPIS (Hubbard et al., 2009; Kuchar et al., 2012). IMIS drain an area of 140,000 km^2 and 66,000 km^2 respectively (Bingham and Siegert, 2009), whilst MPIS drained an area of 15,000 – 20,000 km^2 (Bradwell et al., 2007; Bradwell and Stoker, 2015). Institute Ice Stream is up to 82 km wide and the fast flowing section of the main trunk is 100 km long (Scambos and others, 2004). MPIS was 40-50 km wide and 200 km long in total (Bradwell and Stoker, 2015). MPIS had a discharge flux of 12-20 Gt a^{-1} (Bradwell and Stoker, 2015) compared to 21.6 and 6.4 Gt a^{-1} for Institute and Möller Ice Streams respectively (Joughin and MacAyeal, 2005).

For contemporary ice streams in Antarctica, the data used were RES transects with an along track resolution of 10 m, and a grid spacing of 30 x 10 km (Rippin et al., 2014).

Data were acquired in the 2010/11 austral summer using the Polarimetric Airborne Survey Instrument (PASIN) with a frequency of 150 MHz (Ross et al., 2012). PASIN has retrieved bed-echoes through 4200 m thick ice (Vaughan et al., 2006). Crossover analysis gave RMS differences of 18.29 m for ice thickness (Ross et al., 2012). The location of the data was determined using a differential GPS with a horizontal accuracy of approximately 5 cm. The reflections returned from the ice-stream bed were processed semi-automatically. The ice thickness (calculated every ∼10 m) was subtracted from ice surface elevations to calculate the bed elevations (Ross et al., 2014). For more detail on acquisition and processing of the RES data see Rippin et al. (2014); Ross et al. (2012, 2014). This dataset was used by Rippin et al. (2014) to calculate bed roughness using both FFT analysis and SD.

Two high resolution datasets were used to calculate bed roughness of the Minch Palaeo-Ice Stream. For the onshore area, the NEXTMap DTM with a 5 m horizontal resolution and a 1 m vertical resolution, was used (Bradwell, 2013). NEXTMap DTM tiles were downloaded from the Centre for Environmental Data Analysis (CEDA) Archive (Intermap Technologies, 2009). For the offshore area, Bathymetric Multi Beam Echosounder Survey data (MBES) were used. The MBES data subset has a resolution of 4 m and encompasses the Little Minch and the southern area of the Minch (Fig. 4.1). The surveys around NW Scotland were undertaken by the Maritime & Coastguard Agency (MCA) between 2006 and 2012. For more detail on acquisition and processing of MBES data see Bradwell and Stoker (2015) or the Reports of Survey, which can be requested from MCA, the UK Hydrographic Office, the British Geological Survey or the Natural Environment Research Council. MPIS is characterised by numerous elongate landforms that show a higher elongation ratio than those in adjacent areas (Bradwell, Stoker and Krabbendam, 2008). Onshore, the bed of the palaeo-ice stream is dominated by bedrock (i.e. hard-bed) landforms (Krabbendam and Bradwell, 2010; Clark et al., 2018) including bedrock megagrooves, crag and tails, whalebacks and roches moutonnées (partly within a cnoc-and-lochan landscape, especially characteristic of Scotland's northwest region, Assynt), with few soft-sediment covered landforms (e.g. Bradwell et al., 2007; Bradwell, Stoker and Krabbendam, 2008; Krabbendam and Glasser, 2011; Bradwell, 2013). In the Minch and further offshore on the Hebrides Shelf, the bed of the palaeo-ice stream comprises more soft-sediment landforms, such as drumlinoid features, although streamlined bedrock, crag-and-tail features, and megagrooves are also present, particularly in the inner Minch (Bradwell and Stoker, 2015, 2016; Ballantyne and Small, 2018).

Overdeepened basins occur, in particular close to the present-day coast, which is in part characterised by a fjord system (Bradwell and Stoker, 2016; Bradwell et al., 2016). Increases in ice velocity are inferred from changes to landform elongation ratios located on the central Minch inner shelf (East Shiant Bank), which Bradwell and Stoker (2015) suggested is caused by the bed substrate changing from rough bedrock to smooth sediment.

4.2.2 Methods

Bed roughness along RES tracks in the Antarctic Ice Sheet and Greenland Ice Sheet has predominantly been quantified using either Fast Fourier Transform (FFT) analysis (e.g. Bingham and Siegert, 2009; Rippin, 2013; Rippin et al., 2014), or standard deviation (SD) of bed elevations (e.g. Layberry and Bamber, 2001; Rippin et al., 2014). FFT analysis transforms bed elevations into wavelength spectra (Gudlaugsson et al., 2013), producing a power spectrum (Bingham and Siegert, 2009), which is a measure of the intensity (power) of different wavelength obstacles along a transect. SD is a measure of variation in amplitude. Applied to elevation data, a higher standard deviation implies a greater spread between the high and low elevations, and thus a rougher bed. Both methods were used on MPIS and IMIS datasets to provide a comparison.

Both roughness methods were applied to a 2D dataset from a deglaciated terrain, MPIS, and were compared with a 1D dataset from a glaciated terrain, IMIS. We constructed an 'artificial' grid of transects spaced 30 x 10 km apart over the high resolution NEXTMap DTM and MBES bathymetry of the deglaciated MPIS to mimic a gridded RES survey over the glaciated IMIS (Fig. 4.1). The transect spacing replicates the spacing and resolution of RES transects used by Rippin et al. (2014) on IMIS. Points were constructed every 10 m along all transects, and the x, y and z coordinates were extracted from NEXTMap DTM and MBES bathymetry. Before bed roughness can be calculated using SD or FFT analysis, the elevation data have to be detrended to remove large wavelengths caused by mountains and valleys, which would otherwise dominate roughness measurements (Shepard et al., 2001; Smith, 2014). We are interested in roughness obstacles at a smaller scale than this i.e. those which affect drag. The elevation data for each transect were detrended in R using the difference function (where difference = 2). This detrending method does not require a moving window, which removes one of many variables that affect the final bed-roughness results (Prescott, 2013; Smith, 2014). Standard deviation was then calculated along transects

using a moving window size of 320 m (32 points) following previous studies (e.g. Taylor et al., 2004; Li et al., 2010). Where transects crossed lakes and coast, bed roughness values were removed to prevent bias towards smooth surfaces(Gudlaugsson et al., 2013) using the Ordnance Survey Meridian 2 lake regions shapefile (Survey, 2017). FFT analysis requires continuous along-track data. For gaps of >100 m long (10 points), the transects were 'cut' (Rippin et al., 2014). Note that, in the onshore DTM analysis, a lake functions like a data gap. FFT analysis was not calculated across these gaps. Following previous studies (e.g. Taylor et al., 2004; Bingham and Siegert, 2009; Rippin et al., 2014), FFT analysis was calculated along transects using a window of 2^N points, where N = 5 giving a window length of 320 m (32 points). The total roughness parameter was then defined by calculating the integral of the power spectra for every window. Roughness at all scales up to the length of the window was integrated.

The bed-roughness calculations from both methods were then interpolated using the Topo to Raster tool in ArcMap, with a 1 km output cell size. The interpolated values were smoothed with a 10 km radius circle and a buffer of 2.5 km was applied either side of the transects. This allowed us to replicate the type of processed results that would be extracted from a RES survey. The same method as described above was applied to the RES transects for IMIS. The difference in bed roughness values was calculated for MPIS and IMIS at locations where transects crossed. Most SD results presented here are not normalised, but shown as absolute values in metres. However, when presented alongside the FFT results, the SD results were normalised, to enable a comparison. Following the post processing stages of interpolation, buffering, and smoothing, the data were normalised using a linear transformation. The results from both sites and both methods were re-scaled so that values range between 0 and 1.

A grid of transects spaced 2 x 2 km apart was also created for the Ullapool megagroove area (Fig. 4.1), a well-characterised part of the onset zone of MPIS (Bradwell, Stoker and Krabbendam, 2008). This finer grid was used to measure roughness in between the gaps created when widely spaced RES grids are used underneath contemporary ice sheets. A 2 x 2 km grid allowed interpolation between transects, and was aligned approximately parallel and orthogonal to palaeo-ice flow. Roughness was calculated using the same method as the larger grid, but the interpolation resolution was 200 m, and the values were smoothed using a 2 km radius circle. Roughness was also calculated for transects parallel and orthogonal to

palaeo-ice flow, allowing differences in bed roughness between palaeo-ice flow directions to be calculated. Within the area of the 2 x 2 km grid, (Bradwell, Stoker and Krabbendam, 2008) identified a bedform continuum, which equates to an erosional transition. This transition was interpreted as a thermal boundary by Bradwell, Stoker and Krabbendam (2008), and bed roughness values from the inferred areas of warm and cold bed conditions were extracted from the smoothed interpolation, to quantify differences in roughness between these areas.

Finally, bed roughness was calculated over the entire onshore study area of the MPIS using a 2D approach. The 2D approach uses standard deviation to calculate bed roughness across surfaces, rather than along 1D transects. The 2D method allows the full coverage and resolution of the NEXTMap data to be analysed, so that bed roughness can be calculated for the gaps in between 1D transects. For every pixel, a circular window with a 320 m diameter was used for detrending and calculating bed roughness to match the results from the 1D approach. The NEXTMap DTM was detrended by subtracting a smoothed bed from the original terrain. Standard deviation was calculated from the detrended raster for each 320 m circular window. We present both unsmoothed and smoothed 2D data, to enable comparison with the smoothed 1D results. Unsmoothed 2D data allow us to look at the roughness calculations in more detail, whereas smoothed data show broader trends. Bed roughness was also calculated using the same approach above (except with a smaller 100 m window size) for all north-south pixels and all east-west pixels to assess directionality.

4.3 Results

The 1D roughness results calculated using SD for IMIS (Fig. 4.2c) are, as expected, similar to those found by Rippin and others (2014) using FFT analysis (Fig. 4.2b). The locations of high and low values are similar but the relative magnitude of roughness trends appears reduced for SD (Fig. 4.2). Table 4.1 shows a slightly smaller range in roughness values for IMIS SD and similar means for both methods. It should be noted that SD roughness results are reported in the text as real values, but are normalised in Fig. 4.2 and Table 4.1 to enable comparison with FFT analysis. IMIS SD roughness values vary between c. 0.5 – 4 m. Lower roughness values of 0.5 – 1 m are generally located underneath the ice-stream tributaries, whereas higher roughness values (2.5 – 3.8 m) are associated with the Pirrit Hills and Nash Hills in the intertributary areas. The Ellsworth Tributary, a tributary of Institute

Ice Stream, has low bed roughness values except where it joins the main trunk (2.7 m). Similarly, Area D, a tributary of Möller Ice Stream, has mostly low roughness values, but with some higher bed roughness values (up to 2.8 m). Areas B and C, tributaries of Institute Ice Stream, generally have rougher beds than Areas A and D (up to 3.4 m). Parts of the inter-tributary area, however, have low roughness values (1 m). Thus, although there is a broad correlation between roughness and ice velocity, there are significant exceptions.

The SD bed roughness values for MPIS have a lower range (0 – 1 m) compared to IMIS (0.5 – 4 m). This also applies to the normalised SD values. The FFT bed roughness values for MPIS also have a lower range compared to IMIS (Table 4.1). The SD bed roughness values are lower (0.1 – 0.5 m) in the trunk of MPIS compared to the onset zones onshore (Fig. 4.2c). Most of the bed in the Minch is sediment covered, but some bedrock has been mapped (Fyfe and others, 1993; Bradwell and Stoker, 2015), which is slightly rougher (0.2 m) than the sediment dominated areas (0.1 m). The bedrock in the Minch is significantly smoother than the onshore bedrock of the cnoc-and-lochan landscape (Fig. 4.2c, d) in the onset zone (by up to 0.7 m). The 30 x 10 km grid is too low in resolution to give a detailed analysis of the transition between rough bedrock and smooth sediment in the Minch (Fig. 4.2). Within the Minch (bathymetry data), the flowlines coincide with smooth values (0.1 m) (Fig. 4.2). This pattern contrasts with most of the flowlines in MPIS onset zones (Fig. 4.2), where values are rougher (0.2 – 0.9 m). This compares to higher bed roughness values from IMIS, which vary from 1 – 2.9 m and 1 – 3.8 m in the tributary and intertributary areas respectively (Fig. 4.2). The highest roughness values on the mainland of NW Scotland are found in the southern area (the Aird) of the 30 x 10 km grid (1 m) (Fig. 4.2), whilst the lowest values are concentrated in the centre and east (0.2 m) (Fig. 4.2). The bed roughness results from SD and FFT analysis show similar trends in high and low values for MPIS (Fig. 4.2c, d). For example, over the Ullapool megagrooves, both methods produce bed roughness values of 0.1 (normalised values). However, the results calculated using SD are higher overall than those calculated from FFT analysis (higher mean in Table 4.1). This difference is largest over the cnoc-and-lochan area, where the SD results are up to 3.5 times higher. SD bed roughness results show slightly more variation than those calculated from FFT (Fig. 4.2c, d). For example, bed roughness values from the top east-west transect (Fig. 4.2c, d) are 0.01 when calculated using FFT analysis, but vary between 0.06 and 0.1 when calculated using SD.

The bed roughness trends from the 30 x 10 km grid (Fig. 4.3c) match those calculated from the smoothed 2D approach (Fig. 4.3b) relatively well, particularly, the high roughness values over the cnoc-and-lochan landscape (3 m compared to 1 m), and low roughness values over the central and NE areas. The unsmoothed 2D results (Fig. 4.3a) give a much more detailed picture of bed roughness. Within the cnoc-and-lochan terrain there are significant local variations in roughness that are not apparent in the smoothed 2D data (Fig. 4.3a, b), whilst the bedrock of the East Shiant Bank is visible in the unsmoothed roughness data but not the smoothed (Fig. 4.3a, b).

The 2 x 2 km grid records higher roughness over the Ullapool megagrooves compared to the larger grid (0.3 m compared to 0.7 m) (Figs. 4.4 and 4.2 respectively). The distribution of bed roughness values between the areas interpreted by Bradwell and others (2008b) as cold and warm bed conditions (Fig. 4.4a) over the Ullapool megagrooves show a clear difference. The area with a cold bed has predominantly lower bed roughness values, with a mean of 0.2 m, compared to the area where the bed was warm, with mean of 0.4 m (Fig. 4.5). There is a clear transition to higher bed roughness values over the megagrooves compared to the surrounding areas (Fig. 4.4a).

4.4 Discussion

Our results show that similar patterns of bed roughness are found in both contemporary and palaeo-ice stream settings, using the same transect spacing and along-transect resolution (Fig. 4.2). High and low roughness values can generally be found in areas of fast ice flow. This suggests that bed roughness is not always a controlling factor on the location of ice streaming. Overall, the bed roughness results for IMIS are higher than MPIS. One reason for this difference could be the vertical resolution of RES data, which is lower compared to DTM data (5 m vs. 1 m respectively). Postglacial sedimentation could be one of the causes of this. For example, a thin layer (0.1 – 10 m) of postglacial sediment deposition occurs in the Minch (Fyfe et al., 1993; **?**), which will reduce the amplitude of small scale glacial features. Yet this is unlikely to be the case onshore, where predominantly exposed bedrock with more localised areas of postglacial sediment prevails (Krabbendam and Bradwell, 2010). Conversely, topographic profiles collected using RES are an average of the radar trace (King et al., 2016), which could cause such data to be slightly smoothed in comparison to data

from visible surfaces e.g. DTMs. Without being able to see the entire bed of IMIS it is difficult to provide a definitive answer. We suggest that the reason for higher bed roughness in IMIS could be due to the difference in elevation range between the two locations. MPIS has an elevation range of 1493 m, whilst IMIS has an elevation range of 3582 m (Fretwell et al., 2013).

4.4.1 SD vs. FFT analysis methods

Our comparison between SD and FFT analysis at the 1D scale for MPIS and IMIS showed similar broad trends of bed roughness, but there were differences (Fig. 4.2). For MPIS, the cnoc-and-lochan landscape appears rougher in the SD than in FFT (Fig. 4.2). Cnoc-and-lochan landscapes typically contain abundant lakes, which appear on a DTM as a flat surface. These are removed from the dataset to avoid bias towards a smooth surface. For FFT analysis to be carried out, transects measuring ¡320 m between lakes are also removed from the data, causing data gaps. Where there are multiple lakes along a transect with ¡320 m between them, the SD method measures a high roughness value. FFT analysis cannot capture this variation in terrain. Some transects that are not impacted by lakes also have higher bed roughness values calculated from SD compared to FFT analysis. Both methods essentially measure the amplitude of the bed obstacles (Rippin et al., 2014), but FFT analysis measures the frequency of vertical undulations (Bingham and Siegert, 2009). We suggest that the FFT analysis is measuring similar frequencies of elevation change. The results from the SD method for the same landscape are rougher than FFT analysis, because it is measuring large amplitude changes between the numerous hills and lakes. Furthermore, FFT analysis (total roughness parameter) integrates roughness at all scales up to the window size, whereas SD is calculated for the window size only. This will cause higher roughness results measured using SD because the values are calculated over a larger horizontal length-scale (Shepard et al., 2001). Both methods have advantages and disadvantages in their application. FFT analysis emphasises roughness frequency whilst SD provides a more intuitive measure of roughness scales.

4.4.2 Transect spacing vs. complete coverage: what is missed?

Measuring bed roughness on a palaeo-ice stream allows us to assess the validity of RES transect spacing used to measure bed roughness on contemporary ice streams. The 30 x 10

km grid misses key areas of glacial landforms used to interpret MPIS ice dynamics, such as the transition from rough bedrock to smooth sediments in the bathymetry data (Fig. 4.2) (Bradwell and Stoker, 2015). For the onshore data, shifting the 30 x 10 km grid by a few km north or south would miss the Ullapool megagrooves altogether (Fig. 4.2). Entire inselbergs and mountain massifs are missed (blue boxes on Fig. 4.3): in the 2D roughness maps these areas appear as very rough and it is known these had a profound effect on local ice dynamics (Bradwell, 2005, 2013; Finlayson et al., 2011). Conversely, some areas appear rough on the 1D transect, but appear on the 2D maps as fairly smooth (red boxes on Fig. 4.3). A much more detailed picture of 2D bed roughness trends can be achieved without the smoothing employed by previous studies (Fig. 4.3a) (e.g. Rippin et al., 2014). For example, all the cnoc-and-lochan area appears rough on the smoothed 2D data, but the unsmoothed data show that some parts are smooth (Fig. 4.3a, b). The 2D method surpasses the detail that can be captured by the 1D transects, but does not allow for analysis of the bed roughness directionality (anisotropy). It is clear that exploring palaeo-ice-stream roughness is possible at much higher resolutions than for contemporary ice streams, and important insights regarding the roughness of subglacial terrain may thus be learnt from these environments (Gudlaugsson et al., 2013). A 30 x 10 km grid is too widely spaced to capture bed roughness of some landform assemblages. The question of what grid size should be used is an important one. The Ullapool megagrooves for example, cover an area of 6 x 10 km, and individual grooves are up to 4 km long (Krabbendam et al., 2016). A grid size of 2 x 2 km is arguably more suitable (Fig. 4.4). The size of glacial landforms that can be measured at DTM resolution varies largely, approximately 10-10 m^5 (Clark, 1993; Bennett and Glasser, 2009), and a grid size that can measure mega-groove bed roughness might not be appropriate for other landform assemblages. The landscape underneath ice streams has been captured in detail using RES grids with transects spaced 500 m apart (King et al., 2009, 2016; Bingham et al., 2017). Importantly, these studies only used orthogonal transects because RES can pick up multiple landform crests parallel to ice flow (King and others, 2016). Acquiring RES tracks at 500 m spacing for large areas is very challenging, but future surveys could be focused on locations where rough, streamlined topography is thought to be present (Bingham et al., 2017), or areas that could cause a future sea level rise through rapid retreat e.g. Thwaites Glacier (Joughin et al., 2014; DeConto and Pollard, 2016). Drones or Unmanned Aerial Vehicles (UAVs) have the potential to make RES data collection with

small track spacing more viable over large areas (e.g. Leuschen et al., 2014).

4.4.3 The importance of transect orientation

The locations of high roughness values over MPIS, measured by both SD and FFT analysis along transects, do not always reflect qualitative roughness seen in the DTM and bathymetry data. This problem has been investigated previously for bed roughness (e.g. Gudlaugsson et al., 2013; Rippin et al., 2014) and englacial layers (e.g. Ng and Conway, 2004; Bingham et al., 2015), and transect orientation was shown to be important. To explore the influence of transect orientation on bed roughness we calculated bed roughness separately for north-south and east-west transects for both MPIS and IMIS (Fig. 4.6). Where transects cross each other, the difference in roughness was calculated (Fig. 4.6c, f). This was also done for transects on a pixel scale spacing for MPIS (Fig. 4.7). The difference in roughness of cross-cutting transects can be seen as a measure of directionality (anisotropy). In MPIS some areas show a difference between east-west and north-south transects, suggesting significant anisotropy. The north-south transect along the West coast has higher roughness values (Fig. 4.6), notably for the lower part of the cnoc-and-lochan landscape on the exposed gneiss bedrock in the Assynt area (Krabbendam and Bradwell, 2014) and the edge of Ullapool megagrooves area (Bradwell, Stoker and Krabbendam, 2008). This same pattern is also apparent in more detail at the pixel scale (Fig. 4.7). In the Minch the east-west pixels are rougher over the exposed bedrock (East Shiant Bank) (Fig. 4.7c), which is not shown in Fig. 4.6 because of the wide transect spacing. In both cases, the rougher transects are orthogonal to palaeo-ice flow, and support previous observations of bedrock smoothing by streaming ice (Bradwell and Stoker, 2015; Ballantyne and Small, 2018). The east-west transects crossing the Aird are rougher than the north-south transects (Fig. 4.6). Closer inspection of the NEXTMap DTM reveals these rough values are located where the east-west transects cross deeply incised river valleys. Post-glacial erosion or sediment deposition can impact on palaeo-ice-stream bed roughness values. In IMIS east-west transects have higher roughness values predominantly in the tributaries labelled C and D, whilst the north-south transects have higher roughness values under tributaries A and B (Fig. 4.6). Although the direction of these transects is not related to ice flow as analysed by Rippin et al. (2014), it shows that the direction of transects influences the bed roughness results for both contemporary and palaeo-ice streams. For contemporary ice streams it has been shown that the transect orientation

in relation to ice flow can bias interpretation (e.g. Rippin et al., 2014; Bingham et al., 2015, 2017). Parallel to ice flow, the data tend to show smooth beds (Lindbäck and Pettersson, 2015) and undisrupted ice layering (Bingham and others, 2015), whereas data orthogonal to ice flow can show rough topography (Rippin et al., 2014; Bingham et al., 2017), which can be caused by streamlined features, e.g. megagrooves or mega-scale glacial lineations (MSGLs). These landforms have strong anisotropy (Spagnolo et al., 2017). The advantage of looking at palaeo-ice-stream beds compared to contemporary ice-stream beds is that the landforms can be observed directly. The strong anisotropy of the Ullapool megagrooves, already known from traditional geomorphological studies (Bradwell et al., 2007; Krabbendam et al., 2016), is well captured by the 2 x 2 km grid results (Fig. 4.4b, c, d). Flow parallel transects are smoother (0.4 m), than the orthogonal transects (1 m). The roughness orthogonal to palaeo-ice flow is up to 2 x higher than parallel palaeo-ice flow. The same pattern is shown in Fig. 4.7. The formation of hard-bed megagrooves smooths the bed along ice-flow, but may lead to increased roughness orthogonal to ice flow, for instance by lateral plucking (Krabbendam and Glasser, 2011; Krabbendam et al., 2016).

4.4.4 Roughness as a control on ice-stream location

The bed-roughness measurements extracted across MPIS using the 1D and 2D SD methods show that high roughness values occur in some areas interpreted as having hosted fast palaeo-ice flow (see MPIS flow paths, Fig. 4.2, 4.3). A rough bed underneath fast flowing ice is not typically assumed and is at odds with some previous findings from contemporary ice streams that show low roughness values i.e. a smooth bed, beneath fast flowing ice (e.g. Siegert et al., 2004; Bingham et al., 2007; Rippin et al., 2011). Warm basal ice will be present in fast flowing areas whilst ice underneath slow flowing regions is likely to be frozen at the bed (Benn and Evans, 2010). Bradwell and others (2008b) interpreted areas of cold and warm basal conditions for the Ullapool megagrooves and adjacent areas (Fig. 4.6). Bed roughness values are lower for the areas with cold basal conditions compared to the areas with warm basal conditions (Fig. 4.5). Bradwell, Stoker and Krabbendam (2008) identified a marked change in the bedform continuum between cold-based and warm-based zones and suggested this was due to increased ice velocity. Thus, we suggest that areas of inferred slow palaeo-ice flow can be associated with a smooth bed. Higher erosion rates under the fast flowing palaeo-ice have produced larger, elongated bedforms, which have left behind

a rougher bed overall (particularly orthogonal to palaeo-ice flow). It must be noted that this is for an area of exposed bedrock, with no sediment cover. Krabbendam (2016) argued that if there is a thick layer of temperate basal ice, fast flow can occur on a rough hard bed. In this setting, less basal drag occurs and thick temperate basal ice is maintained by frictional heating, which produces high basal melt rates. The Laxfjord Palaeo-Ice Stream is a tributary to MPIS, identified by Bradwell (2013) (Fig. 4.1). Erosional landforms such as whalebacks and roches moutonnées were mapped on the bed of the Laxfjord Palaeo-Ice Stream, in the cnoc-and-lochan landscape (Bradwell, 2013). These landforms are indicative of warm based ice with meltwater present at the bed (Bennett and Glasser, 2009; Benn and Evans, 2010; Roberts et al., 2013). Bradwell (2013) suggested that topographic funnelling of ice was the driver of palaeo-fast ice flow in the Loch Laxford area. MPIS has a dendritic network of overdeepened valleys that channelled ice into a main trough, and is thought to be topographically controlled (Bradwell and Stoker, 2015). It thus appears that rough beds are possible in topographically steered ice streams, and that topographic steering may 'trump' roughness as a control on ice-stream location (see also Winsborrow et al., 2010). Recent insights from contemporary ice streams support our results from MPIS. Schroeder et al. (2014) demonstrated that the lower trunk of the fast flowing Thwaites Glacier is underlain by rough bedrock. Jordan et al. (2017) found that warm-based areas, predicted by MacGregor and others (2016), underneath the northern part of the Greenland Ice Sheet, are relatively rough compared to predicted cold-based areas. A tributary to Institute Ice Stream, Ellsworth Tributary (Fig. 4.2), is topographically controlled (Ross et al., 2012), and Siegert et al. (2016)suggest that this explains why fast flow occurs over rough areas of the bed. The suggested reasons for a rough bed underneath the Ellsworth Tributary are an absence of sediment deposition or excavation of pre-existing sediment (Siegert et al., 2016). In MPIS in Scotland and surrounding areas, there is a strong geological control on roughness (Bradwell, 2013; Krabbendam and Bradwell, 2014; Krabbendam et al., 2016). This could be the underlying cause for the rough bed underneath the Ellsworth Tributary. Our results suggest that the bed roughness of a palaeo-ice stream and a contemporary ice stream are comparable, and support the notion that palaeo-ice streams can be used as analogues for contemporary ice streams (Bradwell et al., 2007; Rinterknecht et al., 2014; Bradwell and Stoker, 2015).

4.4.5 Interpreting sediment cover from roughness calculations

Bed roughness values from IMIS were smoother underneath the ice-stream tributaries compared to the intertributary areas (Fig. 4.2). Smooth beds beneath ice streams are typically explained by the inferred presence of soft sediment Siegert et al. (2005); Li et al. (2010); Rippin (2013). However, the Ullapool megagrooves (exposed bedrock features, without sediment cover) Bradwell, Stoker and Krabbendam (2008), are smooth, particularly parallel to palaeo-ice flow (Fig. 4.4 and 4.7). Equally the East Shiant Bank includes bedrock, but is barely rougher than the adjacent, sediment-covered parts of the MPIS (Fig. 4.2). Smooth areas of below present-day ice streams may therefore not necessarily be sediment covered.

4.4.6 Recommendations for future studies

The direction of transects influences the bed roughness results on palaeo- and contemporary ice streams. We suggest that future acquisition of RES tracks over contemporary ice streams are orientated parallel and orthogonal to flow where possible. Fine spacing of RES tracks i.e. 500 m orthogonal to ice flow only, could be focussed on locations where the bed is thought to be rough underneath fast flowing ice as this has been shown to have an impact on ice flow Bingham et al. (2017). Further analysis of the relationship between grid size, bed roughness, and landforms assemblages is needed on palaeo-ice streams to give recommendations on the appropriate grid sizes. For palaeo-ice streams, including MPIS, bed roughness could be explored parallel and orthogonal to inferred flow lines (e.g. Gudlaugsson et al., 2013) to increase our understanding of the relationship between bed roughness and ice flow direction. The bed roughness of palaeo-ice streams dominated by sediment landforms (soft bed), could be compared with contemporary ice streams that are thought to have similar bed properties. Palaeo-ice streams provide an opportunity to improve our understanding of the relationship between landforms and bed roughness, and in turn, ice dynamics. The difference in what the SD and FFT analysis methods are measuring should be taken into account when these methods are applied in future studies. The effect of post-glacial erosion or sediment deposition on palaeo-ice-stream bed roughness values should also be taken into consideration.

4.5 Conclusion

We compared the bed roughness of the deglaciated Minch Palaeo-Ice Stream (MPIS) in Scotland, to the contemporary Institute and Möller Ice Streams (IMIS) in West Antarctica, using two analysis methods. We also investigated whether different grid spacing and orientation impact bed roughness measurements. The 30 x 10 km grid, which matches a previous RES transect distribution used for bed roughness studies over a large area on contemporary ice streams, is too coarse to confidently capture all the different landforms on a typical ice sheet bed. Using a finer 2 x 2 km grid we were able to show that transects parallel to palaeo-ice flow were smoother compared to orthogonal transects over the Ullapool megagrooves in the onset zone of MPIS. A clear difference in bed roughness values was also shown for pixel scale transects for MPIS, demonstrating how transect orientation influences roughness results. RES transects should be closer together in future studies and orientated in relation to ice flow where possible. This would allow for more representative bed roughness measurements because of the importance of flow direction on roughness patterns. SD produced similar results to FFT analysis for the majority of the data, but there were some differences which should be taken into account by future studies. Unsmoothed 2D roughness data for MPIS showed detail that is missed when 2D data are smoothed. Most MPIS flow paths in the onshore onset zones coincided with high bed roughness values, whilst lower roughness values were associated with sediment cover in the main ice stream trunk. Yet, smooth areas of the bed beneath MPIS occurred over bedrock as well as the sediment covered areas. Low bed roughness beneath contemporary ice streams is not a reliable indicator of the presence of sediment. In this study we found that fast palaeo-ice flow has occurred over areas with high bed roughness values. Previous research often assumed that fast flowing ice streams are generally related to areas of low roughness. High and low bed roughness values were also found in the IMIS tributaries, which supports the notion that palaeo- and contemporary ice streams are comparable in terms of bed roughness. The diverse topography underneath ice streams needs to be measured in more detail to increase our understanding on what controls ice stream location. Palaeo-ice streams provide useful analogues for bed roughness underneath contemporary ice streams, and both can be used to inform the other.

Chapter 5

Do glacial landforms have bed-roughness signatures?

5.1 Introduction

Investigating palaeo-glacial landsystems has the potential to provide insights into bed roughness and other basal conditions that cannot be captured from underneath contemporary glaciers and ice sheets (Bingham and Siegert, 2009). Entire beds of palaeo-ice sheets can be observed using high resolution DEMs (e.g. Dowling et al., 2015; Margold et al., 2015), whereas the beds of contemporary-ice sheets cannot be directly observed due to the kilometres of ice covering them (Fretwell et al., 2013). The opportunity provided by palaeo-glacial landsystems to learn more about subglacial bed roughness has yet to be realised fully by the glacial community, with few studies undertaken to date (e.g. Gudlaugsson et al., 2013; Lindbäck and Pettersson, 2015; Chapter 4 of this thesis). These studies have focused on measuring roughness over the entire palaeo-ice-stream bed. However, DEM analyses from palaeo-glacial landsystems show that ice-stream beds are complex, and contain diverse landforms (Fig. 5.1), ranging from stubby drumlins to MSGLs, and from regions of sediment-cover to a hard bed (Benn and Evans, 2010; Krabbendam et al., 2016). Within each landform type there are often further classifications to describe differences; for example, drumlins can vary from spindle to parabolic (Fig. 5.2). As glaciologists can see the whole bed of palaeo-ice streams, it allows measurement and description of the bed using many metrics (including bed roughness), and gives greater detail than can be achieved for contemporary-ice streambeds. Prescott (2013) showed that roughness parameters differed between two palaeo-glacial

regions, e.g., the Tweed Ice Stream (MSGL) and the Cheviots, northern England (upland non-glacially modified). Roughness was calculated for a 10 x 10 km test area rather than using a moving window returning a single value for the entire palaeo ice-stream bed, but spatial patterns of roughness over glacial landforms were not explored.

The question then arises: do different fields or sets of glacial landforms (e.g. a drumlin field or a megagroove field) have ranges of bed-roughness values that are unique to them? Using palaeo-glacial landsystems, we can test whether homogeneous areas of landforms have unique bed-roughness signatures (Bingham and Siegert, 2009; Stokes, 2018). If glacial landform sets have a bed-roughness signature, it could be used to suggest where landforms exist underneath contemporary-ice sheets (Stokes, 2018).

Glacial landforms have been identified underneath small areas of contemporary-ice sheets using high-resolution radio echo sounding (RES; e.g. King et al., 2007; Smith et al., 2007; King et al., 2009; Jezek et al., 2011; Schroeder et al., 2014; Bingham et al., 2017). Smith et al. (2007) identified the development of a drumlin on the Rutford Ice Stream bed, West Antarctica. King et al. (2007) were the first to show that a link existed between ice velocities and landform elongation underneath contemporary-ice streams. They observed a drumlinised ribbed moraine underneath ice moving at a rate of 72 m a^{-1} and drumlins underneath ice moving at a rate of 125 m a^{-1} (King et al., 2007). King et al. (2009) also identified MSGLs beneath an area (∼20 x 20 km) of Rutford Ice Stream, West Antarctica (Fig. 5.3). Similarly, elongate erosional features were identified underneath an area (5x20 km) on Jakobshavn Isbrae, Greenland Ice Sheet by Jezek et al. (2011). Furthermore, Bingham et al. (2017) used high resolution RES to map nine multi-km^2 areas of the bed of Pine Island Glacier, West Antarctica, revealing a varied topography that included MSGLs (Fig. 5.3). However, there are only a handful of high resolution studies beneath small areas of contemporary-ice-stream beds, which ultimately gives glaciologists just a glimpse of landform location and distribution. It is currently not feasible to undertake high resolution studies across the whole area of a contemporary-ice stream.

If subglacial landforms have specific bed-roughness signatures, then it might be possible to use low-resolution RES to infer that particular landforms exist underneath contemporary-ice streams. This would provide more knowledge about contemporary-ice-stream beds, such as the link between ice speed and types of landforms (e.g. King et al., 2007). It could in turn improve the reconstruction of palaeo-ice streams by using the known ice-flow regime that is

above specific contemporary-ice-stream landforms.

The approach to this chapter is informed by the results of chapters 3 and 4. It was shown in chapter 4 that roughness measurements of some transects orthogonal and parallel to ice flow can differ significantly. Thus in this chapter, roughness measurements are made both parallel and orthogonal to palaeo-ice flow. In chapter 4 it was shown that a finer transect spacing provides more information about spatial patterns of bed roughness, and that different transect spacing captured different element of roughness pattern. However, a 2x2 km transect grid spacing used over the Ullapool megagrooves in chapter 4 is still relatively coarse considering some studies have used orthogonal transects spaced 500 m and 250 m apart using radar (King et al., 2007, 2009; Bingham et al., 2017). Here, grid sizes are chosen to capture this difference and to use the full resolution of NEXTMap DTM.

In chapter 3 it was shown that both detrending methods (difference and mean) were able to pick out the bed roughness of different areas of the bed. The difference detrended method measured the roughness of the bedrock more successfully due to the bedrock's steep slopes, whilst the mean detrended method was able to better measure the roughness of drumlins (chapter 3, Section 4.2.2). Therefore, the two methods are used in this chapter to see if they show differences in bed-roughness signatures. The comparison between the FFT analysis and SD methods used to calculate bed roughness in chapter 4 demonstrated that similar trends in bed roughness were produced. Here, the SD method is used because it can measure areas in between closely spaced lakes on a cnoc and lochan terrain (Section 4.4.1) and does not require re-sampling or interpolation of data along transects that the FFT analysis needs (Bingham and Siegert, 2009; Rippin et al., 2014; Cooper et al., 2019). Furthermore, the SD method provides a result with units (quantifies bed roughness in metres) which is a more "physically-intuitive metric" (Cooper et al., 2019, p.6). The window size used to calculate bed roughness in chapter 3 had an impact on roughness results. A window of > 500 m picked out landforms but also bedrock troughs, and it could not distinguish between bedrock and drumlins as the larger window sizes merge individual features (chapter 3, Section 4.2.1). A window size between 100 m and 300 m was able to capture individual landforms. Glacial landforms vary in size from micro (0.01 m) to macro (100 km) (linear dimensions) (Bennett and Glasser, 2009). Different window sizes may be able to capture bed-roughness signatures of glacial landforms types due to this size variation of landforms and are used in this chapter.

5.2 Aims and objectives

The overall aim for this chapter is to establish whether different sets of glacial landforms have specific, characteristic bed-roughness signatures. To achieve this, several objectives are identified.

1. To identify type sites of glacial landforms (homogeneous) across the UK from the NEXTMap DTM. Homogeneous glacial landforms refers to an area where a single type of glacial landform predominates, e.g., drumlin swarms. These sites will include examples of drumlins, megagrooves and, cnoc and lochan landsystems.

2. To identify sites of mixed glacial landforms (heterogeneous) such as glaciated uplands and lowlands. Heterogeneous glacial landforms refers to any site that has more than one type of glacial landform, for example, a combination of moraines, drumlins and MSGL. These were included to test whether a site with homogeneous landforms has a distinct bed-roughness signature when compared to a site with heterogeneous landforms.

3. To calculate bed roughness for the sites chosen in objectives 1 and 2, following the approach outlined above (Section 5.1).

4. To investigate how transect spacing and window size affect bed-roughness signatures, and establish whether there is an ideal transect spacing and window size to analyse bed-roughness signatures of glacial landforms.

5. To investigate how anisotropy of bed roughness varies between sites, and whether this metric is important in establishing bed-roughness signatures of glacial landforms.

6. To provide recommendations for future RES studies that allow bed-roughness signatures of glacial landforms to be measured under contemporary-ice streams.

5.3 Data and study sites

The NEXTMap DTM was used to extract elevation data required for bed-roughness calculations (see chapter 3, Section 3.1 for details on NEXTMap). Landform distribution was mapped using BRITICE version 2.0 shapefiles (Clark, 2017).

5.3.1 Sites

Using the literature and BRITICE version 2 (Clark et al., 2018), sites were chosen over the UK that had classical examples of homogeneous landforms i.e. similar to type sites (sites 1-4, Fig. 5.4 & Table 5.1). Individual landforms had to be large enough to be seen on NEXTMap DTM (> 5 m wide and long, and >1 m high), so landforms in the macro and meso-scale categories (Bennett and Glasser, 2009) were chosen. For areas of homogeneous landforms i.e. a drumlin field, the site needed the landforms to have one palaeo-ice-flow direction and other landform types had to be absent. In addition, two sites were chosen that had a mix of different landforms, one upland and one lowland (sites 5 & 6, Fig. 5.4 & Table 5.1).

5.3.1.1 Site 1: Ullapool megagrooves

The Ullapool megagrooves are located north of Ullapool, in Northwest Scotland (Figs. 5.4 & 5.5). These landforms were formed by fast flowing ice in the onset zone of the Minch Palaeo-Ice Stream, which reached its maximum extent between 30 and 27 ka (Ballantyne and Small, 2018). Megagrooves are erosional, macroscale landforms that are strongly anisotropic. They are described as metre-scale deep grooves in rock and can be kilometres long (Bradwell, 2005; Krabbendam et al., 2016; Newton et al., 2018). The Ullapool megagrooves are located in an area measuring 6 by 10 km (Krabbendam et al., 2016). The megagrooves have a typical length of 1000 – 2000 m, width of 50 – 120 m, depth of 10 – 20 m and elongation ratios of 6 – 25:1 (Bradwell, Stoker and Krabbendam, 2008). The underlying geology has clearly influenced the formation of these landforms as the bedrock strike is parallel to ice flow (Krabbendam and Glasser, 2011).

5.3.1.2 Site 2: Ribblesdale drumlins

The Ribblesdale drumlins are located in Ribblesdale, Yorkshire Dales (Figs. 5.4 & 5.6). To the north of site 2 is the Ribblehead viaduct, to the south is Horton in Ribblesdale, whilst the peaks of Ingleborough and Pen-y-ghent are to the east and west respectively. Drumlins are sediment and/or rock formed, smooth, mesoscale landforms, generally oval-shaped hills with the appearance of an inverted spoon (Menzies, 1979; Benn and Evans, 2010). However drumlins can vary from long and thin (spindle) to broad, asymmetrical forms (parabolic; Fig. 5.2; Benn and Evans, 2010). The Ribblesdale drumlins have been described as 'classically-

shaped' because they are half egg-shaped features, which appear as blisters superimposed on the landscape (Clark et al., 2009; Spagnolo et al., 2012). The drumlins in Ribblesdale have a length of 95 – 530 m, widths of 55 – 355 m, and elongation ratios of 1 – 4:1 (Mitchell, 1994; Clark et al., 2009). The formation of the drumlins is suggested to have occurred during deglaciation of the BIIS at 21-17.3 ka because the drumlins have a local alignment i.e. ice flow was more valley-confined (Chiverrell et al., 2016).

5.3.1.3 Site 3: Assynt cnoc and lochan

The Assynt cnoc and lochan terrain is located on the Northwest coast of Scotland, north of site 1 (Fig. 5.4 & 5.7). Cnoc and lochan terrain (also referred to as areas of areal scour) is a macroscale landscape of glacial erosion. Cnoc and lochan derives from Scottish Gaelic words cnoc, meaning 'knoll' or 'hillock' and lochan, meaning 'small lake' (Benn and Evans, 2010). These areas of exposed bedrock often have whalebacks and roches moutonnées (Bennett and Glasser, 2009), although these are generally too small to be mapped using NEXTMap DTM. The cnoc and lochan terrain in Northwest Scotland has been formed on fractured Lewisian Gneiss, which is the primary control on the landform morphology (Rea and Evans, 1996; Bennett and Glasser, 2009; Krabbendam and Bradwell, 2014). The bedrock was locally subjected to more intense glacial modification underneath a palaeo-ice stream (Bradwell, 2013) and it has been suggested that the roughness of exposed cnoc and lochan terrain can be used to constrain bed roughness of contemporary-ice sheets with gneiss at the base (Krabbendam and Bradwell, 2014). The Assynt cnoc and lochan terrain is located at the onset zone of the Minch palaeo-ice stream that was active during the Devensian glaciation (Bradwell et al., 2007).

5.3.1.4 Site 4: Tweed MSGLs

The Tweed MSGL landsystem is located north of the Cheviot Hills, close to Berwick upon Tweed (Fig. 5.4 & 5.8). MSGL are highly elongate, macroscale landforms. They are described as very elongated ridges, which are spaced parallel to each other (Clark, 1993; Spagnolo et al., 2014). The Tweed MSGLs were first noted by Clapperton (1971) as exceptionally elongated and further described by Everest et al. (2005). The Tweed MSGL are 2 – 16.5 km long and have elongation ratios of 8 – 23:1 (Everest et al., 2005; Hughes et al., 2010). The Tweed Palaeo-Ice Stream was active during the last BIIS (Devensian; Hughes et al.,

2014). The MSGLs show a clear swing in orientation. Hence, the site was split into three sections, also to avoid the River Tweed, which has visibly cut across the MSGL between the central and eastern segments of the site, and Leet Water. Splitting the site avoids roughness returns from fluvial features that are demonstrably post-glacial.

5.3.1.5 Site 5: Tyne Gap mixed lowland

Site 5 is part of the Tyne Gap Palaeo-Ice Stream (Livingstone et al., 2015), and is a lowland area that has a mix of depositional and erosional landforms (Fig. 5.4 & 5.9) (Krabbendam and Glasser, 2011). The elevation varies between 50 and 234 m above sea level (a.s.l.). The Tyne Gap Palaeo-Ice Stream formed part of the last BIIS and was topographically controlled at the LGM (Livingstone et al., 2010, 2012). Elongation ratios vary from 1 – 10: 1 (Livingstone et al., 2010, 2012), which are lower than sites 1, 4, and 5 but higher than site 2. The existence of an esker and moraines (Fig. 5.9) suggests that a retreating ice margin was present at this site during deglaciation of the BIIS Livingstone et al. (2008).

5.3.1.6 Site 6: Beinn Dearg mixed upland

Site 6 is located in the Beinn Dearg massif, Northwest Scotland, and is an upland area that has a mix of depositional and erosional landforms (Figs. 5.4 & 5.10; Finlayson et al., 2011). Half of the Beinn Dearg massif is higher than 600 m a.s.l., and the highest point in site 5 is Seana Bhraigh (927 m a.s.l.). This area comprises cirques and glacial valleys, as well as rogen moraines (Hughes et al., 2010; Finlayson et al., 2011). During the last BIIS, this site was located to the east of the Minch palaeo-ice stream onset zone (Bradwell et al., 2007; Bradwell and Stoker, 2015). A plateau icecap existed during the Younger Dryas, where ice flow was topographically constrained, with valley glaciers being fed from the ice plateau (Finlayson and Bradwell, 2007; Finlayson et al., 2011). Ice-flow directions are likely to have changed at this site during deglaciation of the BIIS and readvance during the Younger Dryas (Loch Lomond Stadial).

5.4 Methods

5.4.1 1D method

The approach to this method builds on the method used and described in chapters 3 and 4. To show the effect of transect spacing on bed-roughness results, transect grid sizes were chosen with increasing resolution, right down to the NEXTMap DTM resolution (2x2 km, 1x1 km, 500x500 m, 250x250 m and 5x5 m). The grids were placed parallel and orthogonal to ice-flow direction, with moving windows of 100 m and 1 km. Both mean and difference detrending methods were applied in the bed-roughness calculations to ascertain if these variables show differences in bed-roughness signatures.

5.4.1.1 Creation of transects

The 'Create Fishnet' tool was used in ArcMap for the initial stage in producing the transects. This outputs a grid polyline shapefile, which is orientated north to south. For each site, 5 grids were created that had spacing between the lines of 2 km, 1 km, 500 m, 250 m and 5 m. All of the grids were then rotated in ArcMap to ensure that the transects were positioned approximately parallel and orthogonal to palaeo-ice flow. Ice-flow direction was interpreted from the landform positions. This determination of ice flow is a simplification, as ice-flow direction is not necessarily in a straight line over a given distance. For example, ice flow is curved at sites 2 and 3. At site 3 this was overcome as the study area was easily split to accommodate the change in ice-flow direction. However, this was not possible in site 2 (Ribblesdale) as it would be too complex to split. Site 6 (Beinn Dearg) also has complicated flow directions. During the LGM flow direction was approximately east to west, but in the Younger Dryas a plateau icecap formed and ice flow was strongly topographically constrained. Ice-flow direction probably switched approximately north to south, but the valleys also curve. The transects were positioned approximately east to west to match the dominant flow direction during the last BIIS because this larger ice mass may have had more impact on the roughness values. Knowledge of the flow direction changes are considered in the interpretation of results. Complex flow directions also exist for contemporary-ice streams (Conway et al., 2002), so site 6 could provide interesting insight into this complexity and the decisions researchers take in the positioning of transects for contemporary-ice streams.

Once the grids had been rotated, the 'QChainage' Plugin in QGIS was used to create a

point shapefile by placing points at 5 m intervals (resolution of the NEXTMap DTM) along the grid polylines. This tool also adds a new ID column to the attribute Table, which links the points to the original line. Thus all points along one transect have the same number. This number was then used later in the process to separate the transects into individual files for bed roughness calculations. All point grids were clipped to the site outlines. Using a shape file with lake outlines, the OS Meridian 2 Lake shapefile (Ordnance Survey, 2017), the transects were clipped to remove any points that exist over a lake. This is to reduce smoothing bias caused by lakes in the bed-roughness calculations (Gudlaugsson et al., 2013). The next processing stages were done in R. The NEXTMap DTM pixel values (elevation) were added to the grid point shapefiles. Using the ID column that links each point to a transect, the grid point shapefiles were split into individual transects. This was done to enable bed roughness for parallel and orthogonal to ice-flow transects to be calculated separately.

5.4.1.2 Bed roughness calculation

bed-roughness calculations were carried out in the same way as in chapters 3 (Sections 3.2.2 & 3.2.3) and 4 (Section 4.2.2). To avoid repetition, the method is only briefly described here. All of the stages within this section were carried out using R. Both difference and mean detrending methods were applied to the elevation data before bed roughness was calculated. The transects' elevation data were detrended using the difference function (difference = 2). For the mean detrending method, the transects' elevation data were detrended using moving windows of 100 m and 1 km radius. Here, the mean was calculated for each point along a transect within the window, and subtracted from the original to leave the detrended output.

Bed roughness was calculated using standard deviation. Standard deviation was calculated along every transect using a moving window. Moving window sizes matched those used for mean detrending (100 m and 1 km). Once the bed roughness had been calculated for all transects that made up one grid size in a site, the transects were outputted as a point shapefile. Figures were then created to display the spatial variation of bed-roughness calculations at each site for all the variations. No interpolation was done for the figures and the data were displayed for each point.

Statistics were calculated in QGIS using the 'Basic Statistics for Fields' plugin for all variations of the bed-roughness calculations at each site. For example, site 1, difference

detrended, 100 m window, parallel to palaeo-ice flow, would be one variation. The minimum, maximum, mean and range of the bed-roughness values were calculated.

5.4.1.3 Directionality (anisotropy) calculation

Directionality (anisotropy) is a useful metric for interpreting bed-roughness measurements as it allows quantification of the difference between parallel ($R_{\parallel}$) and orthogonal ($R_{\perp}$) to ice-flow bed roughness (Smith, 2014). Directionality can only be calculated at the point where parallel and orthogonal transects cross. Consequently, only 1D roughness measurements (R) can be used. For transects with a spacing of 250 m - 2 km, a point shapefile was created in ArcGIS Pro for the crossover points. This is not needed for the 5 x 5 m spaced transects as all points crossover because this is resolution of NEXTMap. The crossover points shapefile was created by using the 'Select by Attributes' tool to select the X coordinates that match between parallel and orthogonal transects. This isolated the crossover points, which were then exported to a new shapefile. This was done for both the parallel transects and the orthogonal transects, creating two crossover shapefiles. The attribute tables of the two crossover shapefiles were joined. A new column in one of the crossover shapefile attribute tables was created, and called anisotropy. The anisotropy ratio (Ω) was calculated (with the 'Calculate Field' function builder) using the following equation from Smith et al. (2006):

$$\Omega = \frac{R_{\parallel} - R_{\perp}}{R_{\parallel} + R_{\perp}} \tag{5.1}$$

where Ω is closer to 1 when $R_{\parallel}$ (parallel to ice flow) is higher than $R_{\perp}$, is 0 when bed roughness is isotropic, and closer to -1 when $R_{\perp}$ (orthogonal to ice flow) is higher than $R_{\parallel}$.

5.4.2 2D method

The NEXTMap DTM (elevation data) was clipped to the extent of all the study sites. The clipped raster was then detrended using the mean detrending method. This was done with the Focal Statistics tool in ArcMap that produces a mean raster using window sizes of 100 m and 1 km i.e. two separate mean rasters were produced. The mean rasters were subtracted from the original clipped raster, creating two detrended rasters. Standard deviation was calculated using the Focal Statistics tool. This time, the detrended raster was the input, and standard deviation was calculated using a moving window. The moving window sizes

correspond to those used to detrend the data, i.e. 100 m and 1 km. Statistics (same as in Section 5.4.1.2) were calculated for the raster at each site in QGIS using the Zonal Statistics plugin, which limits the raster data included to the extent of a polygon layer. The 2D bed-roughness rasters do not have to be individually clipped to each site to calculate the statistics.

5.5 Results

At each site a large amount of data was generated. To avoid repetition, observations and patterns that are common to all sites are presented at the end of the results section (Section 5.5.8). The results that are site specific are recorded with the appropriate figures in Sections 5.5.1-5.5.7.

5.5.1 Area 1: Ullapool megagrooves

Figs. 5.11-5.15 show that megagrooves are rougher orthogonal to palaeo-ice-flow direction than parallel to it. This is summarised in Table 5.2 for the mean detrended results (see mean column). Table 5.3 shows that there is no clear difference between the flow direction roughness values for the difference detrended data. The anisotropy values also show that the majority of the bed-roughness values are higher orthogonal to palaeo-ice-flow direction (Figs. 5.17 & 5.18), with overall mean anisotropy between -0.2 and -0.4 (Table 5.4). The mean and median values are either the same, or the orthogonal to palaeo-ice-flow bed-roughness values are higher than parallel values (Table 5.2). The deeper megagrooves are rougher orthogonally (up to 6 m) than the shallower ones (up to 3 m). This difference is best seen in the mean detrended, pixel-scale, orthogonal data (black boxes in Fig. 5.15h) but is also picked up where orthogonal transects cross from lower resolution data, e.g., black boxes in Fig. 5.14h. These trends are also shown in the 2D data for the 100 m window size (Fig. 5.16b) but are lost in the 1 km window data (Fig. 5.15f & Fig. 5.16a). Bed-roughness values derived from difference detrended data at the pixel-scale, parallel to palaeo-ice flow (Fig. 5.15a, c), pick out the pattern of megagrooves more strongly compared to the mean detrended data (Fig. 5.15e, g). Parts of the pre-existing geological faults, likely gouged out to form narrow topographic valleys by subglacial meltwater, that cut across the megagrooves (Fig. 5.5a) are picked out by the pixel-scale data, orientated parallel to palaeo-ice flow (Fig. 5.15c & g) and

2D data calculated using a 100 m window (Fig. 5.16b), but also appear to a lesser extent in the orthogonal direction pixel-scale data (Fig. 5.15d & h). This is also shown in the pixel-scale anisotropy calculations calculated using a 100 m window (Fig. 5.18). The geological faults have a similar range of roughness as the megagrooves, 4-6 m for the roughness values calculated using mean detrending and a 100 m window compared to 3-6 m respectively.

5.5.2 Reduction in displayed site variables

The results from site 1 show that the bed-roughness trends between the different grid sizes were relatively consistent (Figs. 5.11-5.15). These are also supported by very similar bed-roughness means (Table 5.2 & 5.3). For example, all the 1km window mean values are between 0.5 and 0.6. More variation was shown by the mean detrended results in comparison to the difference detrended results (Figs. 5.11-5.16). For example, all the 1D 1km window mean values are between 7.5 and 12.3. To avoid repetition and to make the results more accessible, the amount of variables shown for the remaining sites are reduced. Only the mean detrended results for one large grid size (1x1 km) and one fine grid size (250x250 m) are shown. The pixel-scale transects (5x5 m) are also shown for the complete picture of bed-roughness trends.

5.5.3 Site 2: Ribblesdale drumlins

Figs. 5.19 and 5.20 show that the drumlins are rougher orthogonal rather than parallel to palaeo-ice-flow direction. The same spatial pattern is shown by the anisotropy values, with higher roughness values orthogonal to palaeo-ice flow (Figs. 5.21 & 5.22). This is also demonstrated in Table 5.5 (mean column): the mean value from the 5x5 m grid with a 1 km window orthogonal is 6.8 whilst parallel is 5.7, and the mean anisotropy values of -0.1 & -0.2 (Table 5.6). However, the difference in bed-roughness values between the flow directions is not as pronounced as it is for site 1 (Section 5.5.1). The roughest values are located over small post-glacial streams and are best seen in Figs. 5.20b & d: whilst these are real results, they are not the direct result of glacial processes. Individual drumlins can be seen using the 100 m window size over the 5x5 m spaced transects and 2D data (Fig. 5.20 c & d & 5.23 b). Here, the bed-roughness values are highest on the drumlin sides compared to the crests (Fig. 5.24). High roughness values are located on the western edge of site 2 in Fig. 5.23a only. There are more high roughness values calculated using the 1 km window compared

to the 100 m window (Figs. 5.20 & 5.23). For example, the median value for the 5x5 m, orthogonal data, calculated using a 1 km window is 6.5 compared to 0.5 when using a 100 m window (Fig. 5.20b & 5.20d).

5.5.4 Site 3: Assynt cnoc and lochan

The overall roughness values for site 3 are significantly higher than for sites 1 and 2. For example, the mean orthogonal bed roughness for the 5x5 m grid size, calculated using a 1 km window is 14.1 for site 3, 6.8 for site 2 and 12.3 for site 1 (Tables 5.7, 5.5 & 5.2). The roughest locations (red areas) calculated using a 1 km window (Fig. 5.26a & b) are not picked up when using a 100 m window (Fig. 5.26c & d). These areas are located over bedrock highs with steep slopes. The roughest locations (red areas) calculated using a 100 m window are located at lake edges (Figs. 5.26c & d). In general, the cnoc and lochan has fairly low anisotropy values. Figs. 5.28 and 5.29 show that the cnoc and lochan is somewhat rougher orthogonal to palaeo-ice-flow direction rather than parallel when using the 1 km sized window. The data in Table 5.7 (mean column) show that the bed-roughness values orthogonal to palaeo-ice flow are rougher for the 1 km window data and the 100 m window data. However, the anisotropy values (Figs. 5.28 and 5.29), have a mean of -0.1 for the 1 km window values compared to 0 for the 100 m window values (Table 5.8).

5.5.5 Site 4: Tweed MSGLs

Figs. 5.30 and 5.31 show the MSGL are significantly rougher orthogonal rather than parallel to palaeo-ice-flow direction; see also Table 5.9 (mean column). It is also shown by the anisotropy data (Figs. 5.32 & 5.33) and the mean anisotropy values of -0.4 - -0.2 (Table 5.10). Mean anisotropy is higher for bed-roughness values calculated using a 1 km window (-0.4) compared to mean anisotropy of bed roughness calculated using a 100 m window (-0.2) (Table 5.10). This is also shown in the spatial distribution of anisotropy values, with the anisotropy values for the eastern most section having a higher proportion of purple dots (higher parallel to palaeo-ice-flow roughness values) for the 100 m window compared to the 1 km window (Figs. 5.32 & 5.33). The bed-roughness values for site 4 are lower compared to sites 1, 2 and 3 (see Table 5.15). For example, the mean bed roughness for all grid sizes, calculated using a 1 km window, is 6.2 for site 2 (smoothest site so far) compared to 2.5 for site 4. However, anisotropy values are similar to those from site 1 (Table 5.15). The crests

of the MSGls are shown as rough by the parallel to palaeo-ice flow, 1 km window size results (Fig. 5.30a & c, Fig. 5.31a). Individual MSGL are shown as rough by orthogonal, 100 m window, results (Figs. 5.31h & 5.32d). However, not all MSGL are rough when comparing the mapped locations to mapped bed-roughness trends (Fig. 5.8 compared to Fig. 5.31d & 5.35b). The bed roughness data parallel to palaeo-ice flow, calculated using a 100 m window, is very smooth (mean value of 0.1) (Figs. 5.30e & g, & 5.31c).

5.5.6 Site 5: Tyne Gap

Figs. 5.35 and 5.36 show that this glaciated lowland site is rougher orthogonal rather than parallel to palaeo-ice-flow direction. This can also be seen in Table 5.11 (mean column). The anisotropy values also show that site 5 is rougher orthogonal rather than parallel to palaeo-ice-flow direction, but this is not the case for roughness values derived using a 100 m window for the 250 x 250 m and 5 x 5 m spaced transects (Table 5.12). The spatial distribution of anisotropy values shows that there are more values below 0 for the roughness values derived using a 1 km window, but not for the roughness values derived using a 100 m window (Figs. 5.37 & 5.38). The bed-roughness values for site 5 are similar to those from site 4, thus these sites are the smoothest (Table 5.15). For example, the mean orthogonal bed roughness for the 5x5 m grid size, calculated using a 1 km window is 3.4 for site 4 compared to 3.3 for site 5. The roughest area (in red) shown in the 1 km window results is an area of exposed bedrock (Figs. 5.9 & 5.36a-b). This bedrock is also shown as rough (red) in the 100 m window results, as are some of the meltwater channels (Figs. 5.9 & 5.36c-d). The esker and moraines that are positioned orthogonal to palaeo-ice flow at the far east of site 5 (Fig. 5.8) are picked out as rough by the 100 m window data (Fig. 5.36c) and have >0 anisotropy value (Fig. 5.38b). The majority of the drumlins (Fig. 5.9) are not shown as rough on the 100 m window data (Figs. 5.36c-d & Fig. 5.39b). Those that are rough appear to be rock cored.

5.5.7 Site 6: Beinn Dearg

The mean bed-roughness values derived from the 100 m window are the same for 250x250 m and 5x5 m grid size, and the median values are the same for 1x1 km and 5x5 m grid sizes (Table 5.13). The mean bed-roughness values derived from the 1 km window are higher orthogonal to palaeo-ice-flow direction, e.g., 17.1 vs 16.1, but the median values are higher

parallel to palaeo-ice-flow direction, e.g., 10.5 vs 11.8 (Table 5.13). The mean anisotropy for all grid and window sizes is 0 (Table 5.14), and there is no clear spatial pattern of anisotropy in relation to the glacial landforms (Figs. 5.42 & 5.43). The highest bed-roughness values (red) are found on the steep cirques (Figs. 5.10 & 5.41). Both parallel and orthogonal to palaeo-ice flow results derived from a 100 m window size show the ribbed moraines as rougher than the surrounding areas (Figs. 5.10, 5.41c & d). However, these landforms are not shown in the 1 km window size results (Figs. 5.41a & b, 5.44a) and cannot be seen in the anisotropy data (Figs. 5.42 & 5.43). The change in bed roughness derived from the 1 km window, moving from east to west across the rogen moraines, is caused by a valley (lower end of SM in Fig. 5.10). The 100 m window has medium bed-roughness values for the rogen moraines (yellow) and does not pick up the valley (Fig. 5.41c & d). However, there are other features in close proximity to the rogen moraines that have similar roughness values and spatial patterns. These have not been mapped as glacial landforms by BRITICE (Clark et al., 2018) or by the detailed field mapping carried out by Finlayson et al. (2011).

5.5.8 Common results across all sites

As the spacing between transects is reduced, the spatial trends in bed-roughness values are clearer. For example at the Ribblesdale site, more detail can be seen in Fig. 5.20d compared to Fig. 5.19f. However, the statistics (Tables 5.2, 5.3, 5.5, 5.7, 5.9, 5.11 & 5.13) do not show a distinct change as the spacing between the transects is reduced and in some cases the numbers are consistent from 1 x 1 km through to 5 x 5 m transect spacing. For example, the mean and median values for bed roughness derived using a 100 m window are identical for Tyne Gap (site 5, Table 5.11). This is also commonly the case for the mean anisotropy values, e.g., Beinn Dearg (site 6, Table 5.13).

To summarise all the bed roughness and anisotropy data across the sites, mean values for each window size were calculated using the data from both flow directions (orthogonal and parallel) (Table 5.15). These mean values were then used to plot bed roughness against anisotropy for each site to determine whether landforms have a unique bed-roughness signature (Fig. 5.45). Due to the striping in the anisotropy results for the eastern section of Tweed (MSGL; Fig. 5.34) and Tyne Gap (lowland; Fig. 5.39), these data were not included in Fig. 5.46 to ensure they did not bias the results. The cause of the striping is discussed in Section 5.6. With the striping included for the MSGL, the mean anisotropy is the same as

the drumlins when a 100 m window size is used (Table 5.15). The lowland and MSGL have very similar mean bed-roughness values (2.4 and 2.5 respectively) but the lowland site has low anisotropy (depending on the window size used, see Table 5.15) whereas the MSGL are very anisotropic (Fig. 5.45). With the striping removed, the mean anisotropy for the MSGL is the same for the 1 km window (-0.4), but is higher for the 100 m window (-0.2 vs -0.3) (Table 5.15). It is clear that the MSGL are the most anisotropic of all the landforms when a 1 km window size is used (Fig. 5.46a). The heterogeneous upland site (Beinn Dearg) is the roughest site when a 1 km window is used, and is the only one that is isotropic with the 1 km window size (Fig. 5.46a). At this window size, the megagrooves and cnoc and lochan sites have very similar mean bed roughness and anisotropy values (Fig. 5.46a). Using the 100m window size, the megagrooves and cnoc and lochan sites can be distinguished more clearly with a small difference in mean bed roughness (1 vs 1.2) and a large difference in anisotropy (-0.4 vs 0; Fig. 5.46b). At this window size, both upland and cnoc and lochan sites are isotropic, whilst all the other sites have a negative anisotropy (Fig. 5.46b).

To further test whether bed roughness and anisotropy data from the sites fall into landform groups, cluster analysis was carried out (Figs. 5.47 - 5.50). The data used were from the 250 x 250 m spaced transects over sites 1 - 4, and site 6. Site 5 was not included due to striping in the anisotropy data. The 250 x 250 m data were chosen because they were a more manageable data set in terms of size in comparison to the 5 x 5 m data, and the results have shown little difference between the mean bed-roughness values when using these two transect spacings. The bed roughness and anisotropy data used were between the 1st and 3rd quartiles. Cluster analysis places data into groups and the number of groups is specified by the user. The kmeans function in R was used, and individual data points were placed into a group that has the nearest centroid (multidimensional equivalent of the mean) (Crawley, 2007). Cluster analysis was applied for both window sizes separately. For each window size, cluster analysis was carried out for sites 1 - 4 and 6 (Figs. 5.47 & 5.49), and then just for sites 1 - 4 (Figs. 5.48 & 5.50) to see if just the homogeneous landform types could be grouped more easily without the heterogeneous site. Statistics on how well the cluster analysis performed when compared to the landform groupings were calculated for Figs. 5.47c, 5.48c, 5.49c & 5.50c. These are reported in the figure captions, and the full statistics output is in the appendix.

The results from the cluster analysis also show that the MSGLs can be clearly grouped

for both the 1 km window and 100 m windows (Figs. 5.47c, 5.48c, 5.49c & 5.50c). The accuracy of the cluster analysis (how accurate it is at placing values from the MSGLs in the same cluster group) is ≥96%. The 1 km window (100% accuracy: Figs. 5.47c & 5.48c) is slightly better than the 100 m window, as for the 100 m window there are values from other cluster groups that are placed into the MSGLs cluster group (96% and 97% accuracy: Figs. 5.49c & 5.50c).

The cluster analysis also show that the megagrooves and cnoc and lochan terrain are separated more using the 100 m window (Figs. 5.49c & d,5.50c & d) compared to the 1 km window (Figs. 5.47c& d, 5.48c& d). The accuracy for the megagrooves and cnoc and lochan terrain when groups 1 - 4 and 6 were used in the cluster analysis was 49% and 64% respectively for the 1 km window data, and 80% and 67% respectively for the 100 m window data. When the upland area (site 6) was removed from the cluster analysis, the accuracies for the megagrooves and cnoc and lochan terrain was 78% and 74% respectively for the 1 km window data, and 85% and 71% respectively for the 100 m window data. The accuracy for placing values correctly in the megagroove cluster group shows a marked improvement from the 1 km window compared to the 100 m window. The accuracy improvement for the cnoc and lochan terrain is not as large from the 1 km window to the 100 m window. The difference between the accuracy improvement of the megagrooves and cnoc and lochan terrain could be that the megagrooves anisotropy values become more anisotropic for the 100 m window, where as there is more crossover between the cnoc and lochan terrain with other landform groups in the raw 100 m window data (Figs. 5.47a vs 5.49a).

For the drumlins, the cluster analysis performed well for the 1 km window data with accuracies of 98% and 100% (Figs. 5.47c & 5.48c). However, for the 100 m window data, the cluster analysis had accuracies of 40% and 39% as there was a lot of crossover with other cluster groups (Figs. 5.49c & 5.50c).

Removing the upland area (site 6) from the cluster analysis improves the overall accuracies from 58% to 71% for the 1 km window data and 60% to 65% for the 100 m window.

The 2D bed-roughness results are useful because they show similar spatial patterns to the 1D results. There is less processing of the data to produce the 2D results, so they can provide a quick assessment of an areas' bed roughness. However, the 2D results cannot show the anisotropy of bed-roughness values, and this is key to distinguishing between areas of glacial landform assemblages.

5.6 Discussion

5.6.1 Do glacial landforms have unique bed-roughness signatures?

The results show that glacial landforms do have characteristic bed-roughness signatures when anisotropy values are used alongside bed-roughness measurements (Fig. 5.46). Megagrooves, MSGL, and drumlins are anisotropic (< -0.2) i.e. they are markedly rougher orthogonal to palaeo-ice-flow direction. In other words, megagrooves, MSGL, and drumlins are streamlined along the ice-flow direction. The megagrooves and MSGL have the highest mean anisotropy compared to the drumlins, which is consistent with the reported elongation values (6-25:1, 8-23:1, & 1-4:1 respectively; Mitchell, 1994; Everest et al., 2005; Bradwell, Stoker and Krabbendam, 2008). The cnoc and lochan have slightly anisotropic values derived from the 1 km window size but are isotropic when derived from the 100 m window size. It is not surprising that the cnoc and lochan of Assynt are isotropic in one window because the bed roughness is inherited from the bedrock geology, consisting of gneiss (Krabbendam and Bradwell, 2014). Cnoc and lochan is a glacially eroded hard-bed landform assemblage (Eyles, 2012), made up of hills and lakes, as well as star shaped basins and linear valleys, whose primary architecture is pre-glacial (Krabbendam and Bradwell, 2014). The fracture and joints of gneiss in Assynt happen to be isotropic (or rather they form an orthogonal fracture network) whereas sedimentary rocks often have highly anisotropic bedding planes (Krabbendam and Bradwell, 2014), which can be preferentially eroded to form megagrooves (e.g. Krabbendam and Glasser, 2011; Krabbendam et al., 2016). It is possible that cnoc and lochan terrains in other areas could be more anisotropic if the bedrock structures are more aligned parallel to ice flow. For example, Charles Island in the Hudson Strait (Canada) has megagrooves and elongate lakes (elongation ratios >1:20) even though it is underlain by gneiss (Krabbendam et al., 2016). The Ullapool megagrooves are an example of an area where bedrock geology is aligned with ice flow (Bradwell, Stoker and Krabbendam, 2008; Krabbendam et al., 2016), which enhanced the existing anisotropy of the landscape.

Both the Ullapool megagrooves and the Assynt cnoc and lochan are underlain by hard bedrock, with very little sediment cover. Using the 1 km window size, both sites produce similar mean bed roughness and anisotropy (Table 5.15 & Fig. 5.45). Yet, at smaller roughness scales, the values derived using the 100 m window show that there is a clear difference in the values caused by the anisotropic nature of the megagrooves and the isotropic nature

of the cnoc and lochan. The accuracy of the cluster analysis in grouping the megagrooves increased from 49% to 80% for the 1 km window and 100 m window respectively (Figs. 5.47c & 5.49c). The difference in mean anisotropy values between the window sizes for the megagrooves is likely to be caused by the size of the landforms. Although the megagrooves are 1000 – 2000 m long, they are only 50 – 120 m wide. Thus, transects orientated orthogonal to the megagrooves are rougher at the 100 m window size because the change in elevation from crest to trough to crest is measured. For the cnoc and lochan, the highest roughness values are often located around the highest elevations using the 1km window. When the 100 m window is used there is no spatial pattern in anisotropy because the bed roughness is inherited from the bedrock geology, so that the cnoc and lochan are isotropic at the smaller scale (Fig. 5.29).

The MSGL terrain in the Tweed has a higher anisotropy when the 1km window is used, but it has a lower anisotropy when the 100 m window is used. The MSGLs are the only homogeneous landform site where this occurs (Fig. 5.45). The Ullapool megagrooves and the Tweed MSGL are similar landforms in terms of their size and shape. However, the MSGL often have a larger spacing between landforms (200 – 800 m) compared to the megagrooves (100 – 500 m), and can be more than 200 m wide (megagrooves are 50 – 150 m wide; Bradwell, Stoker and Krabbendam, 2008). Therefore, the bed-roughness signature is more distinct for the MSGL when using the 1 km window size because the 100 m window is too small to capture some of the bed roughness. This is also shown by the cluster analysis, which had a 100% accuracy for placing the MSGLs 1 km window data into a cluster group (Fig. 5.47c). This reduced slightly to 96% for the 100 m window data as some data from other cluster groups were placed into the MSGLs cluster group (Fig. 5.49c). However, the difference between the megagrooves compared to cnoc and lochan and uplands is clearer when the 100 m window is used (Figs. 5.45 & 5.49). At this scale, the isotropic nature of the cnoc and lochan and uplands is apparent, distinguishing these two sites from the others.

This is the first time that bed-roughness signatures of glacial landforms have been investigated. The results from this chapter indicate that by using a combination of bed roughness and bed-roughness anisotropy, it is possible to distinguish homogeneous areas of landforms i.e. sites 1, 2, & 4 from each other, as well as from heterogeneous areas of landforms i.e. sites 5 & 6 (depending on the window size used). The cnoc and lochan landscape (site 3) is the only homogeneous area that plots with the heterogeneous landforms (when the 100 m

window is used) due to the isotropic nature of the bed roughness. However, there is crossover between other sites such as the drumlins and megagrooves (when the 100 m window is used) which is not surprising as some subglacial bedforms are on a size-shape continuum (Ely et al., 2016). Both window sizes are needed to determine for bed-roughness signatures. If bed-roughness signatures are consistent across large areas of glacial landforms, it will allow bed roughness from contemporary-ice streams to be used to infer the geomorphology that might exist at the bed (Stokes, 2018). This creates a new avenue of research to explore, and the potential to answer questions about ice-stream beds. For example, if areas of homogeneous landforms can be identified beneath contemporary-ice streams, then this information can be used to refine velocities that are applied to model palaeo-ice streams. Once areas of landforms have been identified, these locations can be monitored because the initiation, evolution and potential decay of landforms over time will change the bed roughness of ice streams, which in turn is likely to be a control on ice velocity and related to subglacial water routing (Schoof, 2002; Stokes, 2018). Additionally, identification of landforms could allow ice streams to be identified as either soft-bedded or hard-bedded, which can be used to quantify if there is a difference in bed-roughness values between the two (Stokes, 2018). The existing understanding of landform evolution is limited and there is no current consensus on certain landform formation mechanisms (e.g. drumlins and MSGLs Clark, 2010; Spagnolo et al., 2014). If bed roughness can be used to infer where these landforms exist underneath contemporary-ice sheets, it will allow observations of how these landforms change over time in relation to ice dynamics and to address whether landforms are in a steady state (Hillier et al., 2013), and may give some insights into landform initiation. Furthermore, observations of landforms at the bed of contemporary-ice streams could be used to create statistical models that link subglacial process to bedform metrics (Hillier et al., 2016).

5.6.2 The importance of window size

This chapter shows that the choice of window size has a significant impact on the bed-roughness results. The window size changes the bed-roughness values reported for each site. There is an order of magnitude difference between the mean bed-roughness values for all sites (except Beinn Dearg site 6; Table 5.15) because of the order of magnitude difference between the window sizes. Importantly, changing the window size will give different bed-roughness values for landforms because the window size sets the horizontal scale range of

the landforms being measured and it determines how much spatial averaging occurs (Smith, 2014). This needs to be taken into consideration in future bed-roughness studies and means that bed-roughness measurements are only comparable between studies that use the same window size, as well as the same bed-roughness calculation.

The 1km window captures bed roughness over larger scales. For example, large areas of the cirques in Beinn Dearg (site 6) have high roughness values when using a 1 km window, but a much smaller area has high roughness values when the 100 m window is applied (Fig. 5.42). This is because roughness for one point is calculated over a larger distance using the 1 km window. The change in elevation from one side of a cirque to the other side is large due to the nature of the landform, which causes high bed roughness. The 100 m window will only capture this change over a small part of the cirque, e.g., 100 m either side of the ridge, whereas the 1 km window will show this change to be over a larger area.

Spatially, the bed-roughness values derived using the 100 m window size pick out individual glacial landforms more clearly than the 1 km window, even in the area of mixed glacial landforms, e.g., Beinn Dearg (site 6). However, this is not the case for the MSGLs (Tweed, site 4), demonstrating that one window size does not fit all glacial landforms. It is not just length and width of landforms that need to be taken into account but also spacing, as already detailed in Section 5.1 when comparing the megagrooves and MSGL. For anisotropic glacial landforms >100 m wide, the 100 m window size does not show the anisotropic nature as clearly as the 1 km window size. Thus, the 100 m window size is more appropriate for mesoscale glacial landforms such as drumlins, and some highly anisotropic macroscale landforms such as megagrooves, whilst the 1 km window size is better suited to macroscale glacial landforms.

When defining bed-roughness signatures the window size was important. The 1 km window size data performed well for defining the MSGLs, and separating the drumlins from the megagrooves in the cluster analysis (Figs. 5.47 & 5.48). The 100 m window size data were better for separating the megagrooves from the cnoc and lochan terrain (Figs. 5.49 & 5.50). Both window sizes are important for defining bed-roughness signatures.

5.6.3 The importance of anisotropy

Glacial landforms range from having isotropic bed roughness to anisotropic bed roughness. In the latter case this is normally where bed roughness is higher orthogonal to palaeo-ice-flow

direction (related to ice streamlining; Fig. 5.45). The sites that have a mix of landforms (heterogeneous) are more isotropic, particularly when using the 100 m window, compared to the sites of homogeneous landforms (sites 1, 2, 4) that have clear elongation ratios. It has been shown that anisotropy needs to be considered to differentiate bed-roughness signatures between landforms (Section 5.5), and these can only be calculated using the 1D results. For example, the megagrooves and cnoc and lochan (sites 1 & 3) have similar overall bed-roughness values (Table 5.15), but the megagrooves are anisotropic.

The results of this chapter show that transect orientation influences bed roughness analysis and is key to identify bed-roughness signatures of glacial landforms. This chapter builds on the results from chapter 4 (Falcini et al., 2018) and previous work by other authors who identified the importance of transect orientation on bed-roughness results (Gudlaugsson et al., 2013; Rippin et al., 2014; Bingham et al., 2015). Transects orientated parallel and orthogonal to ice flow are needed to calculate the anisotropy of bed roughness, and there are large datasets in Antarctica and Greenland that fit this criterion (e.g. Bingham and Siegert, 2009; King et al., 2009; Rippin, 2013; Lindbäck and Pettersson, 2015; Bingham et al., 2017). These data could be used to infer where landforms exist underneath contemporary-ice sheets. Furthermore, the quantification of parameters at the bed of contemporary-ice streams such as roughness and landforms will improve ice-sheet models (Stokes, 2018). Improving future predictions of ice-sheet behaviour is of high importance as it will increase the accuracy of sea-level rise predictions, enabling appropriate mitigation against the impacts of climate change (Hanna et al., 2013).

5.6.4 The importance of transect spacing

The spacing of transects is less important when analysing bed-roughness values alone because there is a consistency in the statistics between low to high resolution grid sizes i.e. the mean values of the 1 x 1 km spaced transects are similar or identical to the mean values of the 5 x 5 m spaced transects. As bed-roughness values are dependent upon window size (Smith, 2014), one might assume that bed-roughness values for a site will also vary if the spacing of transects changes. Therefore, this is an unexpected, yet interesting finding, and could be useful for future RES surveys. A prospective RES survey focused on finding landforms at the bed of contemporary-ice streams would not need to be undertaken at 5 x 5 m spacing, because the bed-roughness values and anisotropy will give similar results for a larger spacing.

However, more spatial detail can be obtained with smaller spacing between transects, which should be taken into consideration when designing future RES surveys. It can be difficult to distinguish bed-roughness of landforms from other areas of similar bed roughness without prior knowledge of landform distribution (see Section 5.6). In effect, this finding creates a catch 22 situation. It suggests that high resolution grid sizes are not required to find areas of homogeneous landforms underneath contemporary ice streams, but the spatial detail obtained from high resolution grid sizes is needed to separate landforms from other areas of the topography. This needs to be taken into account by future studies.

5.6.5 Recommendations for future studies

This is the first study that has attempted to find bed-roughness signatures of homogeneous glacial landforms using 1D methods. Repetition of this study at other sites, and other landform assemblages such as rogen moraines, would be beneficial in order to constrain further the novel measurement of landform bed-roughness signatures.

Another important aspect of future work would be to test an area underneath a contemporary ice sheet where homogeneous glacial landforms exist. This could for example be undertaken on the MSGL underneath Rutford Ice Stream (King et al., 2007, 2009) or lineated bedforms underneath Pine Island Glacier (Bingham et al., 2017). Investigating whether landforms underneath contemporary-ice streams have similar bed roughness to those underneath palaeo-ice streams would allow a better understanding of basal conditions.

Using the results of chapters 3 and 4, it was suggested that RES surveys should have a transect spacing of 500 m orthogonal to ice flow only (Falcini et al., 2018). For more spatial detail and to be able to separate glacial landforms from areas that do not have landforms, it is clear that a transect spacing of 250 m would be preferable, with both parallel and orthogonal transects. However, this would not be practical over large areas, so undertaking RES surveys with high resolution grids could be focused on areas where a rough bed has been inferred (Bingham et al., 2017) and where the existence of landforms has been suggested (e.g. King et al., 2009; Jezek et al., 2011; Rippin et al., 2014; Schroeder et al., 2014; King et al., 2016; Bingham et al., 2017).

5.6.6 Limitations

Prior knowledge of glacial landforms is needed in some cases to distinguish landform bed roughness from similar bed-roughness values in the landscape. For example, in site 6 (Beinn Dearg) there are other features in close proximity to the group of rogen moraines (Fig. 5.10) that have similar roughness values and spatial patterns (Fig. 5.41c & d). This is not too problematic for areas with palaeo landforms because many of these areas have been mapped in great detail by previous studies, e.g., BRITICE (Clark et al., 2018) and, if not, landforms can often be identified using a high resolution DTM such as NEXTMap. However, this would be a problem for studies of contemporary-ice streams and ice sheets as DEMs are created using RES survey data, which at best have a spacing between transects of 250 m (King et al., 2007). If the bed cannot be seen at high resolution (e.g., 5 m), it is difficult to interpret what glacial landforms are there. Bed-roughness anisotropy and other bed-roughness methods that measure spacing could overcome this. Anisotropy can be used to infer whether features are elongated or not, as shown in distinguishing between the roughness results of megagrooves and cnoc and lochan. Spacing methods can measure the number of peaks or troughs along a transect (Prescott, 2013), which can be compared to the spacing between palaeo landforms.

Prior knowledge of palaeo-ice-flow direction at the time of landform formation is important. It has been shown that glacial landforms are often anisotropic, making transect orientation key when measuring bed roughness. There are locations where multiple flow sets are imprinted on top of one another, leaving landforms with different orientations (e.g. Hughes et al., 2014). Although the landforms may be homogeneous (e.g. different sets of drumlins), these areas would not necessarily give clear roughness signatures. This could be problematic for contemporary-ice streams that have changed flow direction (e.g. Conway et al., 2002).

The anisotropy calculations for 5 x 5 m resolution appear to have some DTM artifacts (striping) for sites 4 & 5 (Figs. 5.33 & 5.38). This might be caused by the orientation of the transects. For these sites only, the transects are aligned exactly north south and east west, which is the same as the DTM pixel orientation. The striping is much more prevalent in the 100 m window results compared to the 1 km window results (e.g. Fig. 5.33b vs 5.33a). This could have caused the mean values to shift from lower to higher anisotropy for both sites. For example, the Tweed has a mean anisotropy of -0.2 for the 100 m window results that include the striping data, but a mean of -0.3 when the striping data are removed.

Striping artifacts by their nature are anisotropic, and have been shown to be scale-dependent, having a greater effect on DTM curvature distributions at smaller window sizes (Sofia et al., 2013). Striping artifacts are caused by the way the data are collected. For DTMs created from remote sensing, the data are collected along lines, and this can cause striping artifacts during interpolation that can impact roughness results (Sofia et al., 2013; Trevisani and Cavalli, 2016). NEXTMap DTM data were collected using parallel flight lines, with three orthogonal flight lines per 200 x 200 km block to aid systematic error removal (Mercer, 2007). A visual inspection of the NEXTMap DTM shows that there is no striping at sites 4 & 5. Thus, this was an unexpected error, which was only visible in the anisotropy measurements. Transects should not be aligned with the DTM pixel direction to avoid this error.

5.7 Conclusions

The groups of glacial landforms investigated here have a characteristic bed-roughness signature when bed-roughness anisotropy is taken into account. Anisotropy is key to defining the bed-roughness signatures of glacial landforms because this allows landforms with similar roughness values to be differentiated, e.g., megagrooves and cnoc and lochan. This is the first study to show that glacial landforms have a characteristic bed-roughness signature, and this information could be used to infer the nature of landforms at the bed and where they are located underneath contemporary-ice streams.

The results showed that a window size of 100 m was more appropriate for mesoscale and some macroscale landforms, whereas a window size of 1 km was better suited to macroscale landforms that were wider than 100 m and had a large spacing. However, both window sizes are required to determine the characteristic roughness for certain landform types and to produce bed-roughness signatures. It must be noted that to facilitate comparison between studies, window sizes must be the same. The 1D transects provided more spatial information as the spacing between transects decreased. Yet there was little change in the mean bed-roughness values as the spacing decreased. Prior knowledge of landform distribution is still required in some cases to distinguish bed-roughness measurements of landforms from other areas that have similar bed roughness. This should be noted by future studies.

There are many unanswered questions about the environment at the bed of ice streams. How are landforms created, and what processes are involved in their genesis, growth and

decay over time? How do changes in landform dimensions affect bed roughness, and consequently affect ice velocity? There are certain feedback loops occurring here: the geomorphology of the bed influences ice velocity i.e. a rougher bed causes slower flow, but ice flow can change the shape of the bed, so faster flow can smooth the bed. Finding out more information about this feedback loop is important because it could be key in our understanding of ice-stream beds. If researchers could know where landforms exist underneath contemporary-ice streams, some of these questions can start to be answered.

The results of this chapter show that bed-roughness signatures of glacial landforms can be defined and have the potential to be compared with known and unknown areas of glacial landforms underneath contemporary-ice streams. This information can be used to find out how landforms form under ice streams, and how landforms influence basal dynamics. There are data available to test whether landforms exist underneath contemporary-ice streams, and this should be a focus of future research. Palaeo-ice sheet reconstruction could be improved because the contemporary-ice-flow regime above an area of homogeneous glacial landforms can be applied to areas of palaeo-ice sheets that have the same homogeneous glacial landforms. Bed roughness of both palaeo and contemporary ice sheets is an important metric that needs to be calculated by future studies so that we can begin to understand how landforms are created and their subsequent impact on ice dynamics.

Chapter 6

Discussion and conclusions

The following sub sections provide a summary of the research described in Chapters 3, 4 and 5, and relate these findings to the objectives set out in Chapter 1. For more in depth discussion of the findings, see the discussion sections of Chapters 3, 4 and 5. Using the findings from Chapters 3, 4 and 5, recommendations are made for future RES surveys and future bed-roughness studies on deglaciated terrain.

6.1 Objective 1: Investigating bed-roughness methods (Chapter 3)

The first objective of this study was to compare the different methods of measuring bed roughness used in glaciology and glacial geomorphology. The choice of method and transect orientation in relation to ice flow was shown by previous studies to impact bed-roughness results. Measuring the bed roughness of deglaciated terrains allows for further interpretation of what the methods are measuring, because the entire bed can be seen.

6.1.1 Detrending

Detrending is a key component of bed-roughness calculation, and in this study it was shown that the method of detrending affects the final roughness results (Section 3.4.2). For example, using the mean detrending method, the drumlins on the offshore transect (Fig. 3.2) could be distinguished in the bed-roughness results. Conversely, the difference detrending method allowed areas of exposed bedrock to be distinguished from other areas along the transect (Fig. 3.2) in the bed-roughness results. The advantage of using the difference detrending

method is that it is not calculated using a moving window, and thus removes window size as a variable during the roughness measurement process. However, as both detrending methods used in the bed-roughness calculations were able to distinguish different elements of the topography, it can be argued that both are useful when measuring glacial bed roughness. As the detrending method can impact the final bed-roughness results, it is important that researchers consider how they are going to detrend their data, what the outcome of this will be and report the method clearly.

6.1.2 Bed-roughness method comparison

Out of the four methods tested in this study, FFT analysis and SD produced the most meaningful results in relation to the topography being measured (Section 3.4.4). The overall trends in bed roughness measured by both FFT analysis and SD were similar, but there were some areas that had differences. For example, the two methods measured lower roughness values for the offshore transects compared to the onshore transects, which is likely to have been caused by sediment deposition offshore and higher erosion rates onshore (Fyfe et al., 1993; Bradwell and Stoker, 2015). Yet the cnoc and lochan landscape onshore showed higher roughness values when calculated using SD compared to FFT analysis. This is likely to be a function of what the FFT analysis is measuring. FFT analysis was used to calculate the total roughness parameter, which measures the frequency of features as well as the amplitude. An area that has a similar frequency of undulations, with large amplitude changes between undulations (e.g., cnoc and lochan), will be smoother when measured using the total roughness parameter (FFT analysis) compared to SD. FFT analysis (total roughness parameter) and SD both have advantages and disadvantages (described in Section 3.4.4.3). FFT analysis can provide more information than SD. However, SD can be used on a wider range of data and does not need a large amount of data preprocessing. Thus, both methods can be used by future studies but the method choice will be determined by the data available and the roughness parameters that are going to be investigated.

6.1.3 Window size

Window size was shown to have a clear impact on bed-roughness results (Section 3.4.2.3), because the window size affected which landforms were measured as rough. As glacial landforms vary in scale from micro (0.01 m - 100 m) to macro (1 km - 100 km) scale, no one

window size will capture the roughness of all landforms. A smaller window size (100 m - 300 m) was shown to capture individual landforms (drumlins ∼300 m wide). The larger windows (>500 m) can measure a wider range of landforms, but can also merge the bed-roughness measurements of landforms i.e. multiple landform types within one window.

6.1.4 Directionality of 1D bed-roughness measurements

In Section 3.4.6, the directionality of 1D bed roughness was measured for the first time, down to the pixel-scale of the DTM (5 m). This enabled a comparison of the bed roughness parallel to palaeo-ice flow and the orthogonal to palaeo-ice flow. Orthogonal to palaeo-ice flow, the Ullapool megagrooves can be clearly seen in the bed-roughness results (Fig. 3.14). The results from this small area suggest that bed-roughness values can be linked to glacial landforms, and provided some of the foundations for the work carried out in objective 3. Furthermore, these results emphasised the importance of directionality, either by placement of transects (1D), or by using a DTM aligned with palaeo ice flow direction (2D).

6.2 Objective 2: Quantifying bed roughness (Chapter 4)

The second objective was to investigate how the roughness of contemporary-ice stream and palaeo-ice stream beds compare. The bed roughness of a contemporary-ice stream had not been directly compared to the bed roughness of a palaeo-ice stream before. By doing this, the bed roughness from palaeo-ice streams can be tested as an analogue for contemporary-ice streams. The effect of RES transects spacing on bed-roughness results was tested on a palaeo-ice stream by comparing the roughness results from artificial transects with the roughness of a high resolution DTM dataset.

6.2.1 Transect spacing and orientation

The results from Chapter 4 clearly showed that a 30 x 10 km grid (same transect spacing as some previous RES surveys) was too coarse to capture all glacial landform types present on a typical ice sheet bed (Section 4.4.2). The bed-roughness results from a smaller spaced grid of 2 x 2 km, placed over the Ullapool megagrooves in the Minch Palaeo-Ice Stream (MPIS) onset zone, demonstrated that transects parallel to palaeo-ice flow were smoother compared to orthogonal transects. There was a clear difference between the pixel-scale transects for

the MPIS, which showed that transect orientation had a strong influence on bed-roughness results (Section 4.4.3).

6.2.2 Comparison of contemporary and palaeo-ice stream bed roughness

The overall trends in bed roughness from the Institute and Möller Ice Streams (IMIS) West Antarctica and MPIS were comparable (Sections 4.4.4 & 4.4.5). Previous research often suggested that fast flowing ice generally occurs over areas of low roughness. Both IMIS and MPIS had areas of high bed roughness that were associated with current fast ice flow (IMIS) or areas of inferred palaeo-fast ice flow (MPIS). As the characteristics of the MPIS bed were visible due to high resolution DTMs and bathymetric data, a more detailed interpretation of the bed-roughness results was possible. High bed-roughness values were associated with MPIS flow paths onshore, where there were large areas of exposed bedrock, whilst offshore, lower bed-roughness values occur, associated with sediment cover. However, some areas with lower bed-roughness values occurred over bedrock, which suggests that low bed-roughness values from contemporary ice streams are not always an indication of basal sediment (Section 4.4.5). The results from this chapter demonstrate that palaeo-ice stream bed roughness provides a good analogue for contemporary ice-stream bed roughness.

6.3 Objective 3: Glacial landforms and bed-roughness signatures (Chapter 5)

The third objective was to test whether glacial landforms have unique bed-roughness signatures. If palaeo-glacial landforms do have bed-roughness signatures, the bed-roughness data from the Antarctic and Greenland Ice Sheets could be used to infer the presence of certain landform fields beneath the ice. This could lead to new insights into the processes occurring at contemporary-ice stream beds that could better constrain reconstructions of palaeo-ice streams and ice sheet models.

6.3.1 The bed-roughness signatures of glacial landforms

The results from Chapter 5 show that glacial landforms have a unique bed-roughness signature when both mean roughness and anisotropy are taken into account (Section 5.5.1). For example, the Ullapool megagrooves and the cnoc and lochan terrains have similar mean bed-

roughness values, but the megagrooves are highly anisotropic whereas the cnoc and lochan terrain is isotropic. At the 1 km window size, the drumlins and cnoc and lochan terrain have the same mean anisotropy but the cnoch and lochan terrain is rougher than the drumlins. The calculation of anisotropy alongside bed roughness, is key to defining glacial landform bed-roughness signatures because anisotropy enables landforms to be differentiated.

6.3.2 Transect spacing and window size

Four different grid spacings (transect spacing) and two different window sizes were used to ascertain which was the most appropriate for measuring the roughness of glacial landforms. As spacing between transects decreased, more spatial information was provided (Section 5.5.4). However, a decrease in the spacing provided little change to the mean bed-roughness results. This suggests that RES surveys with widely spaced transects could be used to locate areas with a bed-roughness signature which matches that of palaeo-glacial landform beds. Yet this is likely to be difficult, as detailed in Section 5.6.6, prior knowledge of glacial landform distribution is required to distinguish landform bed roughness from similar bed-roughness values in the landscape. In terms of window size, the smaller 100 m window was better suited to measuring bed roughness of mesoscale (1 m - 1 km) glacial landforms, whilst the 1 km window performed better for macroscale glacial landforms (1km - 100 km; Section 5.5.2). For a good characterisation of roughness for fields of glacial landforms, both window sizes are needed.

6.4 Application of results

6.4.1 Interpretation of bed roughness underneath contemporary-ice streams

The interpretation of bed-roughness results from contemporary-ice streams is more difficult in comparison to palaeo-ice streams because data are sparser. For palaeo-ice streams the whole of the bed is often visible and covered by high resolution DEMs (e.g. Intermap Technologies, 2009; Hughes et al., 2010), which allow for higher spatial coverage of bed-roughness measurements (Falcini et al., 2018). Moreover, there is more information available for other factors that are important for the interpretation of bed-roughness measurements on palaeo-ice stream beds such as knowledge of the geology (e.g. Fyfe et al., 1993). A study that measured bed roughness of the proglacial area and adjacent ice sheet around Kangerlussuaq

in Greenland, used geological information from the proglacial area to interpret what might be influencing bed-roughness values underneath the ice sheet (Lindbäck and Pettersson, 2015). They suggested that gneiss bedrock from the proglacial area could extend underneath the ice sheet.

For contemporary-ice streams, the first obstacle in accessing the bed is the ice. RES can overcome this, but as has been shown in this study (Section 4.4.2), the large gaps between the RES transects in some studies (e.g. Taylor et al., 2004; Siegert et al., 2005; Bingham and Siegert, 2007; Rippin, 2013; Rippin et al., 2014) can miss areas of glacial landforms (Falcini et al., 2018). Furthermore, there are other aspects of the bed that influence not only bed roughness, but also the location of ice streaming (Winsborrow et al., 2010). These include the presence or absence of marine sediments (Studinger et al., 2001; Rippin et al., 2011), bedrock geology (Clark, 1994; Krabbendam et al., 2016), erosion vs deposition (Li et al., 2010; Rippin et al., 2014), basal thermal regime (Blankenship et al., 1993; Siegert et al., 2005), and topographical control (Bennett, 2003; Ross et al., 2012; Winter et al., 2018) (Fig. 2.1). Many of these factors are interlinked (Bingham and Siegert, 2009). For example, bedrock geology may promote topographical control (Ross et al., 2012; Jordan et al., 2013; Winter et al., 2018), and the basal thermal regime is likely to be warm based where ice flows at high velocities through a bedrock trough (Van der Veen et al., 2007). The data available to assess these other factors can be sparse. For example, direct observations of till are limited (e.g. Engelhardt and Kamb, 1998; Tulaczyk et al., 1998), and although seismic techniques and RES have been used to determine the locations of sediment, they are also influenced by the spacing of transects (e.g. Studinger et al., 2001; Peters et al., 2006). In some locations RES data cannot be acquired, for example, RES returns from deep troughs can be weak or intermittent, so estimates of marine sediments deposition are made via isostatically rebounded elevation maps (a map of past sea level where ice is removed) (Winter et al., 2018).

Marine sediments have often been suggested as a reason for smooth beds underneath fast flowing ice streams (e.g. Siegert et al., 2004; Rippin et al., 2006; Bingham and Siegert, 2007; Rippin et al., 2011). Large parts of West Antarctica are below isostatically uplifted sea level elevations and were likely covered by marine sediments during interglacial periods, which would bury preglacial topography and leave a smoother surface (Bingham et al., 2007; Bingham and Siegert, 2009). Marine sediments have been found at the beds of West Antarctic

ice streams using boreholes (Engelhardt et al., 1990; Engelhardt and Kamb, 1998; Kamb, 2001; Smith et al., 2007) and inferred over larger areas from geophysical surveys (RES and airborne gravimetry) which have determined the palaeo-shoreline (Studinger et al., 2001). Areas that have large amounts of sediment correspond with smooth basal reflectors, which have been used to infer that smoothness is an indicator of marine sediments at the bed (Bingham and Siegert, 2007).

Using a two-parameter FFT analysis method, Li et al. (2010) suggested that locations that have low total roughness values but are dominated by long wavelengths, can be interpreted as having marine sediments with fast, warm ice flow. Wright et al. (2012) argued that erosive process could have reduced the amplitude of obstacles, whilst Rippin et al. (2014) suggested streamlined bedforms could cause these bed-roughness results. Furthermore, Rippin et al. (2011) found that the bed of fast flowing tributaries of Pine Island Glacier in West Antarctica were not smooth in all of the tributaries. Other studies have suggested that Pine Island Glacier was deglaciated in the past and that the majority of the basin was a palaeo-seabed (Vaughan et al., 2006; Pollard and DeConto, 2009). Rippin et al. (2011) interpreted this difference in bed roughness between tributaries to be due to a patchy spatial distribution of marine sediments. The interpretations of bed-roughness measurements in relation to marine sediments from the above studies show that whilst the inferences of what is causing a smooth bed are logical, there are complications. Three studies have suggested different interpretations for similar bed-roughness values (Li et al., 2010; Wright et al., 2012; Rippin et al., 2014). The findings from this study on bed roughness of palaeo-ice streams could provide further information to refine interpretations from bed roughness of contemporary-ice streams, as explained below.

bed-roughness results from the MPIS have shown that the presence of sediment which causes a smooth bed does not necessarily correspond with fast flowing ice. In Chapter 4, low bed-roughness values from the 2 x 2 km grid upstream from the Ullapool megagrooves were associated with sediment cover that has been interpreted as being underneath an area of cold-based slow flowing ice (Section 4.4.4). Moreover, areas of exposed bedrock in the MPIS trunk had low bed-roughness values in comparison to the higher bed-roughness values on exposed bedrock onshore. A smooth bed therefore cannot always be associated with sediments (Section 4.4.5). The MPIS is an example of a topographically controlled ice stream (Bradwell et al., 2007; Bradwell and Stoker, 2015, 2016; Krabbendam et al., 2016), which

in turn is heavily influenced by the bedrock geology (Fyfe et al., 1993; Bradwell and Stoker, 2016). Therefore, interpretations of bed-roughness values for contemporary-ice streams that are in deep troughs should consider that a smooth bed could be associated with marine sediments or streamlined bedrock.

Rough values measured on contemporary-ice stream beds have often been associated with slow flow and cold basal ice (Fig. 2.1) but it has been shown in this study that rough, exposed bedrock can be associated with fast flow, and subsequently warm basal ice (Section 4.3 & 4.4.4). This supports findings from some contemporary-ice streams (e.g. Schroeder et al., 2014; Siegert et al., 2016; Diez et al., 2018; Muto et al., 2019) that found rough beds underneath fast flowing ice and the theoretical argument of Krabbendam (2016) that ice streaming over a rough, hard bed, could be explained by a thick layer of warm basal ice. Krabbendam (2016) suggests that continuous frictional heating can cause a thick layer of temperate ice to develop at the ice bed interface. In this situation, ice will flow around bedrock obstacles by stoss-side pressure melting (regelation) or enhanced creep. The presence of meltwater is suggested to aid melting on the stoss-side for bedrock obstacles that are longer than they are high, which is a quicker process than Weertman sliding (Weertman, 1957).

A key finding from this study is that the anisotropy of bed roughness is important for interpreting results. In Chapter 5, the mean bed-roughness values of cnoc and lochan terrain and the Ullapool megagrooves were similar, but the anisotropy measurements were different which enabled these landscapes to have unique bed-roughness signatures. Glacial landforms can potentially be identified underneath ice streams using bed roughness, which could be used to substantiate interpretations such as those from Rippin et al. (2014) who envisioned streamlined bedforms being the cause of bed-roughness values for some areas of the IMIS. Anisotropy is key to defining glacial landforms bed-roughness signatures, and can only be measured from bed-roughness values located at cross-over points between transects orientated parallel and orthogonal to ice flow. Many studies have not used anisotropy in their interpretations (e.g. Rippin et al., 2011). Rippin et al. (2011) used parallel and orthogonal transects to calculate bed roughness for Pine Island Glacier, and they focussed part of their analysis on bed-roughness measurements from transects running parallel to ice flow on Pine Island Glacier and its tributaries. They found that some tributaries had a rough bed and interpreted that marine sediment distribution was patchy to account for the differences in bed roughness beneath fast flowing ice. If they had calculated anisotropy for locations

where parallel and orthogonal to ice flow transects crossed, this could have provided further information to aid their interpretations. For example, if the bed was isotropic and rough, this would suggest exposed bedrock which could be similar to a cnoc and lochan landscape, whereas a rough bed with negative anisotropy would suggest streamlined bedrock or landforms, similar to megagrooves or MSGLs.

This study has demonstrated the value of measuring bed roughness on deglaciated terrain and further studies like this can only improve interpretations of bed-roughness values from contemporary-ice streams.

6.4.2 Recommendations for future RES surveys over contemporary ice

One of the aims of this thesis was to use the information gained from palaeo-ice stream bed roughness to propose best practice for acquiring data from major ice sheets that is appropriate to use in bed-roughness studies. RES surveys vary in their along-transect resolution and the spacing of transects. For example, Rippin et al. (2014) used a RES survey with a grid spacing of 10 x 30 km and an along transect resolution of ∼10 m, whilst Bingham et al. (2017) used orthogonal to ice flow transects spaced 500 m apart with an along transect resolution of ∼4-6 m. The question arises, what is the best transect spacing and along transect resolution to use?

This study focused on testing transect spacing because the along transect resolution used is often high, and comparable to DEMs from deglaciated terrain (e.g. Margold et al., 2015), whereas transect spacing can be coarse. By replicating a RES survey over the MPIS with a grid of transects spaced 10 x 30 km, the results from Chapter 4 demonstrated that the spacing of this grid was too coarse because it was not able to capture the bed-roughness of glacial landforms (Falcini et al., 2018). In Chapter 5, transect spacing of 2 km, 1 km, 500 m, 250 m and 5 m were tested on the bed-roughness of glacial landforms. Whilst the spatial roughness information increased as the spacing between transects decreased, overall there was little difference between the bed-roughness means for each site (Section 5.5.4). This suggests that over areas of homogeneous glacial landforms, 2 km spacing of RES transects would be sufficient to capture bed roughness, and define bed-roughness signatures. However, glacial beds are not made up of discrete areas of homogeneous glacial landforms. Although these areas are found in the the palaeo record such as the Ullapool megagrooves (Bradwell, Stoker and Krabbendam, 2008) or Ribblesdale drumlins (Mitchell, 1994), there are large

areas of complex heterogeneous landforms (e.g. central BIIS; Evans et al., 2009). Without previous knowledge of landform distributions, it can be argued that the smallest spacing possible between transects is required. Yet due to the nature of RES surveys, transect spacing of less than 500 m is difficult. This is because RES can pick up multiple landform crests parallel to ice flow (Welch et al., 1998; King et al., 2016), therefore studies that have used a transect spacing of 500 m or less mainly collect orthogonal to ice flow transects, with a few parallel transects to check for errors (e.g. King et al., 2016). As the parallel transects are not collected at 500 m spacing, this does not allow for anisotropy measurements to be made, which has been shown to be key to measuring unique landform bed-roughness signatures (Section 5.5.1), and for measuring bed roughness underneath conetmporary-ice streams (e.g. Gudlaugsson et al., 2013; Rippin et al., 2014). Furthermore, collecting RES surveys with small spacing between transects may not be practical over large areas due to cost and time. For example, it took King et al. (2016) three weeks with a two person team using snowmobiles to collect orthogonal transects spaced 500 m apart for an area of 18 x 40 km. Rutford Ice Stream is ∼200 km long and 20-30 km wide (Doake et al., 2013). Drones or Unmanned Aerial Vehicles could make RES data collection with small track spacing viable over large areas in the future. These systems are still relatively new and have only been tested for a few flightlines (e.g. Leuschen et al., 2014; Arnold et al., 2018), yet they could provide RES data in the future, and are likely to be cheaper compared to aircraft.

Taking the above discussions into account, the recommendations for acquiring future RES surveys to measure bed roughness are as follows:

1. Focus on areas where a rough bed is inferred (Bingham et al., 2017) and where existence of landforms has been suggested (e.g. King et al., 2009; Jezek et al., 2011; Rippin et al., 2014; Schroeder et al., 2014; King et al., 2016; Bingham et al., 2017). It is not currently feasible to carrying out RES surveys with small track spacing over large areas, therefore specific areas should be targeted.

2. As small as possible spacing between transects is the target to get the best spatial information on bed-roughness trends. However, this is constrained by cost, time and the need to collect parallel and orthogonal transects. 250 m transect spacing would be preferable but 1 km transect spacing is likely to be more realistic at present to get both orthogonal and parallel to ice flow transects. 1 km spacing would be suitable for MSGLs but smaller landforms such as drumlins are likely to need higher resolution

spacing.

6.4.3 Recommendations for future bed-roughness studies of deglaciated terrain

The second part to proposing best practice for bed-roughness studies on major ice sheets is to suggest recommendations for future bed-roughness studies on deglaciated terrain. To date, there have been few studies on bed roughness of palaeo-ice streams and palaeo-ice sheets (Hubbard et al., 2000; Winsborrow, 2007; Prescott, 2013; Gudlaugsson et al., 2013; Lindbäck and Pettersson, 2015; Tegowski et al., 2016; Spagnolo et al., 2017) and the results from Chapter 4 demonstrated that palaeo-ice streams can be used as an analogue for contemporary-ice stream bed roughness (Falcini et al., 2018). Furthermore, the results from Chapter 5 showed that glacial landforms do have bed-roughness signatures when anisotropy measurements are taken into account.

6.4.3.1 Framework for approach and method

The first consideration for future bed-roughness studies is whether to take a 1D or 2D approach. This depends on the focus of the study, but arguably a 1D approach is better suited to bed-roughness of deglaciated terrain because this allows the anisotropy of bed roughness to be measured. To provide meaningful anisotropy measurements, transects need to be orientated parallel and orthogonal to palaeo ice flow where possible. Transect orientation has been shown to be important not only for bed-roughness measurements on palaeo-ice streams (Gudlaugsson et al., 2013; Lindbäck and Pettersson, 2015; Falcini et al., 2018), but also on contemporary-ice streams (Rippin et al., 2014; Falcini et al., 2018).

If a 1D approach is taken, the spacing of transects is the next consideration. Initially this will be dictated by the resolution of available DEMs for a study area. However, there is a wealth of high resolution DEMs available that, like NEXTMap, have resolutions of 5 m or better (e.g. ArcticDEM; Morin et al., 2016; Dai and Howat, 2017). A 5 m resolution is perfectly adequate for measuring bed roughness of most mesoscale glacial landforms such as drumlins (Bennett and Glasser, 2009). Setting up transects at the pixel-scale will provide the best measure of bed roughness, but this is currently time consuming. It is further complicated by areas where previous flow direction was not in a continuous straight line, such as the Tweed Palaeo-Ice Stream (Fig. 5.8; Everest et al., 2005; Livingstone et al.,

2015). This is because multiple grids at different orientations would be needed to capture the change in flow direction. Automated placing of transects would be a useful method that could be developed. If measurement of bed roughness of a palaeo-ice sheet was the aim of a future project, pixel-scale transects would be feasible if there was automated placing of transects and access to a high performance computing facility (computing cluster; Dongarra et al., 2005; Lee et al., 2011) to process the bed-roughness calculations. However, if this was not possible, transect spacing of 1 km or less would be adequate (Section 5.5.4). Ideally, transect spacing should match high resolution RES studies, which are typically 500 m spacing (e.g. King et al., 2009, 2016; Bingham et al., 2017) as this would enable comparisons of bed-roughness measurements (if identical methods are followed).

The next consideration is the method to be used, and the moving window size employed. To allow comparisons between studies, the same method and window size must be used to ensure that bed roughness is measured at the same scale (Smith, 2014). To measure bed roughness in terms of amplitude, either FFT analysis or SD can be used, as these methods tend to show similar bed-roughness trends (Section 3.4.4 & 4.4.1; Falcini et al., 2018). Other parameters of bed roughness can be measured such as spacing, and these could be useful for further defining unique bed-roughness signatures of glacial landforms. A brief discussion of other methods was provided in Section 2.1.5. Window size has been shown to influence bed-roughness measurements by previous studies (e.g. Grohmann et al., 2011; Smith, 2014) and this research (Section 3.4.2.3 & 5.5.2), as this changes the scale over which calculations are made. This study tested many different window sizes, from 100 m - 1 km. The smaller 100 m window was better suited to measuring bed roughness of mesoscale glacial landforms, whilst the 1 km window performed better for macroscale glacial landforms (Section 5.5.2). Arguably both window sizes are required for defining bed-roughness signatures. From these findings, it can be suggested that both a 100 m and a 1 km window size could be applied to future studies to enable different scales of glacial landform bed roughness to be measured.

Taking the above discussions into account, the framework for measuring bed roughness on deglaciated terrain are as follows:

1. *Purpose of the research.* This will define what scale of measurements to make, and the method. For example, is the purpose of the research to measure bed-roughness of MSGL or whalebacks?

2. *Data and computing power available.* The resolution of the data will be a limiting factor

in terms of the smallest scale of roughness measurements that can be made. The same also applies to the available computing power, and whether researchers have access to machines that can process thousands of transects with thousands of data points. For example, a 10 km transect will have 2000 points if the DEM has a resolution of 5 m. A 10 x 10 km grid, with a DEM resolution of 5 m, equates to 4000 transects in total, with 8 million points. For reference, the BIIS is estimated to have had an areal extent of $\sim$ 840,000 km^2 (Clark et al., 2012; Ó Cofaigh et al., 2019).

3. *1D or 2D?* If the direction of palaeo-ice flow in relation to bed roughness is an important consideration for a study, then 1D transects would be required. However, if a general overview of bed-roughness trends was needed, then a 2D approach could be more appropriate.

4. *If 1D, what transect spacing?* This will be dictated by points 1 and 2. But once the limits have been defined i.e. what is not possible with the data and computing power available, then it will come down to user choice and what is most appropriate for the scale of bed roughness being measured. For example, if a researcher wants to measure bed-roughness of drumlins, should they choose a 500 m spacing between transects or 250 m? The consideration of spatial trends gained from these two grid sizes is likely to help the decision making process. The differences between two grid spacings could be tested on a small area first.

5. *Window size* Again, this will be dictated by points 1 and 2. Particular focus should be given to the scale of the features being measured. For example, what is the largest landform in the study site that a researcher wants to measure?

6. *Roughness measurement method.* Researchers should consider whether they want to measure more than one variable (e.g., amplitude and frequency). The advantage of measuring more than one variable is that it will provide more bed-roughness information and could help distinguish between areas that have similar roughness measurements but are qualitatively different.

6.4.3.2 Recommendations for future research focus

This study has shown that bed-roughness studies on deglaciated terrain are highly valuable to glaciology. Palaeo-ice streams provide a good analogue for bed-roughness of contemporary-

ice streams and allow for a more detailed interpretation of bed-roughness results. So far there have been fewer than ten studies on bed-roughness of palaeo-ice streams (Hubbard et al., 2000; Winsborrow, 2007; Gudlaugsson et al., 2013; Prescott, 2013; Ebert, 2015; Lindbäck and Pettersson, 2015; Tegowski et al., 2016; Spagnolo et al., 2017; Falcini et al., 2018). There is clearly more work needed on this subject. This study measured bed-roughness of a topographically controlled palaeo-ice stream, which was strongly influenced by bedrock geology. It would be useful to measure bed-roughness of a palaeo-ice stream that was not topographically constrained, which could then be used as an analogue for 'pure' contemporary-ice streams such as the Siple Coast Ice Streams, West Antarctica (Stokes and Clark, 1999; Winsborrow et al., 2010). Glaciologists could investigate whether 'pure' ice streams have a smoother bed compared to topographically controlled ice streams or whether their bed are just as variable. The majority of the Siple Coast Ice Streams have a smooth bed compared to the surrounding bed underneath slower flowing ice, which is thought to be caused by the presence of marine sediments (Siegert et al., 2004; Bingham and Siegert, 2007). There are examples of 'pure' ice streams in the palaeo record such as the Dubawnt Lake palaeo-ice stream (Stokes and Clark, 2003) and M'Clintock Channel corridor palaeo-ice streams (De Angelis and Kleman, 2005). Another interesting focus would be measuring the roughness of an entire palaeo-ice sheet bed using a high resolution DEM. This would allow for a comparison with contemporary studies (e.g. Rippin, 2013) and also enable further investigation into how bed roughness varies over a larger spatial scale rather than just one ice stream. Measuring the bed-roughness of an entire palaeo-ice sheet could also allow researchers to parametrise bed roughness for ice sheet modelling (Ritz et al., 2015; Stokes, 2018).

This study is the first to show that glacial landforms have unique bed-roughness signatures. A focus for future research would be to test this on other sites to refine the bed-roughness signature values. This is important because glacial landforms have a range of sizes and shapes within each category (Benn and Evans, 2010; Krabbendam et al., 2016). Drumlins, for example, can be spindle or more parabolic (Fig. 5.2). It is possible that the bed-roughness signatures of spindle drumlins are different to parabolic drumlins. Transects should be orientated parallel and orthogonal to allow for anisotropy calculations to be made as this value is key to defining unique bed-roughness signatures. The same window sizes must be used to allow for comparisons between studies.

An important step in further developing bed-roughness signatures is to test glacial land-

forms that have already been identified underneath contemporary-ice streams (Section 5.5.5). This would allow for a comparison between the bed-roughness of palaeo landforms and those currently forming underneath contemporary-ice streams.

6.5 Conclusions

The overall aim for this thesis was to explore bed roughness of palaeo-ice streams and to use this information as an analogue for bed roughness underneath contemporary-ice streams. To achieve this aim, the methods that have been used by previous studies to calculate bed roughness underneath ice streams were investigated. The results showed that the choices made by researchers on data resolution, window size, detrending and roughness methods have a significant impact on a studies results. It was shown that window size affects which landforms are measured as rough or smooth. Landforms are on a size continuum, therefore no one window size will capture the roughness of all landforms. Different window sizes were tested to find out what was most appropriate for glacial landforms found in deglaciated terrains. A window size of 100 m was most appropriate for measuring bed roughness of mesoscale (1 m - 1 km) and some macroscale landforms (1 km - 100 km). Conversely, a window size of 1 km was better for measuring bed roughness of macroscale landforms that were wider than 100 m and had large spacing between individual landforms. Arguably, both window sizes are needed to determine roughness for certain landform types and to define bed-roughness signatures. It is important to note that window sizes need to be the same size for comparison between studies.

Detrending the data before bed roughness is calculated is an important step as this removes large scale topography such as hills and valleys, that can otherwise dominate the roughness results. Here, two detrending methods were tested, and the results showed that both methods were adept at producing bed-roughness measurements that picked out certain features of the topography. For example, the *mean detrending* method led to bed-roughness measurements of drumlins, whereas the *difference detrending* method led to bed-roughness measurements of exposed bedrock. Both detrending methods are useful when measuring glacial bed roughness, potentially being more robust when used together.

Roughness methods that have been used in glaciology were compared, and out of the four methods, Fast Fourier Transform (FFT) analysis and Standard Deviation (SD) provided the

most useful results. FFT analysis and SD methods were used to calculate bed roughness along a flow parallel transect of the Minch Palaeo-Ice Stream (MPIS), north west Scotland, and a 10 x 30 km grid of transects over the MPIS and the Institute and Möller Ice Streams (IMIS), West Antarctica. The results showed FFT analysis and SD produced similar results for the majority of the data, but there were some differences which should be taken into account by future studies. For example, both methods measured lower roughness values for the onshore transects of the MPIS vs the offshore transects, which is likely to have been caused by sediment deposition offshore and higher erosion rates onshore. However, for the cnoc and lochan terrain located on the north west coast of Scotland, higher roughness values were calculated using SD compared to FFT analysis. This is likely to be caused by what the FFT analysis is measuring. In this study, FFT analysis was used to calculate the total roughness parameter, which measures the frequency of features as well as the amplitude. The cnoc and lochan terrain will have lower roughness values when measured using the total roughness parameter (FFT analysis) compared to SD because this terrain has a similar frequency of undulations, with large amplitude changes between undulations. Both FFT analysis (total roughness parameter) and SD have advantages and disadvantages. FFT analysis can provide more information than SD. However, SD can be used on a wider range of data and does not need a large amount of data preprocessing. Thus, both methods can be used by future studies but the method choice will be determined by the data available and the roughness parameters that are going to be investigated.

Data resolution was an important focus of this study because of the variation between contemporary and palaeo-ice streams. Data for bed-roughness studies of contemporary ice-streams comes from radio echo sounding (RES) transects, and whilst the along-transect resolution can be high (e.g., 10 m), the spacing between transects if often wide (10s km). In comparison, high resolution DEMs are available for large numbers of palaeo-ice streams, e.g., NEXTMap (5 m) and ArcticDEM (2 m). To test the impact of RES transect spacing on ice streams, and directly compare a contemporary and palaeo-ice stream, a RES survey was replicated over the MPIS. This artificial grid of transects spaced 10 x 30 km matched the RES survey from the IMIS. The results showed that the spacing of this grid was too coarse because it was not able to capture the bed-roughness of glacial landforms visible in the DTM. By using a smaller 2 x 2 km grid over the Ullapool megagrooves in the onset zone of MPIS, it was shown that transects orientated parallel to palaeo-ice flow had lower

bed-roughness values compared to orthogonal transects.

Bed roughness was calculated for pixel-scale transects over the MPIS, which also demonstrated a clear difference in bed-roughness values depending on transect orientation. The main flow paths of the MPIS in the onshore onset zones corresponded with high bed-roughness values and lower roughness values were associated with sediment cover in the main ice stream trunk. However, it was found that smooth areas of the bed beneath MPIS occurred over bedrock as well as the sediment covered areas. This is an important finding as some previous studies on contemporary-ice stream bed roughness have found that a smooth bed is associated with fast flowing ice, whilst a rough bed is associated with the slower flowing ice stream margins. Furthermore the bed-roughness results from the MPIS demonstrated that the presence of sediment, which can cause a smooth bed, does not necessarily correspond with fast flowing ice. The MPIS is a topographically controlled ice stream that is largely influenced by bedrock geology. Therefore, when making interpretations of bed-roughness values of contemporary-ice streams situated in deep troughs, researchers should consider that a smooth bed could be related to marine sediments or streamlined bedrock. In the IMIS tributaries, high and low bed-roughness values were also measured, which supports the notion that the bed roughness of palaeo and contemporary-ice streams can be compared. This study has shown that palaeo-ice streams provide useful analogues for bed roughness underneath contemporary ice streams, and findings from both environments can be used to inform the other.

Glacial landforms are important features from the bed of palaeo-ice sheets, as they provide information that researchers can use to reconstruct former ice. In terms of palaeo-ice streams, glacial landforms are key to defining the margins of fast ice flow, e.g., from elongation ratios or landform type. There are unanswered questions about the nature of ice stream beds, including how glacial landforms affect bed roughness, and in turn, ice velocity. To start the process of answering these questions, glacial landforms first need to be identified at the base of contemporary-ice streams so that researchers can measure how ice dynamics and the bed changes over time. A few areas of glacial landforms underneath contemporary-ice streams have been found such as the Rutford Ice Stream MSGLs from RES data with closely spaced transects (King et al., 2009, 2016). However, it is not currently feasible to carry out these high resolution RES studies over large areas. This study investigated whether different homogeneous glacial landforms have a range of bed-roughness

measurements that are unique (bed-roughness signature), which could be used by future studies to locate areas where those landforms exist underneath contemporary-ice streams. This was achieved by measuring the bed roughness and anisotropy of fields of landforms, using closely spaced grids of transects orientated parallel and orthogonal to palaeo-ice flow. This study is the first to show that groups of glacial landforms have a unique bed-roughness signature when bed-roughness anisotropy is taken into account. Anisotropy is significant for defining the bed-roughness signatures of glacial landforms because landforms with similar roughness values can be differentiated using the anisotropy measurement. However, prior knowledge of landform distribution is required in some cases to distinguish bed-roughness measurements of some landforms. The bed-roughness signatures of glacial landforms have the potential to be compared with known and unknown areas of glacial landforms at the bed of contemporary-ice streams, and this should be a priority of future research. If locations of homogeneous glacial landforms can be found at the bed of contemporary-ice streams, it could improve palaeo-ice sheet reconstruction because researchers would be able to apply the appropriate contemporary-ice flow regime to a matching deglaciated area of homogeneous glacial landforms. Bed roughness of both palaeo and contemporary ice sheets is an important metric that needs to be calculated by future studies so that researchers can understand how landforms are formed and how they affect ice dynamics.

Following this study, there are numerous recommendations for future research into ice stream bed roughness. The transect spacing of many RES surveys has been shown to be too wide to capture areas of glacial landforms. The smallest possible transect spacing is needed to get the best spatial coverage of bed roughness, but this is controlled by money, time available and the importance of aqcuiring parallel and orthogonal transects. Future studies should focus on acquiring RES transects from areas where a rough bed is inferred and where glacial landforms are thought to be located at the bed. 250 m transect spacing would be desirable but 1 km transect spacing is likely to be more practical because it would allow orthogonal and parallel transects to be acquired. Using a transect spacing of 1 km would be appropriate for macroscale glacial landforms (e.g., MSGLs), but mesoscale glacial landforms (e.g., drumlins) are likely to require smaller transect spacing. The results suggest that to define unique bed-roughness signatures over homogeneous glacial landforms, a 2 km spacing of RES transects would be adequate. However, glacial beds are not always composed of distinct areas of homogeneous glacial landforms, which should be taken into

account. Furthermore, if there is no previous knowledge of glacial landform distributions, the smallest spacing possible between transects is likely to be required.

In terms of the focus of future studies on bed-roughness of palaeo-ice streams, there are other avenues to explore. For example, this study focused on a topographically controlled palaeo-ice stream that is influenced by bedrock geology. Researchers could explore whether an ice stream that is not topographically constrained i.e. a 'pure' ice stream has a bed that shows variable bed-roughness values. A different focus would be to calculate the bed-roughness of a palaeo-ice sheet bed such as the British and Irish Ice Sheet, using a high resolution DEM. The results from such a study could be compared with findings from contemporary ice sheets and allow researchers to parametrise bed roughness in ice sheet models. Lastly, this study demonstrated that glacial landforms have unique bed-roughness signatures when anisotropy is taken into account. Future studies should test whether other sites not tested here show similar results. This would be useful because glacial landforms have a range of shapes and sizes, and it would allow bed-roughness signatures to be further refined.

This project demonstrated not only the importance of calculating bed roughness on deglaciated terrains, but also that palaeo-ice streams provide a useful analogue for contemporary-ice stream bed roughness. The bed-roughness signatures of glacial landform were defined for the first time, and future studies should focus on refining bed-roughness signatures and using them to locate glacial landforms underneath ice sheets.

Appendix A

Appendices

A.1 Examples of R scripts used for roughness calculations

All the roughness calculations in this thesis were performed using R. Examples of the scripts are shown in the following subsections. Explanations of what each line of the script does is provided following the # symbols. The file paths have been left blank and the window sizes can be changed for use in future studies.

A.1.1 Script to calculate Fast Fourier Transform (FFT) analysis

This is an example script that was used in Chapter 3 to calculate roughness using both detrending methods, along multiple transects (1D).

```
#loop to calculate roughness using Fast Fourier Transform (FFT) analysis for
#multiple transects


#Install required libraries.


library(caTools)
library(flux)
library(foreign)
library(maptools)
library(plyr)
library(psd)
```

```
library(raster)
library(rgdal)
library(scatterplot3d)
library(zoo)

window_size=32 #moving window size to calculate roughness, in data points,
#i.e. it will use 32 data points in calculations

#Have to set the working directory to where the transect files are located
#otherwise it won't work

setwd("") #put in file path where shapefile is stored
#Tell it where the transect files are located
path = "" #put in file path where shapefile is stored
#Create blank file for the loop to write to
out.file<-""
#Tell it where to write the output file to. Needs to be in a separate location
#to the input files.
outfile="" #put in file path to folder where files will be stored
file.names <- dir(path, pattern =".txt") #gets the names of all files

#loop that reads each file, then calculates the roughness for each transect
#using FFT over a moving window and writes this to individual output files.

for(i in 1:length(file.names)){
  files <- read.table(file.names[i],header=FALSE, stringsAsFactors=FALSE)
  #in data
  data.subset <- as.vector(files\$V5) #extract the elevation data
  detrended <- diff(data.subset, differences=2) #detrend the data
  PSD_result_window <- "" #empty vector to put the pspectrum output data in
  #have to call the spectra and freuency data separatley and put it into a
  #separate table. Otherwise the list produced doesn't have all the values
```

```
#stored in it.
PSD_result_window_spectra <- matrix(nrow = (nrow(files)-33),
ncol = window_size) #empty matrix to put the spectra output in
PSD_result_window_frequency <- matrix(nrow = (nrow(files)-33),
ncol = window_size) #empty matrix to put the frequency output in

 for (j in 1:length(detrended))
{
  PSD_result_window <- pspectrum(detrended[j:(window_size - 1 + j)],
  log="no") #returns the power spectral density
  PSD_result_window_spectra [j,] <- PSD_result_window\$spec
  PSD_result_window_frequency [j,] <- PSD_result_window\$freq
}
PSD_result_window_frequency2 <- na.omit(PSD_result_window_frequency)
#remove na
PSD_result_window_spectra2 <- na.omit(PSD_result_window_spectra)
#remove na
PSD_result_window_frequency3 <- as.vector(t(PSD_result_window_frequency2))
PSD_result_window_spectra3 <-as.vector(t(PSD_result_window_spectra2))
Total_Roughness_32_window <- "" #empty vector to put the pspectrum output
#data in

for (k in 1:length(PSD_result_window_spectra3)) #Now need to calculate
  #total roughness by intergrating the spectra for each window i.e.
  #integrate for each row of PSD_result_window_spectra
{
  Total_Roughness_32_window [k] <- flux::auc(PSD_result_window_frequency3
  [k:(window_size - 1 + k)], PSD_result_window_spectra3
  [k:(window_size - 1 + k)])
}

Total_Roughness_32_window2<- as.numeric(Total_Roughness_32_window)
```

```
  Total_Roughness_32_window2 <- rollapply(Total_Roughness_32_window2,
  width = 32, by = 32, FUN = mean, align = "left")
  xy <- data.frame(files\$V3, files\$V4) #data frame with the xy coordinates
  #from original file
  xy <- head(xy, -32) #remove last two values so it's the same length as
  #detrended
  xy <- data.frame(xy, Total_Roughness_32_window2) #data frame with xy
  #coordinates and roughness values
  out.file <- rename(xy, c("files.V3"="X", "files.V4"="Y",
  "Total_Roughness_32_window2"="Roughness")) #change column names to x and
  #y coordinates
  filename <- file.names[i]
  tn <- unlist(strsplit(filename,"[.]")[[1]][1]) #separate filename and keep
  #the first half e.g. t1.txt becomes t1
  fn <- paste(tn, "_rough.dbf", sep="") #create new filename
  write.dbf(out.file, file.path(paste0(outfile,fn)), factor2char = TRUE)
  #out file placed in separate folder to working directory
}
```

A.1.2 Script to calculate Standard Deviation (SD)

This is an example script that was used in Chapter 5 to calculate roughness using both detrending methods, along multiple transects (1D). The input shapefile is made using Qchainage, as detailed in section 5.4.1.1.

```
#This script is to split a point grid shapefile into multiple transects and
#calculate roughness using SD


rm(list = ls()) #clear the environment tab. Needs to be done otherwise final
#shapefiles will include previous sites


#First set the working directory:
setwd("")  #put in file path where shapefile is stored
```

```
#Then install required libraries.
library(bioimagetools)
library(Rcpp)
library(plyr)
library(caTools)
library(PBSmapping)
library(raster)
library(maptools)
library(foreign)
library(raster)
library(rgdal)

#Now identify the path where the input data is
infile=""  #put in file path where shapefile is stored

#Import point data and put in correct format

data=importShapefile(infile) #shapefile with xy coordinates, but no
#elevation values
data2=data[,c(2,3)] #Isolate the xy coordinates to use in the extract
#function
data2=data.matrix(data2) #Convert data to correct format for extract
#function, first into a matrix
data_sp=SpatialPoints(data2) #Then convert to a spatial points file
result=data.frame() #Blank data frame for extracted data

#Import raster to extract elevation values from

infile="" #file path where DEM is stored
raster_Ullapool=raster(infile) #import DEM
newproj <- "+proj=tmerc +lat_0=49 +lon_0=-2 +k=0.9996012717 +x_0=400000
+y_0=-100000 +ellps=airy +datum=OSGB36 +units=m +no_defs"
```

```
raster_Ullapool2=projectRaster(raster_Ullapool, crs=newproj) #Make sure
#raster is in correct projection to point data
result<-extract(raster_Ullapool2, data_sp, method='simple', df=TRUE)
#Extract DEM data using points

data <- data.frame(data, result$w001001) #Combine original point file data
#and DEM data
data <- rename(data, c("result.w001001" = "RASTERVALU")) #Change the name of
#DEM data column

#Individual tansects are will now be extracted from the point grid shapefile
#prepare the data, and create objects needed to loop the data

data <-data[,c(2, 3, 4, 5, 6)] #Selects the columns required i.e. X, Y,
#Rastervalu
file.names <- seq(1:84) #1km grid. Sequence of numbers used to name each
#transect
file.names <- file.names[-(35:36)] #remove any transects that are smaller than
#window size
file.names <- file.names[-(1)]
outfile="" #put in file path to folder where individual transects will be stored
result <- data.frame(stringsAsFactors = FALSE) #empty data frame for results

#Split into individual transects

uniq <- unique(unlist(data$fid))
for (i in 1:length(uniq)){
  result <- subset(data, fid == uniq[i])
  filename <- file.names[i] #number selected to name each indivdual transect
  fn <- paste(filename, ".txt", sep="") #create new filename
  write.csv(result, file.path(paste0(outfile,fn)))#out file placed in separate
  #folder to working directory
```

```
}

#Need to separate transect files into orthogonal and parallel folders before next
#step.

#Move orthogonal transects to orthogonal folder

# identify the folders
current.folder <- "" #put in file path for all individual transects
new.folder <- "" #put in file path for just orthogonal transects
setwd("") #put in file path for all individual transects
list.of.files <- paste(37:84, ".txt", sep = "") #names of files required
# copy the files to the new folder
file.copy(list.of.files, new.folder, overwrite = TRUE)

#Move parallel transects to parallel folder

# identify the folders
current.folder <- "" #put in file path for all individual transects
new.folder <- "" #put in file path for just parallel transects
setwd("") #put in file path for all individual transects
list.of.files <- paste(2:34, ".txt", sep = "") #names of files required
# copy the files to the new folder
file.copy(list.of.files, new.folder, overwrite = TRUE)

##########################################################################
#Calculate roughness for orthogonal transects

#window size (number of data points)
runm_win=20 #100 m window for a resolution of 5m

#Have to set the working directory to where the txt files are located
```

```
#otherwise it won't work
setwd("") #put in file path for just orthogonal transects
#Tell it where the files are located
path = "" #put in file path for just orthogonal transects
#Create blank file for the loop to write to
out.file<-""
#Tell it where to write the output file to. Needs to be in a separate
#location to the input files.
outfile="" #put in file path for orthogonal transects output
file.names <- dir(path, pattern =".txt") #gets the names of all files

#loop that reads each file, then calculates the roughness for each transect
#using SD over a moving window and writes this to individual output files.
#Detrend method = mean


for(i in 1:length(file.names)){
  files <- read.table(file.names[i], header=TRUE, sep =",",
  stringsAsFactors = FALSE) #in data
  data.subset <- as.vector(files$RASTERVALU) #extract the elevation data
  mean <- runmean(data.subset,runm_win,endrule='NA') #detrend the data
  detrended <- data.subset-mean
  runstd <- runsd(detrended, runm_win, endrule = 'NA')
  xy <- data.frame(files$X, files$Y) #data frame with the xy coordinates from
  #original file
  xy <- data.frame(xy, detrended, runstd) #data frame with xy coordinates and
  #roughness values
  xy <- na.omit(xy) #removed the na values at beginning and end of file
  #padded from running sd
  #calculations i.e. same number of na values as window size at beginning and
  #end of file)
  out.file <- rename(xy, c("files.X"="X", "files.Y"="Y", "runstd"="Roughness"))
```

```
  #change column names to x and y coordinates
  filename <- file.names[i]
  tn <- unlist(strsplit(filename,"[.]")[[1]][1]) #separate filename and keep the
  #first half e.g. t1.txt becomes t1
  fn <- paste(tn, "_rough.txt", sep="") #create new filename
  write.csv(out.file, file.path(paste0(outfile,fn)))#out file placed in separate
  #folder to working directory
}

#Repeat the above section for parallel transects (copy and paste script and
#change infiles and outfiles

################################################################################


#Run the same code, but for the difference detrend method. Orthogonal
#transects.

#window size (number of data points)
runm_win=20 #100 m window for a resolution of 5m

#Have to set the working directory to where the txt files are located
#otherwise it won't work

setwd("") #put in file path for just orthogonal transects

#Tell it where the files are located
path = "" #put in file path for just orthogonal transects

#Create blank file for the loop to write to
out.file<-""
#Tell it where to write the output file to. Needs to be in a separate location
```

```
#to the input files.
outfile="" #put in file path for orthogonal transects output

file.names <- dir(path, pattern =".txt") #gets the names of all files

#loop that reads each file, then calculates the roughness for each transect
#using SD over a moving window and writes this to individual output files.

for(i in 1:length(file.names)){
  files <- read.table(file.names[i],header=TRUE, sep = ",",
  stringsAsFactors=FALSE) #in data
  data.subset <- as.vector(files$RASTERVALU) #extract the elevation data
  detrended <- diff(data.subset, differences=2) #detrend the data
  runstd <- runsd(detrended, runm_win, endrule = 'NA')
  xy <- data.frame(files$X, files$Y) #data frame with the xy coordinates from
  #original file
  xy <- head(xy, -2) #remove last two values so it's the same length as
  #detrended
  xy <- data.frame(xy, detrended, runstd) #data frame with xy coordinates and
  #roughness values
  xy <- na.omit(xy) #removed the na values at beginning and end of file
  #(padded from running sd calculations i.e. same number of na values as window
  #size at beginning and end of file)
  out.file <- rename(xy, c("files.X"="X", "files.Y"="Y", "runstd"="Roughness"))
  #change column names to x and y coordinates
  filename <- file.names[i]
  tn <- unlist(strsplit(filename,"[.]")[[1]][1]) #separate filename and keep
  #the first half
  #e.g. t1.txt becomes t1
  fn <- paste(tn, "_rough.txt", sep="") #create new filename
  write.csv(out.file, file.path(paste0(outfile,fn)))#out file placed in
  #separate folder to working directory
```

```
}

#Repeat the above section for parallel transects (copy and paste script and
#change infiles and outfiles

################################################################################
#Finally, shapefiles can be created from by merging all of the individual
#transects that now have roughness data

#Merge all transects into one data frame so this can be converted into a
#shapefile.

rm(list = ls()) #clear the environment tab. Needs to be done otherwise final
#shapefiles will include previous sites
setwd("") #put in file path for just orthogonal transects with mean detrended
#data
file_list <- list.files(pattern = ".txt")

for (file in file_list){

  # if the merged dataset doesn't exist, create it
  if (!exists("all_orthogonal_transects")){
    all_orthogonal_transects <- read.table(file, header=TRUE, sep=",")
  }

  # if the merged dataset does exist, append to it
  if (exists("all_orthogonal_transects")){
    temp_dataset <-read.table(file, header=TRUE, sep=",")
    all_orthogonal_transects<-rbind(all_orthogonal_transects, temp_dataset)
    rm(temp_dataset)
  }
```

```
}

outfile = "" #file path and name of new shapefile
xy <- all_orthogonal_transects [,c(2, 3)]
shapefile <- SpatialPointsDataFrame(xy, all_orthogonal_transects,
proj4string = CRS("+proj=tmerc+lat_0=49 +lon_0=-2 +k=0.9996012717 +x_0=400000
+y_0=-100000 +ellps=airy +datum=OSGB36 +units=m +no_defs")) #create shapefile
filename = "Roughness_100m_win" #shapefile name
writeOGR(shapefile, outfile, filename, driver = "ESRI Shapefile",
overwrite_layer = TRUE) #output shapefile

#repeat for parallel data, and difference detrended roughness data (copy and
paste script and change infiles and outfiles
```

A.1.3 Example script to calculate roughness using a raster (DEM)

The following script is used to calculate roughness using the SD method with mean detrended data. The script calculates roughness using the rows and columns of a raster.

```
#This script is to calculate roughness for rows and columns of a raster

#Install required libraries.

library(raster)
library(rgdal)
library(caTools)
library(plyr)
library(maptools)
library(foreign)
library(PBSmapping)
library(scatterplot3d)
library(rio)
library(purrr)
```

```
setwd("")  #put in file path where DEM is stored
dtm <- raster("") #put in file name of DEM

cells <-cellFromRowColCombine(dtm, 1:200, 1:200) #gives cell numbers for all
#rows and columns
xy <- xyFromCell(dtm, cells) #extract xy coordinate data
dtm_vals <- extract(dtm, xy) #extract xy coordinate data and elevation values
dtm_vals_xy <-data.frame(xy, dtm_vals) #create data frame from xy coordinate
#data and elevation values

#For the horizontal transects

#Calculate roughness for dtm values
#Prepare the data, and create objects needed to loop the data

file.names <- seq(1:200) #Sequence of numbers used to name each transect
window=199 #moving window size to separate dtm into transects using rows
#and columns
step=200 #step size
total <- nrow(dtm_vals_xy) #total length of dtm
spots <- seq(from=1, to=(total-window), by=step) #sequence used to create
#moving window
result <- data.frame(stringsAsFactors = FALSE) #empty data frame for results
#Create blank file for the loop to write to
out.file<-""
outfile="" #Tell it where to write the output files to.
runm_win=20 #moving window size for detrending and roughness calculations
file.names <- seq(from=1, to=200, by=1) #names of output files


for(i in 1: length(spots)) {
```

```
  result <- dtm_vals_xy[spots[i]:(spots[i]+window), ] #selects the first 200
  #lines, and then the next 200, and so on
  mean <- runmean(result$dtm_vals,runm_win,endrule='NA') #detrend the data
  detrended <- result$dtm_vals-mean
  runstd <- runsd(detrended, runm_win, endrule = 'NA')
  xy <- data.frame(result$x, result$y) #data frame with the xy coordinates
  #from original file
  xy <- data.frame(xy, detrended, runstd) #data frame with xy coordinates
  #and roughness values
  xy <- na.omit(xy) #removed the na values at beginning and end of file
  #(padded from running sd calculations i.e. same number of na values as
  #window size at beginning and end of file)
  out.file <- rename(xy, c("result.x"="x", "result.y"="y",
  "runstd"="Roughness")) #change column names to x and y coordinates
  filename <- file.names[i]
  fn <- paste(filename, "_transect_rough.txt", sep="") #create new filename
  write.csv(out.file, file.path(paste0(outfile,fn)))#out file placed in
  #separate folder to working directory
}

##############################################################################
#For the vertical transects

#Calculate roughness for dtm values
#prepare the data, and create objects needed to loop the data

dtm_vals_xy <-arrange(dtm_vals_xy, x) #Reorders the rows in ascending order
#using the X coordinates.
file.names <- seq(1:200) #Sequence of numbers used to name each transect
window=199 #moving window size to separate dtm into transects using rows
#and columns
step=200 #step size
```

```
total <- nrow(dtm_vals_xy) #total length of dtm
spots <- seq(from=1, to=(total-window), by=step) #sequence used to create moving
#window
result <- data.frame(stringsAsFactors = FALSE) #empty data frame for results
#Create blank file for the loop to write to
out.file<-""
outfile="" #Tell it where to write the output files to.
runm_win=20 #moving window size for detrending and roughness calculations
file.names <- seq(from=1, to=200, by=1) #names of output files

for(i in 1: length(spots)) {
  result <- dtm_vals_xy[spots[i]:(spots[i]+window), ] #selects the first 200
  #lines, and then the next 200, and so on
  mean <- runmean(result$dtm_vals,runm_win,endrule='NA') #detrend the data
  detrended <- result$dtm_vals-mean
  runstd <- runsd(detrended, runm_win, endrule = 'NA')
  xy <- data.frame(result$x, result$y) #data frame with the xy coordinates
  #from original file
  xy <- data.frame(xy, detrended, runstd) #data frame with xy coordinates and
  #roughness values
  xy <- na.omit(xy) #removed the na values at beginning and end of file
  #(padded from running sd calculations i.e. same number of na values as window
  #size at beginning and end of file)
  out.file <- rename(xy, c("result.x"="x", "result.y"="y",
  "runstd"="Roughness"))
  #change column names to x and y coordinates
  filename <- file.names[i]
  fn <- paste(filename, "_transect_rough.txt", sep="") #create new filename
  write.csv(out.file, file.path(paste0(outfile,fn)))#out file placed in
  #separate folder to working directory
}
```

```
################################################################################

#Merge all transects into one data frame so this can be converted into a
#raster.

setwd("") #put in file path for horizontal transects
file_list <- list.files()

for (file in file_list){

  # if the merged dataset doesn't exist, create it
  if (!exists("all_horizontal_transects")){
    all_horizontal_transects <- read.table(file, header=TRUE, sep=",")
  }

  # if the merged dataset does exist, append to it
  if (exists("all_horizontal_transects")){
    temp_dataset <-read.table(file, header=TRUE, sep=",")
    all_horizontal_transects<-rbind(all_horizontal_transects, temp_dataset)
    rm(temp_dataset)
  }

}

setwd("") #put in file path for vertical transects
file_list <- list.files()

for (file in file_list){

  # if the merged dataset doesn't exist, create it
  if (!exists("all_vertical_transects")){
```

```
    all_vertical_transects <- read.table(file, header=TRUE, sep=",")
  }

  # if the merged dataset does exist, append to it
  if (exists("all_vertical_transects")){
    temp_dataset <-read.table(file, header=TRUE, sep=",")
    all_vertical_transects<-rbind(all_vertical_transects, temp_dataset)
    rm(temp_dataset)
  }

}

#sort the data for raster output

#organise correct data into data frames
all_h_detrended <-all_horizontal_transects[,c(2, 3, 4)]
all_h_roughness <-all_horizontal_transects[,c(2, 3, 5)]
all_v_detrended <-all_vertical_transects[,c(2, 3, 4)]
all_v_roughness <-all_vertical_transects[,c(2, 3, 5)]

#create raster from data frames
all_h_detrended_rast <-rasterFromXYZ(all_h_detrended)
all_h_roughness_rast <-rasterFromXYZ(all_h_roughness)
all_v_detrended_rast <-rasterFromXYZ(all_v_detrended)
all_v_roughness_rast <-rasterFromXYZ(all_v_detrended)

setwd("") #put in file path for output of rasters

#output rasters

writeRaster(all_h_detrended_rast, "horizontal_detrended", format = "GTiff")
writeRaster(all_h_roughness_rast, "horizontal_roughness", format = "GTiff")
```

```
writeRaster(all_v_detrended_rast, "vertical_detrended", format = "GTiff")
writeRaster(all_v_roughness_rast, "vertical_roughness", format = "GTiff")
```

A.2 Cluster analysis statistics

The percentage accuracy of the cluster analysis placing the data associated with each site in the correct landform groups is presented below. The percentages that were reported in the captions of Figs. 5.47 - 5.50 were taken from these statistics. The statistics were produced using the confusionMatrix function in R. The first table (confusion matrix) has the real values (truth) in the columns and the predicted values from the cluster analysis (pred). Confusion matrices were only produced for Figs. 5.47c - 5.50c and not Figs. 5.47d - 5.50d. This was because an equal number of cluster groups and landform groups are needed to use the confusionMatrix function.

A.2.1 Statistics for Fig. 5.47c

Statistics for cluster analysis where all sites were used except site 5. The data used were roughness and anisotropy derived using a 1 km moving window.

```
Confusion Matrix and Statistics


          truth
pred       Site 1 Site 2 Site 3 Site 4 Site 6
  Site 1      31      0    430      0     62
  Site 2       3     95      0      0     81
  Site 3      92      0    423      0     47
  Site 4       0      0      0    495      0
  Site 6       0      0    138      0     90


Overall Statistics

                Accuracy : 0.5707
                  95% CI : (0.5486, 0.5926)
```

```
    No Information Rate : 0.4987
    P-Value [Acc > NIR] : 7.586e-11

                  Kappa : 0.4349
 Mcnemar's Test P-Value : NA

Statistics by Class:
```

	Site 1	Site 2	Site 3	Site 4	Site 6
Sensitivity	0.24603	1.00000	0.4268	1.0000	0.32143
Specificity	0.73563	0.95560	0.8604	1.0000	0.91916
Pos Pred Value	0.05927	0.53073	0.7527	1.0000	0.39474
Neg Pred Value	0.93511	1.00000	0.6014	1.0000	0.89198
Prevalence	0.06341	0.04781	0.4987	0.2491	0.14092
Detection Rate	0.01560	0.04781	0.2129	0.2491	0.04529
Detection Prevalence	0.26321	0.09009	0.2828	0.2491	0.11475
Balanced Accuracy	0.49083	0.97780	0.6436	1.0000	0.62029

A.2.2 Statistics for Fig. 5.48c

Statistics for cluster analysis where sites 1 - 4 were used. The data used were roughness and anisotropy derived using a 1 km moving window.

```
Confusion Matrix and Statistics

          truth
pred      Site 1 Site 2 Site 3 Site 4
  Site 1    110      0    487      0
  Site 2      0     95      0      0
  Site 3     16      0    504      0
  Site 4      0      0      0    495

Overall Statistics
```

```
               Accuracy : 0.7053
                 95% CI : (0.6831, 0.7269)
    No Information Rate : 0.5806
    P-Value [Acc > NIR] : < 2.2e-16

                  Kappa : 0.5851
 Mcnemar's Test P-Value : NA
```

Statistics by Class:

	Site 1	Site 2	Site 3	Site 4
Sensitivity	0.87302	1.00000	0.5086	1.00
Specificity	0.69197	1.00000	0.9777	1.00
Pos Pred Value	0.18425	1.00000	0.9692	1.00
Neg Pred Value	0.98559	1.00000	0.5897	1.00
Prevalence	0.07381	0.05565	0.5806	0.29
Detection Rate	0.06444	0.05565	0.2953	0.29
Detection Prevalence	0.34974	0.05565	0.3046	0.29
Balanced Accuracy	0.78249	1.00000	0.7431	1.00

A.2.3 Statistics for Fig. 5.49c

Statistics for cluster analysis where all sites were used except site 5. The data used were roughness and anisotropy derived using a 100 m moving window.

Confusion Matrix and Statistics

	truth				
pred	Site 1	Site 2	Site 3	Site 4	Site 6
Site 1	301	40	51	0	28
Site 2	111	0	393	0	24
Site 3	0	0	332	0	0
Site 4	13	65	0	636	93
Site 6	36	21	179	0	277

```
Overall Statistics

               Accuracy : 0.5946
                 95% CI : (0.5755, 0.6136)
    No Information Rate : 0.3673
    P-Value [Acc > NIR] : < 2.2e-16

                  Kappa : 0.4975
 Mcnemar's Test P-Value : NA
```

Statistics by Class:

	Site 1	Site 2	Site 3	Site 4	Site 6
Sensitivity	0.6529	0.00000	0.3476	1.0000	0.6564
Specificity	0.9444	0.78658	1.0000	0.9129	0.8916
Pos Pred Value	0.7167	0.00000	1.0000	0.7881	0.5400
Neg Pred Value	0.9266	0.93919	0.7253	1.0000	0.9305
Prevalence	0.1773	0.04846	0.3673	0.2446	0.1623
Detection Rate	0.1158	0.00000	0.1277	0.2446	0.1065
Detection Prevalence	0.1615	0.20308	0.1277	0.3104	0.1973
Balanced Accuracy	0.7986	0.39329	0.6738	0.9565	0.7740

A.2.4 Statistics for Fig. 5.50c

Statistics for cluster analysis where sites 1 - 4 were used. The data used were roughness and anisotropy derived using a 100 m moving window.

```
Confusion Matrix and Statistics

          truth
pred      Site 1 Site 2 Site 3 Site 4
  Site 1    348     40     71      0
  Site 2     63      6    467      0
```

```
  Site 3     27      0    417      0
  Site 4     23     80      0    636

Overall Statistics

               Accuracy : 0.646
                 95% CI : (0.6255, 0.6661)
    No Information Rate : 0.4385
    P-Value [Acc > NIR] : < 2.2e-16

                  Kappa : 0.5297
 Mcnemar's Test P-Value : NA

Statistics by Class:

                         Site 1      Site 2         Site 3        Site 4
Sensitivity              0.7549      0.047619       0.4366        1.0000
Specificity              0.9354      0.741715       0.9779        0.9332
Pos Pred Value           0.7582      0.011194       0.9392        0.8606
Neg Pred Value           0.9343      0.926918       0.6897        1.0000
Prevalence               0.2117      0.057851       0.4385        0.2920
Detection Rate           0.1598      0.002755       0.1915        0.2920
Detection Prevalence     0.2107      0.246097       0.2039        0.3393
Balanced Accuracy        0.8451      0.394667       0.7073        0.9666
```

A.3 Published version of Chapter 4

Journal of Glaciology (2018), **64**(247) 822–834 doi: 10.1017/jog.2018.71

Quantifying bed roughness beneath contemporary and palaeo-ice streams

FRANCESCA A.M. FALCINI,[1] DAVID M. RIPPIN,[1] MAARTEN KRABBENDAM,[2] KATHERINE A. SELBY[1]

[1]*Environment Department, Wentworth Way, University of York, Heslington, York, YO10 5NG, UK*
[2]*British Geological Survey, The Lyell Centre, Research Avenue South, Edinburgh, EH14 4AP, UK*
Correspondence: Francesca A.M. Falcini <famf500@york.ac.uk>

ABSTRACT. Bed roughness is an important control on ice-stream location and dynamics. The majority of previous bed roughness studies have been based on data derived from radio-echo sounding (RES) transects across Antarctica and Greenland. However, the wide spacing of RES transects means that the links between roughness and flow are poorly constrained. Here, we use Digital Terrain Model/bathymetry data from a well-preserved palaeo-ice stream to investigate basal controls on the behaviour of contemporary ice streams. Artificial transects were set up across the Minch Palaeo-Ice Stream (NW Scotland) to mimic RES flight lines over Institute and Möller Ice Streams (Antarctica). We then explored how different data-resolution, transect orientation and spacing, and different methods, impact roughness measurements. Our results show that fast palaeo-ice flow can occur over a rough, hard bed, not just a smooth, soft bed, as previous work has suggested. Smooth areas of the bed occur over both bedrock and sediment covered regions. Similar trends in bed roughness values were found using Fast Fourier Transform analysis and standard deviation methods. Smoothing of bed roughness results can hide important details. We propose that the typical spacing of RES transects is too wide to capture different landform assemblages and that transect orientation influences bed roughness measurements in both contemporary and palaeo-ice-stream setting.

KEYWORDS: geomorphology, ice streams, radio-echo sounding, remote sensing

1. INTRODUCTION

This paper aims to measure the bed roughness of contemporary subglacial and deglaciated terrains at analogous length scales. We define bed roughness as the vertical variation of terrain over a given horizontal distance (Siegert and others, 2005; Rippin and others, 2011). Accurate quantification of bed roughness beneath ice sheets is important because it is a primary control on basal drag and therefore ice flow velocity (Siegert and others, 2005; Bingham and others, 2017). Subglacial obstacles of ~0.5–1 m in both amplitude and horizontal wavelength have been shown theoretically to exert critical basal drag (Weertman, 1957; Kamb, 1970; Nye, 1970; Hubbard and Hubbard, 1998; Hubbard and others, 2000; Schoof, 2002); however, these obstacle dimensions lie below the resolution achievable by radio-echo sounding (RES) across ice sheets. Several authors have nevertheless explored the relationship of higher amplitude (several 100 m) and longer wavelength (hundreds of m to several km) bed roughness and ice dynamics across ice sheets using available RES data. These analyses have suggested that beds beneath contemporary ice streams are relatively smooth, with roughness values decreasing downstream, whilst in surrounding areas of slower ice flow, the beds are relatively rougher (Siegert and others, 2004; Rippin and others, 2006, 2011; Callens and others, 2014). As a consequence, basal roughness is regarded as one of the controls on ice-stream location, in particular for ice streams not topographically controlled by deep valleys (Siegert and others, 2004; Bingham and Siegert, 2009; Winsborrow and others, 2010; Rippin, 2013).

While a relationship between bed roughness and ice dynamics is intuitive, quantifying such a relationship has proved elusive and several studies have produced findings that should be explored further. For example, it has been observed that fast flowing ice can also occur over a rough, hard bed (Schroeder and others, 2014). The reasons for a smooth bed underneath fast-flowing ice can be varied, for example the existence of fine-grained sediments vs. streamlined topography (Li and others, 2010; Rippin and others, 2014). Ice-stream beds can be smooth along ice flow (parallel) and rough across flow (orthogonal) (King and others, 2009; Bingham and others, 2017), showing that the direction of bed roughness measurements is extremely important. Palaeo-ice-stream beds show the same pattern (Gudlaugsson and others, 2013; Lindbäck and Pettersson, 2015). Geology can have a strong control on the roughness underneath fast-flowing ice as shown in previously glaciated gneiss terrains (Krabbendam and Bradwell, 2014). An increase in landform elongation ratios in a palaeo-ice stream has been related to the change from a rough to smooth bed (Bradwell and Stoker, 2015). The points raised by these studies demonstrate that bed roughness and its relationship to ice dynamics is complex. By using Digital Terrain Models (DTMs) from now-exposed palaeo-ice streams to calculate bed roughness, we propose that it may be possible to explore these complexities in more detail because the bed of a palaeo-ice stream can be directly observed over its entirety at much higher spatial resolutions than contemporary ice-stream beds.

The bed roughness of contemporary ice sheets has been calculated along 1-D topographic profiles (from RES tracks) predominantly using two different approaches, frequency domain methods for example Fast Fourier Transform (FFT) analysis (e.g. Taylor and others, 2004; Siegert and others, 2005; Bingham and Siegert, 2007; Li and others, 2010; Rippin, 2013) and space domain methods for example Standard Deviation (SD) (Layberry and Bamber, 2001; Rippin and others, 2014). Radar specularity has also been used to infer bed roughness (e.g. Schroeder and others, 2014). The scale of bed roughness measurements has mostly been controlled by the spacing between flight tracks, and the along-track resolution, which is a function of the radar system used. Ice-sheet scale studies have typically used track spacing of several kilometres with an along track resolution of a few metres (Siegert and others, 2004; Rippin and others, 2006; Bingham and others, 2007). Higher resolution radar imaging by King and others (2009, 2016) and Bingham and others (2017) has shown topographic detail that cannot be captured by the larger scale studies, and is similar to the detail available on deglaciated terrains from DTMs and bathymetric data unconstrained by ice cover (e.g. Perkins and Brennand, 2014; Bradwell and Stoker, 2015; Margold and others, 2015). Using DTMs also allows bed roughness to be measured in 2-D and at much smaller scales. The resolution of DTMs is becoming finer, with pixels down to a few metres or less (e.g. LiDAR; Salcher and others, 2010; Putkinen and others, 2017). Analysis of DTMs from deglaciated areas provides an opportunity to show what is being missed when bed roughness measurements are interpolated across widely spaced RES transects. Bed roughness calculations made on this terrain can also be much more easily linked to the geomorphological and geological character of the bed because individual landforms and geological variation can be observed directly.

In this study, we compare the bed roughness of the deglaciated, Devensian, Minch Palaeo-Ice Stream (MPIS) and surrounding areas in NW Scotland, with the contemporary Institute and Möller Ice Streams (IMIS) in West Antarctica. The bed roughness of both ice streams is quantified along transects with the same grid spacing, but for the palaeo-ice stream is also calculated between transects. We test how several parameters influence the measurement and interpretation of bed roughness. Firstly, we gauge whether the method used to measure bed roughness, FFT analysis or SD, produces different results. Secondly, we explore whether RES track spacing is sufficient to capture bed roughness trends. Thirdly, we compare bed-roughness results from transects that have the same grid spacing as RES data with results calculated down to the DTM pixel resolution. Finally, we show how the orientation of transects in relation to ice flow direction influences bed-roughness results.

2. DATA AND METHODS

2.1. Study sites and data

The MPIS drained the NW sector of the British and Irish Ice Sheet during the Devensian (Weichselian) Glacial Period (116–11.5 ka BP) and has a well-documented glacial landform and sediment record (Bradwell and others, 2008a; Bradwell and Stoker, 2015; Fig. 1). Its onset zone lies in the mountainous NW Highlands of mainland Scotland, with peaks up to ~1000 m above present-day sea level (m a.s.l.). At its maximum extent, several ice-stream tributaries flowed from breaches (at ~300 m a.s.l.) in the present-day watershed in the NW Highlands mainland out to the shelf edge, at ~200 m below present-day sea level (Bradwell and others, 2007, 2016; Bradwell and Stoker, 2015; Krabbendam and others, 2016). MPIS likely reached its maximum extent at ~26–28 ka (Chiverrell and Thomas, 2010; Clark and others, 2012; Praeg and others, 2015; Bradwell and others, 2016).

IMIS drain the West Antarctic Ice Sheet into Ronne Ice Shelf (Fig. 1). Ice surface velocities are up to 400 m a^{-1} (Rignot and others, 2011). The inferred occurrence of sediments at the bed of Institute Ice Stream has been interpreted to be associated with a smooth bed (Bingham and Siegert, 2007; Siegert and others, 2016). The Ellsworth Trough Tributary, a tributary of Institute Ice Stream, is topographically controlled (Ross and others, 2012).

We compare MPIS with IMIS due to their relatively comparable scale. IMIS ice thickness varies between ~50 and 3000 m (Fretwell and others, 2013). A maximum ice thickness of 750–1000 m has been modelled for MPIS (Hubbard and others, 2009; Kuchar and others, 2012). IMIS drain an area of 140 000 km^2 and 66 000 km^2, respectively (Bingham and Siegert, 2009), While MPIS drained an area of 15 000–20 000 km^2 (Bradwell and others, 2007; Bradwell and Stoker, 2015). Institute Ice Stream is up to 82 km wide and the fast flowing section of the main trunk is 100 km long (Scambos and others, 2004). MPIS was 40–50 km wide and 200 km long in total (Bradwell and Stoker, 2015). MPIS had a discharge flux of 12–20 Gt a^{-1} (Bradwell and Stoker, 2015) compared with 21.6 and 6.4 Gt a^{-1} for IMIS, respectively (Joughin and Bamber, 2005).

For contemporary ice streams in Antarctica, the data used were RES transects with an along track resolution of 10 m, and a grid spacing of 30 × 10 km (Rippin and others, 2014). Data were acquired in the 2010/11 austral summer using the Polarimetric Airborne Survey Instrument (PASIN) with a frequency of 150 MHz (Ross and others, 2012). PASIN has retrieved bed-echoes through 4200 m thick ice (Vaughan and others, 2006). Crossover analysis gave RMS differences of 18.29 m for ice thickness (Ross and others, 2012). The location of the data was determined using a differential GPS with a horizontal accuracy of ~5 cm. The reflections returned from the ice-stream bed were processed semi-automatically. The ice thickness (calculated every ~10 m) was subtracted from ice surface elevations to calculate the bed elevations (Ross and others, 2014). For more detail on acquisition and processing of the RES data see Rippin and others (2014) and Ross and others (2012, 2014). This dataset was used by Rippin and others (2014) to calculate bed roughness using both FFT analysis and SD.

Two high-resolution datasets were used to calculate bed roughness of the MPIS. For the onshore area, the NEXTMap DTM with a 5 m horizontal resolution and a 1 m vertical resolution, was used (Bradwell, 2013). NEXTMap DTM tiles were downloaded from the Centre for Environmental Data Analysis (CEDA) Archive (Intermap Technologies, 2009). For the offshore area, Bathymetric Multi-Beam Echosounder Survey data (MBES) were used. The MBES data subset has a resolution of 4 m and encompasses the Little Minch and the southern area of The Minch (Fig. 1). The surveys around NW Scotland were undertaken by the Maritime & Coastguard Agency (MCA) between 2006 and 2012. For more detail on acquisition and processing of MBES data see Bradwell and Stoker (2015) or the Reports

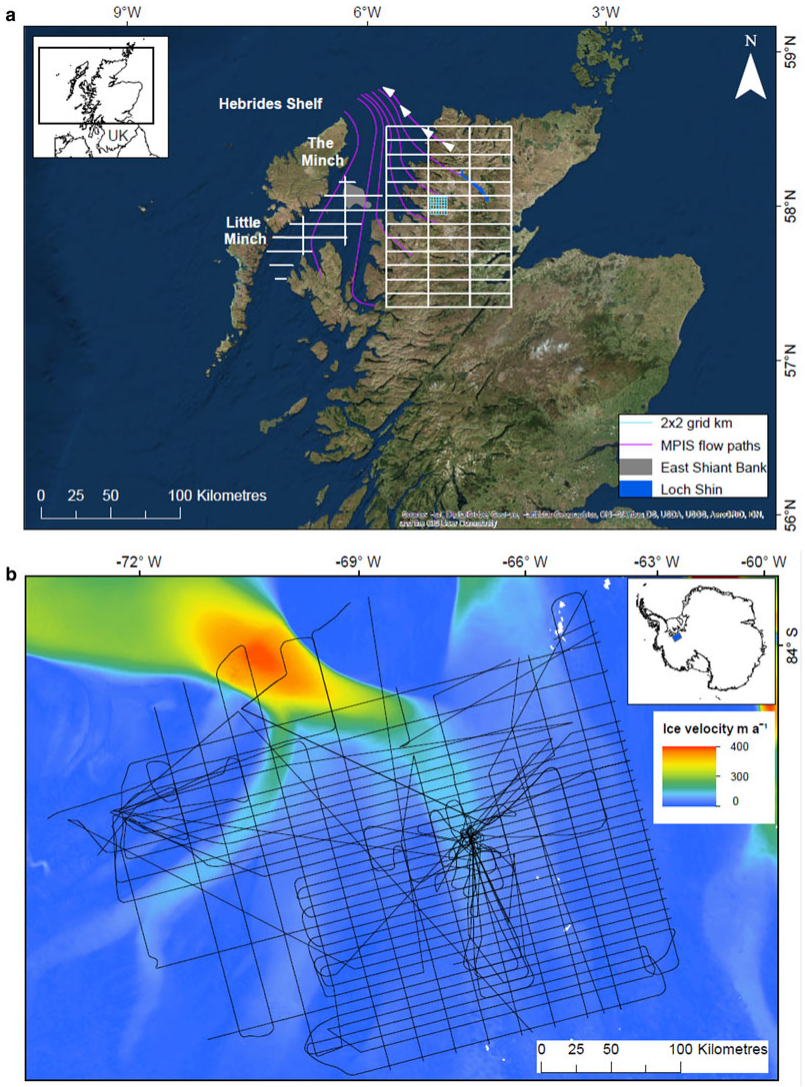

Fig. 1. Study site locations. (a) The Minch Palaeo-Ice Stream (MPIS), in NW Scotland. MPIS flow paths, that is areas of fast-flowing ice, are from Bradwell and others, (2007). The flow path with white arrows is the Laxfjord tributary. The coarse grid (30 × 10 km) set up to mimic RES transects in (b), is shown in white. The fine grid (2 × 2 km) is over the Ullapool megagroove area and is shown in cyan. Inset map shows the location of the main image. (b) Institute and Möller Ice Streams (IMIS), in West Antarctica. RES transects are shown in black. The inset map shows the location of IMIS (blue box). Ice velocity from Rignot and others (2011) and Mouginot and others, (2012).

of Survey, which can be requested from MCA, the UK Hydrographic Office, the British Geological Survey or the Natural Environment Research Council. MPIS is characterised by numerous elongate landforms that show a higher elongation ratio than those in adjacent areas (Bradwell and others, 2008b). Onshore, the bed of the palaeo-ice stream is dominated by bedrock (i.e. hard-bed) landforms (Krabbendam and Bradwell, 2010; Clark and others, 2018) including bedrock megagrooves, crag and tails, whalebacks and roches moutonnées (partly within a cnoc-and-lochan landscape, especially characteristic of Scotland's northwest region, Assynt), with few soft-sediment covered landforms (e.g. Bradwell and others, 2007; Bradwell, and others, 2008b; Krabbendam and Bradwell, 2011; Bradwell, 2013). In the Minch and further offshore on the Hebrides Shelf, the bed of the palaeo-ice stream comprises more soft-sediment landforms, such as drumlinoid features, although streamlined bedrock, crag-and-tail features and megagrooves are also present, particularly in the inner Minch (Bradwell and Stoker, 2015, 2016; Ballantyne and Small, 2018). Overdeepened basins occur, in particular, close to the present-day coast, which is in part characterised by a

fjord system (Bradwell and Stoker, 2016; Bradwell and others, 2016). Increases in ice velocity are inferred from changes to landform elongation ratios located on the central Minch inner shelf (East Shiant Bank), which Bradwell and Stoker (2015) suggested is caused by the bed substrate changing from rough bedrock to smooth sediment.

2.2. Methods

Bed roughness along RES tracks in the Antarctic ice sheet and Greenland ice sheet has predominantly been quantified using either FFT analysis (e.g. Bingham and Siegert, 2009; Rippin, 2013; Rippin and others, 2014), or SD of bed elevations (e.g. Layberry and Bamber, 2001; Rippin and others, 2014). FFT analysis transforms bed elevations into wavelength spectra (Gudlaugsson and others, 2013), producing a power spectrum (Bingham and Siegert, 2009), which is a measure of the intensity (power) of different wavelength obstacles along a transect. SD is a measure of variation in amplitude. Applied to elevation data, a higher SD implies a greater spread between the high and low elevations, and thus a rougher bed. Both methods were used on MPIS and IMIS datasets to provide a comparison.

Both roughness methods were applied to a 2-D dataset from a deglaciated terrain, MPIS, and were compared with a 1-D dataset from a glaciated terrain, IMIS. We constructed an 'artificial' grid of transects spaced 30 × 10 km apart over the high-resolution NEXTMap DTM and MBES bathymetry of the deglaciated MPIS to mimic a gridded RES survey over the glaciated IMIS (Fig. 1). The transect spacing replicates the spacing and resolution of RES transects used by Rippin and others (2014) on IMIS. Points were constructed every 10 m along all transects, and the x, y and z coordinates were extracted from NEXTMap DTM and MBES bathymetry.

Before bed roughness can be calculated using SD or FFT analysis, the elevation data have to be detrended to remove large wavelengths caused by mountains and valleys, which would otherwise dominate roughness measurements (Shepard and others, 2001; Smith, 2014). We are interested in roughness obstacles at a smaller scale than this, that is those which affect drag. The elevation data for each transect were detrended in R using the difference function (where difference = 2). This detrending method does not require a moving window, which removes one of many variables that affect the final bed-roughness results (Prescott, 2013; Smith, 2014). SD was then calculated along transects using a moving window size of 320 m (32 points) following previous studies (e.g. Taylor and others, 2004; Li and others, 2010). Where transects crossed lakes and coast, bed roughness values were removed to prevent bias towards smooth surfaces (Gudlaugsson and others, 2013) using the Ordnance Survey Meridian 2 lake regions shapefile (Ordnance Survey, 2017). FFT analysis requires continuous along-track data. For gaps of >100 m long (10 points), the transects were 'cut' (Rippin and others, 2014). Note that, in the onshore DTM analysis, a lake functions like a data gap. FFT analysis was not calculated across these gaps. Following previous studies (e.g. Taylor and others, 2004; Bingham and Siegert, 2009; Rippin and others, 2014), FFT analysis was calculated along transects using a window of 2^N points, where $N = 5$ giving a window length of 320 m (32 points). The total roughness parameter was then defined by calculating the integral of the power spectra for every window. Roughness at all scales up to the length of the window was integrated.

The bed-roughness calculations from both methods were then interpolated using the Topo to Raster tool in ArcMap, with a 1 km output cell size. The interpolated values were smoothed with a 10 km radius circle and a buffer of 2.5 km was applied either side of the transects. This allowed us to replicate the type of processed results that would be extracted from a RES survey. The same method as described above was applied to the RES transects for IMIS. The difference in bed roughness values was calculated for MPIS and IMIS at locations where transects crossed. Most SD results presented here are not normalised, but shown as absolute values in metres. However, when presented alongside the FFT results, the SD results were normalised, to enable a comparison. Following the post-processing stages of interpolation, buffering and smoothing, the data were normalised using a linear transformation. The results from both sites and both methods were re-scaled so that values range between 0 and 1.

A grid of transects spaced 2 × 2 km apart was also created for the Ullapool megagroove area (Fig. 1), a well-characterised part of the onset zone of MPIS (Bradwell and others, 2008b). This finer grid was used to measure roughness in between the gaps created when widely spaced RES grids are used underneath contemporary ice sheets. A 2 × 2 km grid allowed interpolation between transects and was aligned approximately parallel and orthogonal to palaeo-ice flow. Roughness was calculated using the same method as the larger grid, but the interpolation resolution was 200 m, and the values were smoothed using a 2 km radius circle. Roughness was also calculated for transects parallel and orthogonal to palaeo-ice flow, allowing differences in bed roughness between palaeo-ice flow directions to be calculated. Within the area of the 2 × 2 km grid, Bradwell and others (2008b) identified a bedform continuum, which equates to an erosional transition. This transition was interpreted as a thermal boundary by Bradwell and others (2008b), and bed roughness values from the inferred areas of warm and cold bed conditions were extracted from the smoothed interpolation, to quantify differences in roughness between these areas.

Finally, bed roughness was calculated over the entire onshore study area of the MPIS using a 2-D approach. The 2-D approach uses SD to calculate bed roughness across surfaces, rather than along 1-D transects. The 2-D method allows the full coverage and resolution of the NEXTMap data to be analysed, so that bed roughness can be calculated for the gaps in between 1-D transects. For every pixel, a circular window with a 320 m diameter was used for detrending and calculating bed roughness to match the results from the 1-D approach. The NEXTMap DTM was detrended by subtracting a smoothed bed from the original terrain. SD was calculated from the detrended raster for each 320 m circular window. We present both unsmoothed and smoothed 2-D data, to enable comparison with the smoothed 1-D results. Unsmoothed 2-D data allow us to look at the roughness calculations in more detail, whereas smoothed data show broader trends. Bed roughness was also calculated using the same approach above (except with a smaller 100 m window size) for all north-south pixels and all east-west pixels to assess directionality.

3. RESULTS

The 1-D roughness results calculated using SD for IMIS (Fig. 2c) are, as expected, similar to those found by Rippin

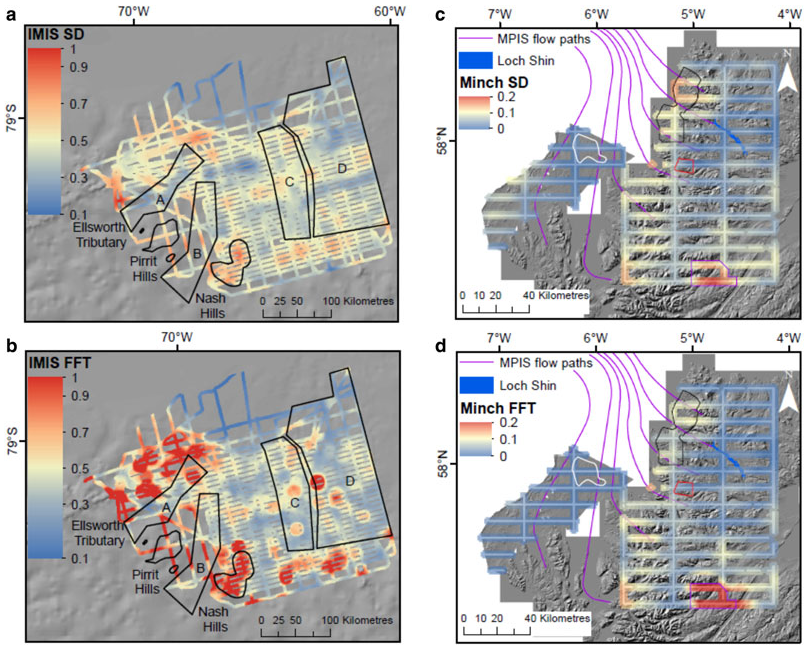

Fig. 2. Bed roughness calculated for MPIS and IMIS using SD and FFT analysis (window size = 320 m). SD and FFT data are normalised. MPIS flow paths after Bradwell and others (2007). For MPIS; the Ullapool megagrooves are outlined in red, the cnoc-and-lochan landscape (including Assynt) to the north is outlined in black, the exposed bedrock (East Shiant Bank) in the Minch is outlined in white, and the Aird is outlined in purple. For IMIS, Institute Ice Stream tributaries are labelled A, B and C, whilst the Möller Ice Stream tributary is labelled D. (a) MPIS roughness derived from SD (m). (b) MPIS roughness derived from FFT analysis (total roughness parameter). (c) IMIS roughness derived from SD (m). (d) IMIS roughness derived from FFT analysis (total roughness parameter).

and others (2014) using FFT analysis (Fig. 2b). The locations of high and low values are similar but the relative magnitude of roughness trends appears reduced for SD (Fig. 2). Table 1 shows a slightly smaller range in roughness values for IMIS SD and similar means for both methods. It should be noted that SD roughness results are reported in the text as real values but are normalised in Figure 2 and Table 1 to enable comparison with FFT analysis. IMIS SD roughness values vary between ~0.5 and 4 m. Lower roughness values of 0.5–1 m are generally located underneath the ice-stream tributaries, whereas higher roughness values (2.5–3.8 m) are associated with the Pirrit Hills and Nash Hills in the intertributary areas. The Ellsworth Tributary, a tributary of Institute Ice Stream, has low bed roughness values except where it joins the main trunk (~2.7 m). Similarly, Area D, a tributary of Möller Ice Stream, has mostly low roughness values, but with some higher bed roughness values (up to 2.8 m). Areas B and C, tributaries of Institute Ice Stream, generally have rougher beds than Areas A and D (up to 3.4 m). Parts of the inter-tributary area, however, have low roughness values (1 m). Thus, although there is a broad correlation between roughness and ice velocity, there are significant exceptions.

Table 1. Statistics of bed roughness results for MPIS and IMIS, using both methods

Site location and roughness method	Range	Minimum	Maximum	Mean
MPIS SD	0.25	0	0.25	0.08
MPIS FFT analysis	0.25	0	0.25	0.03
IMIS SD	0.9	0.1	1	0.46
IMIS FFT analysis	1	0	1	0.49

These are normalised values. The maximum value and minimum value across all datasets was used to normalize.

The SD bed roughness values for MPIS have a lower range (0–1 m) compared with IMIS (0.5–4 m). This also applies to the normalised SD values. The FFT bed roughness values for MPIS also have a lower range compared to IMIS (Table 1). The SD bed roughness values are lower (0.1–0.5 m) in the trunk of MPIS compared with the onset zones onshore (Fig. 2c). Most of the bed in the Minch is sediment covered, but some bedrock has been mapped (Fyfe and others, 1993; Bradwell and Stoker, 2015), which is slightly rougher (0.2 m) than the sediment dominated areas (0.1 m). The bedrock in the Minch is significantly smoother than the onshore bedrock of the cnoc-and-lochan landscape (Fig. 2c, d) in the onset zone (by up to 0.7 m). The 30 × 10 km grid is too low in resolution to give a detailed analysis of the transition between rough bedrock and smooth sediment in the Minch (Fig. 2). Within the Minch (bathymetry data), the flowlines coincide with smooth values (~0.1 m) (Fig. 2). This pattern contrasts with most of the flowlines in MPIS onset zones (Fig. 2), where values are rougher (0.2–0.9 m). This compares to higher bed roughness values from IMIS, which vary from 1 to 2.9 m and 1–3.8 m in the tributary and intertributary areas, respectively (Fig. 2). The highest roughness values on

the mainland of NW Scotland are found in the southern area (the Aird) of the 30 × 10 km grid (1 m) (Fig. 2), whilst the lowest values are concentrated in the centre and east (0.2 m) (Fig. 2). The bed roughness results from SD and FFT analysis show similar trends in high and low values for MPIS (Fig. 2c, d). For example, over the Ullapool megagrooves, both methods produce bed roughness values of 0.1 (normalised values). However, the results calculated using SD are higher overall than those calculated from FFT analysis (higher mean in Table 1). This difference is largest over the cnoc-and-lochan area, where the SD results are up to 3.5 times higher. SD bed roughness results show slightly more variation than those calculated from FFT (Fig. 2c, d). For example, bed roughness values from the top east-west transect (Fig. 2c, d) are 0.01 when calculated using FFT analysis, but vary between 0.06 and 0.1 when calculated using SD.The bed roughness trends from the 30 × 10 km grid (Fig. 3c) match those calculated from the smoothed 2-D approach (Fig. 3b) relatively well, particularly, the high roughness values over the cnoc-and-lochan landscape (3 m compared with 1 m), and low roughness values over the central and NE areas. The unsmoothed 2-D results (Fig. 3a) give a much more detailed picture of bed roughness. Within the cnoc-and-lochan terrain there are significant local variations in roughness that are not apparent in the smoothed 2-D data (Fig. 3a, b), While the bedrock of the East Shiant Bank is visible in the unsmoothed roughness data but not the smoothed (Fig. 3a, b).

The 2 × 2 km grid records higher roughness over the Ullapool megagrooves compared with the larger grid (0.3 m compared with 0.7 m) (Figs 2 and 4 respectively). The distribution of bed roughness values between the areas interpreted by Bradwell and others (2008b) as cold and warm bed conditions (Fig. 4a) over the Ullapool megagrooves show a clear difference. The area with a cold bed has predominantly lower bed roughness values, with a mean of 0.2 m, compared with the area where the bed was warm, with a mean of 0.4 m (Fig. 5). There is a clear transition to higher bed roughness values over the megagrooves compared with the surrounding areas (Fig. 4a).

4. DISCUSSION

Our results show that similar patterns of bed roughness are found in both contemporary and palaeo-ice stream settings, using the same transect spacing and along-transect resolution (Fig. 2). High and low roughness values can generally be found in areas of fast ice flow. This suggests that

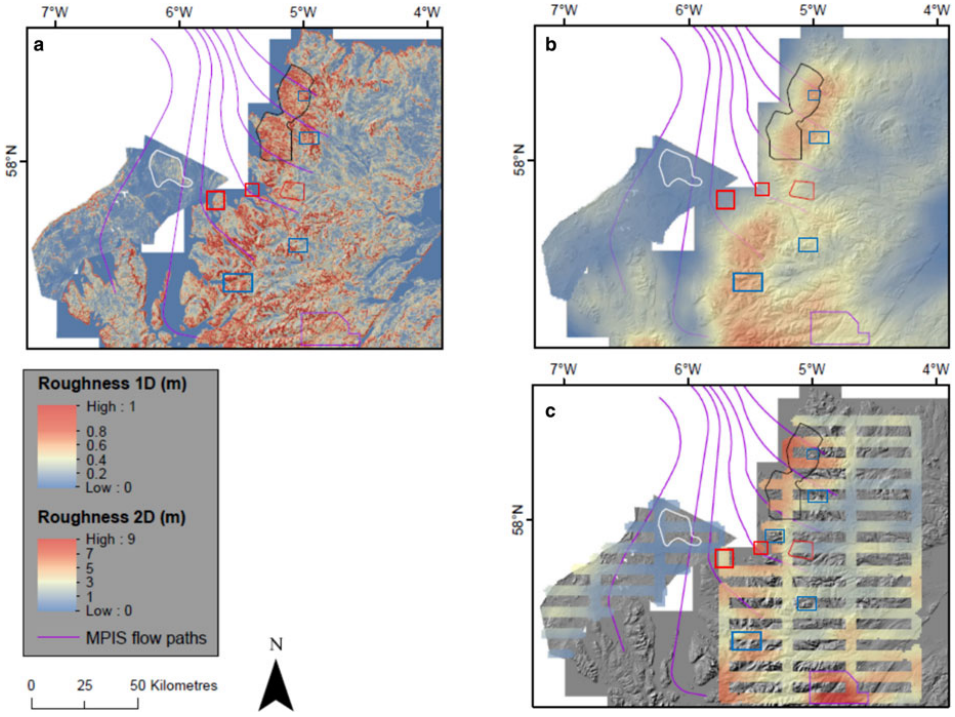

Fig. 3. Bed roughness calculated using SD for all NEXTMap DTM pixels using a moving window of 320 m (2-D). Values are not normalised. The exposed bedrock (East Shiant Bank) in the Minch is outlined in white. The Ullapool megagrooves are outlined in red. The cnoc-and-lochan landscape (including the Assynt) to the north is outlined in black. The Aird is outlined in purple. (a) Bed roughness of MPIS onset zone with flow paths after Bradwell and others (2007). Blue boxes are inselbergs and mountain massifs that are missed by the 1-D 30 × 10 km transects. These include Ben Mor Coigach massif, Ben Stack, the Assynt massif, the Fannichs, and Liathach. Red boxes show Loch Ewe and Little Loch Broom, which appear rough on the 1-D grid but smooth using the 2-D data. (b) Bed roughness from (a) that has been resampled to 1 km resolution and smoothed using the same window size as that used for the bed roughness measurements calculated using the 30 × 10 km grid. (c) Bed roughness from the 1-D 30 × 10 km.

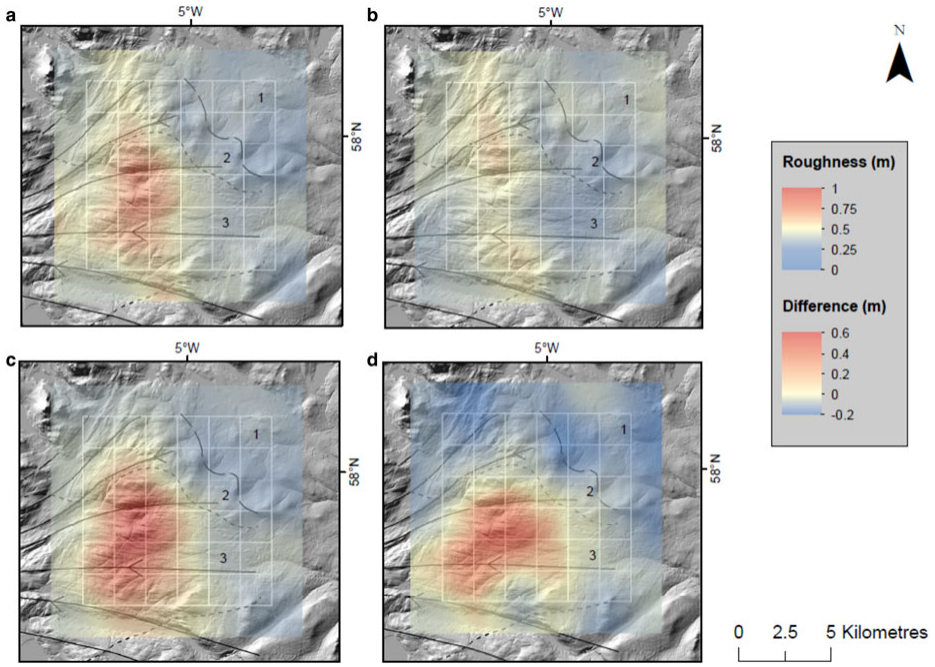

Fig. 4. Roughness measured along transects (white lines, grid spacing of 2 × 2 km) over the Ullapool megagrooves (see Fig. 1 for location). The transects are approximately parallel and orthogonal to palaeo-ice flow (Solid black lines with arrows, east to west). 1 is an area of no glacial streaming (cold-based ice), 2 is an area of subtle streamlined landforms between the dotted and dashed lines (warm-based ice). Between the dotted lines, 3 is an area of strong glacial streamlining (warm-based ice). Palaeo-flow direction and areas of glacial streaming after Bradwell and others (2008b). Values are not normalised. (a) Roughness calculated along all transects. (b) Roughness calculated along transects parallel to flow. (c) Roughness calculated along transects orthogonal to flow. (d) The magnitude difference between (b) and (c).

bed roughness is not always a controlling factor on the location of ice streaming. Overall, the bed roughness results for IMIS are higher than MPIS. One reason for this difference could be the vertical resolution of RES data, which is lower compared with DTM data (5 m vs. 1 m, respectively). Postglacial sedimentation could be one of the causes of this. For example, a thin layer (0.1–10 m) of postglacial sediment deposition occurs in the Minch (Fyfe and others, 1993; Bradwell and Stoker, 2015), which will reduce the amplitude of small-scale glacial features. Yet this is unlikely to be the case onshore, where predominantly exposed bedrock with more localised areas of postglacial sediment prevails (Krabbendam and Bradwell, 2010). Conversely, topographic profiles collected using RES are an average of the radar trace (King and others, 2016), which could cause such data to be slightly smoothed in comparison with data from visible surfaces for example DTMs. Without being able to see the entire bed of IMIS it is difficult to provide a definitive answer. We suggest that the reason for higher bed roughness in IMIS could be due to the difference in elevation range

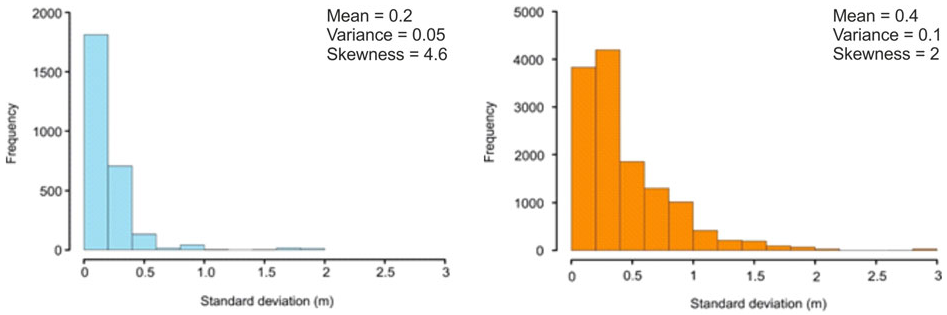

Fig. 5. Bed roughness distributions in cold-based (blue) and warm-based (orange) areas from the 2 × 2 km grid over the Ullapool megagrooves. Cold-based and warm-based areas are defined by Bradwell and others (2008b). Values are not normalised.

between the two locations. MPIS has an elevation range of 1493 m, While IMIS has an elevation range of 3582 m (Fretwell and others, 2013).

4.1. SD vs. FFT analysis methods

Our comparison between SD and FFT analysis at the 1-D scale for MPIS and IMIS showed similar broad trends of bed roughness, but there were differences (Fig. 2). For MPIS, the cnoc-and-lochan landscape appears rougher in the SD than in FFT (Fig. 2). Cnoc-and-lochan landscapes typically contain abundant lakes, which appear on a DTM as a flat surface. These are removed from the dataset to avoid bias towards a smooth surface. For FFT analysis to be carried out, transects measuring <320 m between lakes are also removed from the data, causing data gaps. Where there are multiple lakes along a transect with <320 m between them, the SD method measures a high roughness value. FFT analysis cannot capture this variation in terrain. Some transects that are not impacted by lakes also have higher bed roughness values calculated from SD compared with FFT analysis. Both methods essentially measure the amplitude of the bed obstacles (Rippin and others, 2014), but FFT analysis measures the frequency of vertical undulations (Bingham and Siegert, 2009). We suggest that the FFT analysis is measuring similar frequencies of elevation change. The results from the SD method for the same landscape are rougher than FFT analysis, because it is measuring large amplitude changes between the numerous hills and lakes. Furthermore, FFT analysis (total roughness parameter) integrates roughness at all scales up to the window size, whereas SD is calculated for the window size only. This will cause higher roughness results measured using SD because the values are calculated over a larger horizontal length-scale (Shepard and others, 2001). Both methods have advantages and disadvantages in their application. FFT analysis emphasises roughness frequency whilst SD provides a more intuitive measure of roughness scales.

4.2. Transect spacing vs. complete coverage: what is missed?

Measuring bed roughness on a palaeo-ice stream allows us to assess the validity of RES transect spacing used to measure bed roughness on contemporary ice streams. The 30 × 10 km grid misses key areas of glacial landforms used to interpret MPIS ice dynamics, such as the transition from rough bedrock to smooth sediments in the bathymetry data (Fig. 2) (Bradwell and Stoker, 2015). For the onshore data, shifting the 30 × 10 km grid by a few km north or south would miss the Ullapool megagrooves altogether (Fig. 2). Entire inselbergs and mountain massifs are missed (blue boxes on Fig. 3): in the 2-D roughness maps these areas appear as very rough and it is known these had a profound effect on local ice dynamics (Bradwell, 2005, 2013; Finlayson and others, 2011). Conversely, some areas appear rough on the 1-D transect but appear on the 2-D maps as fairly smooth (red boxes on Fig. 3). A much more detailed picture of 2-D bed roughness trends can be achieved without the smoothing employed by previous studies (Fig. 3a) (e.g. Rippin and others, 2014). For example, all the cnoc-and-lochan area appears rough on the smoothed 2-D data, but the unsmoothed data show that some parts are smooth (Fig. 3a, b). The 2-D method surpasses the detail that can be captured by the 1-D transects but does not allow for analysis of the bed roughness directionality (anisotropy). It is clear that exploring palaeo-ice-stream roughness is possible at much higher resolutions than for contemporary ice streams, and important insights regarding the roughness of subglacial terrain may thus be learnt from these environments (Gudlaugsson and others, 2013).

A 30 × 10 km grid is too widely spaced to capture bed roughness of some landform assemblages. The question of what grid size should be used is an important one. The Ullapool megagrooves for example, cover an area of 6 × 10 km and individual grooves are up to 4 km long (Krabbendam and others, 2016). A grid size of 2 × 2 km is arguably more suitable (Fig. 4). The size of glacial landforms that can be measured at DTM resolution varies largely, ~10–10^5 m (Clark, 1993; Bennett and Glasser, 2009) and a grid size that can measure mega-groove bed roughness might not be appropriate for other landform assemblages. The landscape underneath ice streams has been captured in detail using RES grids with transects spaced 500 m apart (King and others, 2009, 2016; Bingham and others, 2017). Importantly, these studies only used orthogonal transects because RES can pick up multiple landform crests parallel to ice flow (King and others, 2016). Acquiring RES tracks at 500 m spacing for large areas is very challenging, but future surveys could be focused on locations where rough, streamlined topography is thought to be present (Bingham and others, 2017), or areas that could cause a future sea level rise through rapid retreat for example Thwaites Glacier (Joughin and others, 2014; DeConto and Pollard, 2016). Drones or Unmanned Aerial Vehicles have the potential to make RES data collection with small track spacing more viable over large areas (e.g. Leuschen and others, 2014).

4.3. The importance of transect orientation

The locations of high roughness values over MPIS, measured by both SD and FFT analysis along transects, do not always reflect qualitative roughness seen in the DTM and bathymetry data. This problem has been investigated previously for bed roughness (e.g. Gudlaugsson and others, 2013; Rippin and others, 2014) and englacial layers (e.g. Ng and Conway, 2004; Bingham and others, 2015), and transect orientation was shown to be important. To explore the influence of transect orientation on bed roughness we calculated bed roughness separately for north-south and east-west transects for both MPIS and IMIS (Fig. 6). Where transects cross each other, the difference in roughness was calculated (Fig. 6c, f). This was also done for transects on a pixel scale spacing for MPIS (Fig. 7). The difference in roughness of cross-cutting transects can be seen as a measure of directionality (anisotropy).

In MPIS some areas show a difference between east-west and north-south transects, suggesting significant anisotropy. The north-south transect along the West coast has higher roughness values (Fig. 6), notably for the lower part of the cnoc-and-lochan landscape on the exposed gneiss bedrock in the Assynt area (Krabbendam and Bradwell, 2014) and the edge of Ullapool mega grooves area (Bradwell and others, 2008b). This same pattern is also apparent in more detail at the pixel scale (Fig. 7). In the Minch, the east-west pixels are rougher over the exposed bedrock (East Shiant Bank) (Fig. 7c), which is not shown in Figure 6 because of the wide transect spacing. In both cases, the rougher

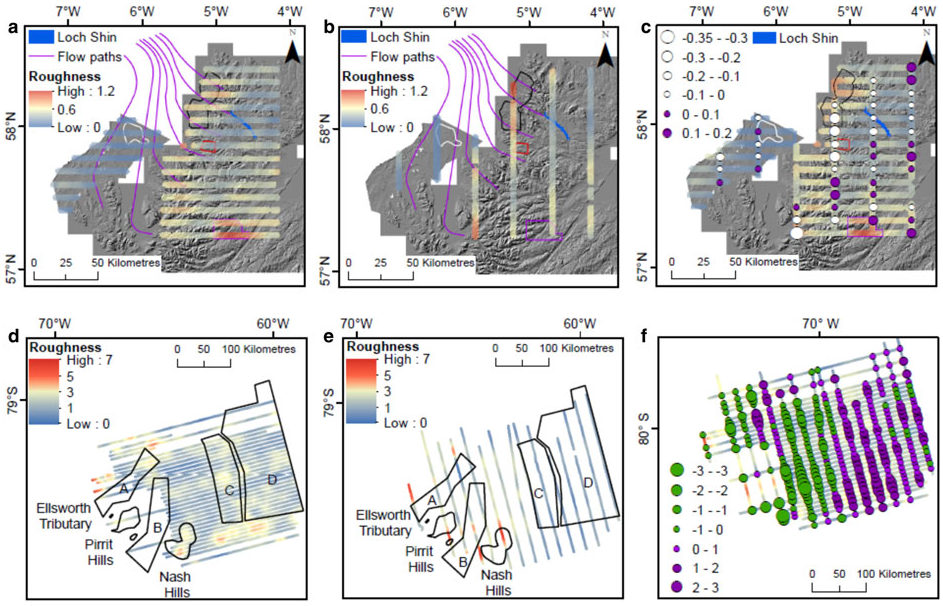

Fig. 6. The relationship between bed roughness measurements and transect orientation for MPIS and IMIS. All bed roughness measurements were calculated using SD and values are not normalised. For MPIS: The exposed bedrock (East Shiant Bank) in the Minch is outlined in white. The Ullapool megagrooves are outlined in red. The cnoc-and-lochan landscape (including the Assynt) to the north is outlined in black. The Aird is outlined in purple. (a) Bed roughness for east-west MPIS transects. (b) Bed roughness for north-south MPIS transects. (c) The proportional circles show the east-west transects minus the north-south for MPIS. (d) Bed roughness for east-west IMIS transects. (e) Bed roughness for north-south IMIS transects. (f) The proportional circles show the east-west transects minus the north-south transects for IMIS.

transects are orthogonal to palaeo-ice flow and support previous observations of bedrock smoothing by streaming ice (Bradwell and Stoker, 2015; Ballantyne and Small, 2018). The east-west transects crossing the Aird are rougher than the north-south transects (Fig. 6). Closer inspection of the NEXTMap DTM reveals these rough values are located where the east-west transects cross deeply incised river valleys. Post-glacial erosion or sediment deposition can impact on palaeo-ice-stream bed roughness values. In IMIS east-west transects have higher roughness values predominantly in the tributaries labelled C and D, whilst the north-south transects have higher roughness values under tributaries A and B (Fig. 6). Although the direction of these transects is not related to ice flow as analysed by Rippin and others, (2014), it shows that the direction of transects influences the bed roughness results for both contemporary and palaeo-ice streams.

For contemporary ice streams it has been shown that the transect orientation in relation to ice flow can bias interpretation (e.g. Rippin and others, 2014; Bingham and others, 2015; Bingham and others, 2017). Parallel to ice flow, the data tend to show smooth beds (Lindbäck and Pettersson, 2015) and undisrupted ice layering (Bingham and others, 2015), whereas data orthogonal to ice flow can show rough topography (Rippin and others, 2014; Bingham and others, 2017), which can be caused by streamlined features, for example mega grooves or mega-scale glacial lineations. These landforms have strong anisotropy (Spagnolo and others, 2017). The advantage of looking at palaeo-ice-stream beds compared with contemporary ice-stream beds is that the landforms can be observed directly. The strong anisotropy of the Ullapool megagrooves, already known from traditional geomorphological studies (Bradwell and others, 2007; Krabbendam and others, 2016), is well captured by the 2 × 2 km grid results (Fig. 4b, c, d). Flow parallel transects are smoother (0.4 m), than the orthogonal transects (1 m). The roughness orthogonal to palaeo-ice flow is up to 2× higher than parallel palaeo-ice flow. The same pattern is shown in Figure 7. The formation of hard-bed megagrooves smooths the bed along ice flow but may lead to increased roughness orthogonal to ice flow, for instance by lateral plucking (Krabbendam and Bradwell, 2011; Krabbendam and others, 2016).

4.4. Roughness as a control on ice-stream location

The bed-roughness measurements extracted across MPIS using the 1-D and 2-D SD methods show that high roughness values occur in some areas interpreted as having hosted fast palaeo-ice flow (see MPIS flow paths, Figs 2 and 3). A rough bed underneath fast-flowing ice is not typically assumed and is at odds with some previous findings from contemporary ice streams that show low roughness values, i.e. a smooth bed, beneath fast-flowing ice (e.g. Siegert and others, 2004; Bingham and Siegert, 2007; Rippin and others, 2011). Warm basal ice will be present in fast flowing areas whilst ice underneath slow flowing regions is likely to be frozen at the bed (Benn and Evans, 2010). Bradwell and others (2008b) interpreted areas of cold and warm basal conditions for the Ullapool megagrooves and adjacent areas (Fig. 6).

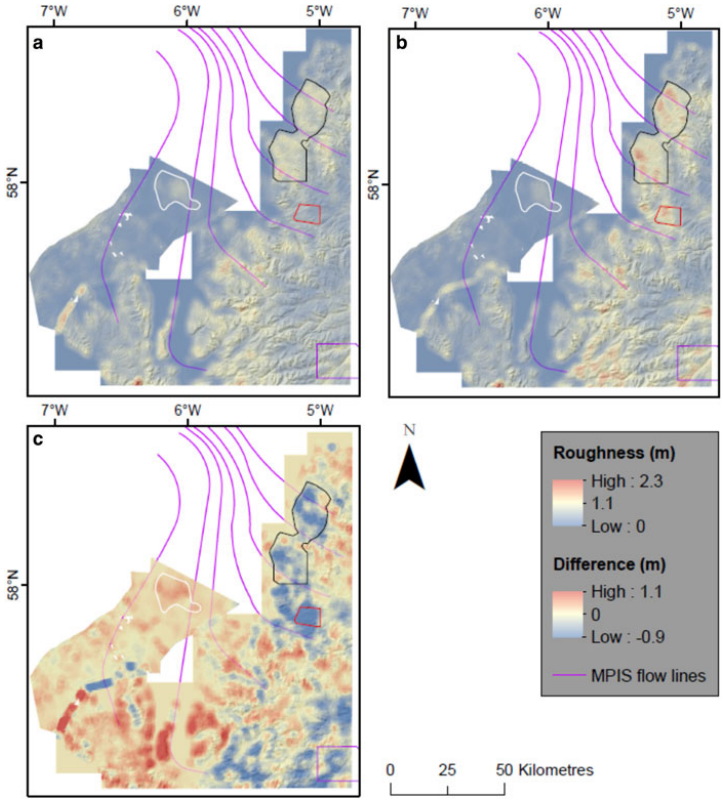

Fig. 7. The relationship between bed roughness measurements and transect direction for MPIS on a pixel scale. All bed roughness measurements were calculated using SD (window size = 100 m) and values are not normalised. The same interpolation and smoothing done for Figure 4 was used here. The exposed bedrock (East Shiant Bank) in the Minch is outlined in white. The Ullapool megagrooves are outlined in red. The cnoc-and-lochan landscape (including Assynt) to the north is outlined in black. The Aird is outlined in purple. (a) Bed roughness values calculated for each row of the DTM (east-west). (b) Bed roughness values calculated for each column of the DTM (north-south). (c) Plot of east-west minus north-south bed roughness.

Bed roughness values are lower for the areas with cold basal conditions compared with the areas with warm basal conditions (Fig. 5). Bradwell and others (2008b) identified a marked change in the bedform continuum between cold-based and warm-based zones and suggested this was due to increased ice velocity. Thus, we suggest that areas of inferred slow palaeo-ice flow can be associated with a smooth bed. Higher erosion rates under the fast-flowing palaeo-ice have produced larger, elongated bedforms, which have left behind a rougher bed overall (particularly orthogonal to palaeo-ice flow). It must be noted that this is for an area of exposed bedrock, with no sediment cover.

Krabbendam (2016) argued that if there is a thick layer of temperate basal ice, fast flow can occur on a rough hard bed. In this setting, less basal drag occurs and thick temperate basal ice is maintained by frictional heating, which produces high basal melt rates. The Laxfjord Palaeo-Ice Stream is a tributary to MPIS, identified by Bradwell (2013) (Fig. 1). Erosional landforms such as whalebacks and roches moutonnées were mapped on the bed of the Laxfjord Palaeo-Ice Stream, in the cnoc-and-lochan landscape (Bradwell, 2013). These landforms are indicative of warm-based ice with meltwater present at the bed (Bennett and Glasser, 2009; Benn and Evans, 2010; Roberts and others, 2013). Bradwell (2013) suggested that topographic funnelling of ice was the driver of palaeo-fast ice flow in the Loch Laxford area. MPIS has a dendritic network of overdeepened valleys that channelled ice into the main trough and is thought to be topographically controlled (Bradwell and Stoker, 2015). It thus appears that rough beds are possible in topographically steered ice streams and that topographic steering may 'trump' roughness as a control on ice-stream location (see also Winsborrow and others, 2010).

Recent insights from contemporary ice streams support our results from MPIS. Schroeder and others (2014) demonstrated that the lower trunk of the fast-flowing Thwaites Glacier is underlain by rough bedrock. Jordan and others (2017) found that warm-based areas, predicted by MacGregor and others (2016), underneath the northern part of the Greenland ice sheet, are relatively rough compared with predicted cold-based areas. A tributary to Institute Ice Stream, Ellsworth Tributary (Fig. 2), is topographically controlled (Ross and others, 2012), and Siegert and others (2016) suggest that this explains why fast flow occurs over rough areas of the bed. The suggested reasons for a rough bed underneath the Ellsworth Tributary are an absence of

sediment deposition or excavation of pre-existing sediment (Siegert and others, 2016). In MPIS in Scotland and surrounding areas, there is a strong geological control on roughness (Bradwell, 2013; Krabbendam and Bradwell, 2014; Krabbendam and others, 2016). This could be the underlying cause for the rough bed underneath the Ellsworth Tributary.

Our results suggest that the bed roughness of a palaeo-ice stream and a contemporary ice stream are comparable, and support the notion that palaeo-ice streams can be used as analogues for contemporary ice streams (Bradwell and others, 2007; Rinterknecht and others, 2014; Bradwell and Stoker, 2015).

4.5. Interpreting sediment cover from roughness calculations

Bed roughness values from IMIS were smoother underneath the ice-stream tributaries compared with the intertributary areas (Fig. 2). Smooth beds beneath ice streams are typically explained by the inferred presence of soft sediment (Siegert and others, 2005; Li and others, 2010; Rippin, 2013). However, the Ullapool megagrooves (exposed bedrock features, without sediment cover) (Bradwell and others, 2008b), are smooth, particularly parallel to palaeo-ice flow (Figs 4 and 7). Equally the East Shiant Bank includes bedrock but is barely rougher than the adjacent, sediment-covered parts of the MPIS (Fig. 2). Smooth areas of below present-day ice streams may therefore not necessarily be sediment covered.

4.6. Recommendations for future studies

The direction of transects influences the bed roughness results on palaeo- and contemporary ice streams. We suggest that future acquisition of RES tracks over contemporary ice streams are orientated parallel and orthogonal to flow where possible. The fine spacing of RES tracks that is 500 m orthogonal to ice flow only, could be focused on locations where the bed is thought to be rough underneath fast-flowing ice as this has been shown to have an impact on ice flow (Bingham and others, 2017). Further analysis of the relationship between grid size, bed roughness and landforms assemblages is needed on palaeo-ice streams to give recommendations on the appropriate grid sizes. For palaeo-ice streams, including MPIS, bed roughness could be explored parallel and orthogonal to inferred flow lines (e.g. Gudlaugsson and others, 2013) to increase our understanding of the relationship between bed roughness and ice flow direction. The bed roughness of palaeo-ice streams dominated by sediment landforms (soft bed), could be compared with contemporary ice streams that are thought to have similar bed properties. Palaeo-ice streams provide an opportunity to improve our understanding of the relationship between landforms and bed roughness, and in turn, ice dynamics. The difference in what the SD and FFT analysis methods are measuring should be taken into account when these methods are applied in future studies. The effect of post-glacial erosion or sediment deposition on palaeo-ice-stream bed roughness values should also be taken into consideration.

5. CONCLUSION

We compared the bed roughness of the deglaciated Minch Palaeo-Ice Stream in Scotland, to the contemporary Institute and Möller Ice Streams in West Antarctica, using two analysis methods. We also investigated whether different grid spacing and orientation impact bed roughness measurements. The 30×10 km grid, which matches a previous RES transect distribution used for bed roughness studies over a large area on contemporary ice streams, is too coarse to confidently capture all the different landforms on a typical ice-sheet bed. Using a finer 2×2 km grid we were able to show that transects parallel to palaeo-ice flow were smoother compared with orthogonal transects over the Ullapool megagrooves in the onset zone of MPIS. A clear difference in bed roughness values was also shown for pixel scale transects for MPIS, demonstrating how transect orientation influences roughness results. RES transects should be closer together in future studies and orientated in relation to ice flow where possible. This would allow for more representative bed roughness measurements because of the importance of flow direction on roughness patterns. SD produced similar results to FFT analysis for the majority of the data, but there were some differences which should be taken into account by future studies. Unsmoothed 2-D roughness data for MPIS showed detail that is missed when 2-D Data are smoothed.

Most MPIS flow paths in the onshore onset zones coincided with high bed roughness values, whilst lower roughness values were associated with sediment cover in the main ice stream trunk. Yet, smooth areas of the bed beneath MPIS occurred over bedrock as well as the sediment-covered areas. Low bed roughness beneath contemporary ice streams is not a reliable indicator of the presence of sediment. In this study, we found that fast palaeo-ice flow has occurred over areas with high bed roughness values. Previous research often assumed that fast-flowing ice streams are generally related to areas of low roughness. High and low bed roughness values were also found in the IMIS tributaries, which supports the notion that palaeo- and contemporary ice streams are comparable in terms of bed roughness. The diverse topography underneath ice streams needs to be measured in more detail to increase our understanding of what controls ice stream location. Palaeo-ice streams provide useful analogues for bed roughness underneath contemporary ice streams, and both can be used to inform the other.

ACKNOWLEDGEMENTS

This research is part of a PhD project, funded by NERC, grant number NE/K00987/1. MBES data are Crown copyright and provided by the British Geological Survey (BGS), and Maritime and Coastguard Agency. OS Meridian data are provided by the Ordnance Survey, Crown copyright and database right 2012. NEXTMap DTM was provided by NERC via the Centre for Environmental Data Analysis (CEDA). RES data came from UK NERC AFI grant NE/G013071/1. Many thanks to Jon Hill and Colin McClean from the Environment Department at the University of York, who provided advice and guidance on the methods used. We thank the editors (Hester Jiskoot and Neil Glasser) and two reviewers (Rob Bingham and one anonymous reviewer) for their helpful and insightful comments, which significantly improved this paper.

REFERENCES

Ballantyne CK and Small D (2018) The last Scottish ice sheet. *Earth Env. Sci. Trans. R. Soc. Edin.*, 1–39

Benn DI and Evans DJA (2010) *Glacier & glaciation*, 2nd edn. Hodder Education, Abingdon

Bennett MR and Glasser NF (2009) *Glacial geology*, 2nd edn. Wiley-Blackwell, Chichester

Bingham RG and Siegert MJ (2007) Radar-derived bed roughness characterization of Institute and Möller ice streams, West Antarctica, and comparison with Siple Coast ice streams. *Geophys. Res. Lett.*, **34**, 1–5

Bingham RG and Siegert MJ (2009) Quantifying subglacial bed roughness in Antarctica: implications for ice-sheet dynamics and history. *Quat. Sci. Rev.*, **28**, 223–236

Bingham RG, Siegert MJ, Young DA and Blankenship DD (2007) Organized flow from the South Pole to the Filchner-Ronne ice shelf: an assessment of balance velocities in interior East Antarctica using radio echo sounding data. *J. Geophys. Res.*, **112**, 1–11

Bingham RG and 9 others (2015) Ice-flow structure and ice dynamic changes in the Weddell Sea sector of West Antarctica from radar-imaged internal layering. *J. Geophys. Res. Earth Surf.*, **120**(4), 655–670

Bingham RG and 5 others (2017) Diverse landscapes beneath pine island glacier influence ice flow. *Nat. Comms.*, **8**(1618), 1–9

Bradwell T (2005) Bedrock megagrooves in Assynt, NW Scotland. *Geomorphology*, **65**, 195–204

Bradwell T (2013) Identifying palaeo-ice-stream tributaries on hard beds: mapping glacial bedforms and erosion zones in NW Scotland. *Geomorphology* **201**, 397–414

Bradwell T and Stoker MS (2015) Submarine sediment and landform record of a palaeo-ice stream within the British−Irish Ice Sheet. *Boreas*, **44**, 255–276

Bradwell T and Stoker MS (2016) Glacial sediment and landform record offshore NW Scotland : a fjord – shelf – slope transect through a Late Quaternary mid-latitude ice-stream system. In Dowdeswell JA, Canals M, Jakobsson M, Todd BJ, Dowdeswell EK and Hogan KA eds. *Atlas of submarine glacial landforms: modern, quaternary and ancient*. The Geological Society of London, London, 421–428

Bradwell T, Stoker M and Larter R (2007) Geomorphological signature and flow dynamics of The Minch palaeo-ice stream, north-west Scotland. *J. Quat. Sci.*, **22**, 609–617

Bradwell T and 11 others (2008a) The northern sector of the last British Ice Sheet: Maximum extent and demise. *Earth-Science Rev.*, **88**, 207–226

Bradwell T, Stoker M and Krabbendam M (2008b) Megagrooves and streamlined bedrock in NW Scotland: the role of ice streams in landscape evolution. *Geomorphology*, **97**, 135–156

Bradwell T and 5 others (2016) Rate and style of ice stream retreat constrained by new surface-exposure ages: The Minch, NW Scotland. In: EGU. Vol. 18. p. 10447.

Callens D and 5 others (2014) Transition of flow regime along a marine-terminating outlet glacier in East Antarctica. *Cryosphere*, **8**, 867–875

Chiverrell RC and Thomas GSP (2010) Extent and timing of the Last Glacial Maximum (LGM) in Britain and Ireland: a review. *J. Quat. Sci.*, **25**, 535–549

Clark CD (1993) Mega-scale glacial lineations and cross-cutting ice-flow landforms. *Earth Surf. Process. Landf.*, **18**, 1–29

Clark CD, Hughes ALC, Greenwood SL, Jordan C and Sejrup HP (2012) Pattern and timing of retreat of the last British-Irish Ice Sheet. *Quat. Sci. Rev.*, **44**, 112–146

Clark CD and 13 others (2018) BRITICE glacial Map, version 2: a map and GIS database of glacial landforms of the last British-Irish Ice Sheet. *Boreas*, **47**(1), 11–27

DeConto RM and Pollard D (2016) Contribution of Antarctica to past and future sea-level rise. *Nature*, **531**, 591–597

Finlayson AG, Golledge N, Bradwell T and Fabel D (2011) Evolution of a Lateglacial mountain icecap in Northern Scotland. *Boreas*, **40**(3), 536–544

Fretwell P and 59 others (2013) Bedmap2: improved ice bed, surface and thickness datasets for Antarctica. *Cryosphere*, **7**, 375–393

Fyfe JA, Long D and Evans D (1993) The geology of the Malin-Hebrides sea area. *UK Offshore Reg. Rep.*,

Gudlaugsson E, Humbert A, Winsborrow M and Andreassen K (2013) Subglacial roughness of the former Barents Sea ice sheet. *J. Geophys. Res. Earth Surf.*, **118**, 2546–2556

Hubbard B and Hubbard A (1998) Bedrock surface roughness and the distribution of subglacially precipitated carbonate deposits: implications for the formation at Glacier de Tsanfleuron, Switzerland. *Earth Surf. Process. Landforms*, **23**(3), 261–270

Hubbard B, Siegert MJ and McCarroll D (2000) Spectral roughness of glaciated bedrock geomorphic surfaces: implications for glacier sliding. *J. Geophys. Res.*, **105**, 21295

Hubbard A and 7 others (2009) Dynamic cycles, ice streams and their impact on the extent, chronology and deglaciation of the British-Irish ice sheet. *Quat. Sci. Rev.*, **28**(7–8), 758–776

Intermap Technologies (2009) NEXTMap British Orthorectified Radar Image (ORI) Data by Intermap. *NERC Earth Obs. Data Cent.* [Internet]. Available from: http://catalogue.ceda.ac.uk/uuid/90de599e45a84d36a16cf01904048705

Jordan TM and 6 others (2017) Self-affine subglacial roughness: consequences for radar scattering and basal thaw discrimination in northern Greenland. *Cryosphere*, **11**, 1247–1264

Joughin I and Bamber JL (2005) Thickening of the ice stream catchments feeding the Filchner-Ronne Ice Shelf, Antarctica. *Geophys. Res. Lett.*, **32**(17), 1–4

Joughin I, Smith BE and Medley B (2014) Marine ice sheet collapse potentially under way for the Thwaites Glacier Basin, West Antarctica. *Science*, **344**, 735–738

Kamb B (1970) Sliding motion of glaciers: theory and observation. *Rev. Geophys.*, **8**, 673–728

King EC, Hindmarsh RCA and Stokes CR (2009) Formation of mega-scale glacial lineations observed beneath a West Antarctic ice stream. *Nat. Geosci.*, **2**, 585–588

King EC, Pritchard HD and Smith AM (2016) Subglacial landforms beneath Rutford Ice Stream, Antarctica: detailed bed topography from ice-penetrating radar. *Earth Syst. Sci. Data*, **8**, 151–158

Krabbendam M (2016) Basal sliding on a rough hard bed; pressure melting and creep mechanisms in temperate basal ice. *Cryosphere*, **10**, 1915–1932

Krabbendam M and Bradwell T (2010) The geology and landscape of the Northwest Highlands: an introduction. In Lukas S and Bradwell T eds. *The quaternary of western Sutherland and adjacent areas: field guide*. Quaternary Research Association, London, 3–12

Krabbendam M and Bradwell T (2011) Lateral plucking as a mechanism for elongate erosional glacial bedforms: explaining mega-grooves in Britain and Canada. *Earth Surf. Process. Landforms*, **36**, 1335–1349

Krabbendam M and Bradwell T (2014) Quaternary evolution of glaciated gneiss terrains: pre-glacial weathering vs. Glacial erosion. *Quat. Sci. Rev.*, **95**, 20–42

Krabbendam M, Eyles N, Putkinen N, Bradwell T and Arbelaez-Moreno L (2016) Streamlined hard beds formed by palaeo-ice streams: a review. *Sediment. Geol.*, **338**, 24–50

Kuchar J and 6 others (2012) Evaluation of a numerical model of the British-Irish ice sheet using relative sea-level data: implications for the interpretation of trimline observations. *J. Quat. Sci.*, **27**(6), 597–605

Layberry RL and Bamber JL (2001) Between dynamics and basal topography. *J. Geophys. Res.*, **106**, 33781–33788

Leuschen C and 6 others (2014) UAS-based radar sounding of the polar ice sheets. *IEEE Geosci. Remote Sens.*, **2**(1), 8–17

Li X and 7 others (2010) Characterization of subglacial landscapes by a two-parameter roughness index. *J. Glaciol.*, **56**, 831–836

Lindbäck K and Pettersson R (2015) Spectral roughness and glacial erosion of a land-terminating section of the Greenland Ice Sheet. *Geomorphology*, **238**, 149–159

MacGregor JA and 11 others (2016) A synthesis of the basal thermal state of the Greenland ice sheet. *J. Geophys. Res. Earth Surf.*, **121**, 1328–1350

Margold M, Stokes CR and Clark CD (2015) Ice streams in the Laurentide Ice Sheet: Identification, characteristics and comparison to modern ice sheets. *Earth-Science Rev.*, **143**, 117–146

Mouginot J, Scheuchl B and Rignot E (2012) Mapping of Ice motion in Antartica using synthetic-aperture radar data. *Remote Sens.*, **4**, 2753–2767

Ng F and Conway H (2004) Fast-flow signature in the stagnated Kamb Ice Stream, West Antarctica. *Geology*, **32**(6), 481–484

Nye JF (1970) Glacier sliding without cavitation in a linear viscous approximation. *Proc. R. Soc. Lond. A.*, **315**, 381–403

Ordnance Survey (2017) Ordnance Survey Meridian 2. Southampton: Ordnance Survey

Perkins AJ and Brennand TA (2014) Refining the pattern and style of Cordilleran Ice Sheet retreat: Palaeogeography, evolution and implications of lateglacial ice-dammed lake systems on the southern Fraser Plateau, British Columbia, Canada. *Boreas*, **44**, 319–342

Praeg D 8 and others (2015) Ice sheet extension to the Celtic Sea shelf edge at the Last Glacial Maximum. *Quat. Sci. Rev.*, **111**, 107–112

Prescott PW (2013) *Quantifying subglacial roughness and its link to glacial geomorphology and ice speed*. (Doctoral thesis, Durham University)

Putkinen N and 13 others (2017) High-resolution LiDAR mapping of glacial landforms and ice stream lobes in Finland. *Bull. Geol. Soc. Finland.*, **29**, 64–81

Rignot E, Mouginot J and Scheuchl B (2011) Ice flow of the Antarctic Ice Sheet. *Science*, **333**, 1427–1430

Rinterknecht V and 7 others (2014) Unstable ice stream in Greenland during the Younger Dryas cold event. *Geology*, **42**, 759–762

Rippin DM (2013) Bed roughness beneath the Greenland ice sheet. *J. Glaciol.*, **59**, 724–732

Rippin DM, Bamber JL, Siegert MJ, Vaughan DG and Corr HFJ (2006) Basal conditions beneath enhanced-flow tributaries of Slessor Glacier, East Antarctica. *J. Glaciol.*, **52**, 481–490

Rippin DM, Vaughan DG and Corr HFJ (2011) The basal roughness of Pine Island Glacier, West Antarctica. *J. Glaciol.*, **57**, 67–76

Rippin DM and 9 others (2014) Basal roughness of Institute and Möller Ice Streams, West Antarctica: process determination and landscape interpretation. *Geomorphology*, **214**, 139–147

Roberts DH, Evans DJA, Lodwick J and Cox NJ (2013) The subglacial and ice-marginal signature of the North Sea Lobe of the British-Irish Ice Sheet during the Last Glacial Maximum at Upgang, North Yorkshire, UK. *Proc. Geol. Assoc.*, **124**, 503–519

Ross N and 9 others (2012) Steep reverse bed slope at the grounding line of the Weddell Sea sector in West Antarctica. *Nat. Geosci.*, **5**, 1–4

Ross N and 8 others (2014) The Ellsworth Subglacial Highlands: Inception and retreat of the West Antarctic ice sheet. *Bull. Geol. Soc. Am.*, **126**, 3–15.

Salcher BC, Hinsch R and Wagreich M (2010) High-resolution mapping of glacial landforms in the North Alpine Foreland, Austria. *Geomorphology*, **122**(3–4), 283–293

Scambos T, Bohlander J, Raup B and Haran T (2004) Glaciological characteristics of Institute Ice Stream using remote sensing. *Antarct. Sci.*, **16**, 205–213

Schoof C (2002) Basal perturbations under ice streams: form drag and surface expression. *J. Glaciol.*, **48**(162), 407–416

Schroeder DM, Blankenship DD, Young DA, Witus AE and Anderson JB (2014) Airborne radar sounding evidence for deformable sediments and outcropping bedrock beneath Thwaites Glacier, West Antarctica. *Geophys. Res. Lett.*, **41**, 7200–7208

Shepard MK and 5 others (2001) A planetary and remote sensing perspective. *J. Geophys. Res.*, **106**, 32,777–32,795

Siegert MJ, Taylor J, Payne AJ and Hubbard B (2004) Macro-scale bed roughness of the Siple Coast ice streams in west Antartica. *Earth Surf. Process. Landforms*, **29**, 1591–1596

Siegert MJ, Taylor J and Payne AJ (2005) Spectral roughness of subglacial topography and implications for former ice-sheet dynamics in East Antarctica. *Glob. Planet. Change*, **45**, 249–263

Siegert MJ and 7 others (2016) Subglacial controls on the flow of Institute Ice Stream, West Antarctica. *Ann. Glaciol.*, **57**, 19–24.

Smith MW (2014) Roughness in the Earth Sciences. *Earth-Science Rev.*, **136**, 202–225

Spagnolo M and 12 others (2017) The periodic topography of ice stream beds: insights from the Fourier spectra of mega-scale glacial lineations. *J. Geophys. Res. Earth Surf.*, **122**, 1355–1373.

Taylor J, Siegert MJ, Payne AJ and Hubbard B (2004) Regional-scale bed roughness beneath ice masses: measurement and analysis. *Comput. Geosci.*, **30**, 899–908

Vaughan DG and 9 others (2006) New boundary conditions for the West Antarctic ice sheet: subglacial topography beneath Pine Island Glacier. *Geophys. Res. Lett.*, **33**(9), 1–4.

Weertman J (1957) On the sliding of glaciers. *J. Glaciol.*, **3**, 33–38

Winsborrow MCM, Clark CD and Stokes CR (2010) What controls the location of ice streams? *Earth-Science Rev.*, **103**, 45–59

MS received 25 February 2018 and accepted in revised form 17 August 2018; first published online 13 September 2018

List of References

Alley, R. B. (1993). In search of ice stream sticky spots, *Journal of Glaciology* **39**: 447–454.

Alley, R. B., Clark, P. U., Huybrechts, P. and Joughin, I. (2005). Ice-sheet and sea-level changes, *Science* **310**: 456–460.

Amaral, R. (2002). Surface roughness, *Applied Surface Science* **193**: 156–166.

Andrle, R. and Abrahams, A. D. (1989). Fractal techniques and the surface roughness of talus slopes, *Earth Surface Processes and Landforms* **14**: 197–209.

Arnold, E., Ewing, M., Hale, R., Keshmiri, S., Leuschen, C., Li, J., Paden, J., Rodriguez-Morales, F. and Berger, V. (2018). Radar sounder platforms and sensors at cresis, *IGARSS 2018 - 2018 IEEE International Geoscience and Remote Sensing Symposium* pp. 7902–7905.

Ballantyne, C. K. (2010). Extent and deglacial chronology of the last British-Irish Ice Sheet: Implications of exposure dating using cosmogenic isotopes, *Journal of Quaternary Science* **25**: 515–534.

Ballantyne, C. K. and Small, D. (2018). The Last Scottish Ice Sheet, *Earth and Environmental Science Transactions of the Royal Society of Edinburgh* **110**: 1–39.

Bamber, J. L., Riva, R. E. M., Vermeersen, B. L. A. and Le Brocq, A. M. (2009). Reassessment of the potential sea-level rise from a collapse of the West Antarctic Ice Sheet, *Science* **324**: 901–3.

Bamber, J. L., Vaughan, D. G. and Joughin, I. (2000). Widespread complex flow in the interior of the Antarctic Ice Sheet, *Science* **287**: 16–19.

Beasom, S. L., Wiggers, E. P. and Giardino, J. R. (1983). A technique for assessing land surface ruggedness, *The Journal of Wildlife Management* **47**: 1163–1166.

Benn, D. I. and Evans, D. J. A. (2010). *Glaciers & Glaciation*, second edn, Hodder Education, Abingdon.

Bennett, M. R. (2003). Ice streams as the arteries of an ice sheet: Their mechanics, stability and significance, *Earth-Science Reviews* **61**: 309–339.

Bennett, M. R. and Glasser, N. F. (2009). *Glacial Geology*, second edn, Wiley-Blackwell, Chichester.

Bigerelle, M., Najjar, D. and Iost, A. (2003). Relevance of roughness parameters for describing and modelling machined surfaces, *Journal of Materials Science* **38**: 2525–2536.

Bingham, R. G., Rippin, D. M., Karlsson, N. B., Corr, H. F. J., Ferraccioli, F., Jordan, T. A., Le Brocq, A. M., Rose, K. C., Ross, N. and Siegert, M. J. (2015). Ice-flow structure and ice dynamic changes in the Weddell Sea sector of West Antarctica from radar-imaged interal layering, *Journal of Geophysical Research* **120**: 656–670.

Bingham, R. G. and Siegert, M. J. (2007). Radar-derived bed roughness characterization of Institute and Möller ice streams, West Antarctica, and comparison with Siple Coast ice streams, *Geophysical Research Letters* **34**: L21504.

Bingham, R. G. and Siegert, M. J. (2009). Quantifying subglacial bed roughness in Antarctica: implications for ice-sheet dynamics and history, *Quaternary Science Reviews* **28**: 223–236.

Bingham, R. G., Siegert, M. J., Young, D. A. and Blankenship, D. D. (2007). Organized flow from the South Pole to the Filchner-Ronne ice shelf: An assessment of balance velocities in interior East Antarctica using radio echo sounding data, *Journal of Geophysical Research* **112**: F03S26.

Bingham, R. G., Vaughan, D. G., King, E. C., Davies, D., Cornford, S. L., Smith, A. M., Arthern, R. J., Brisbourne, A. M., De Rydt, J., Graham, A. G., Spagnolo, M., Marsh, O. J. and Shean, D. E. (2017). Diverse landscapes beneath Pine Island Glacier influence ice flow, *Nature Communications* **8**: 1618.

Blankenship, D. D., Bell, R. E., Hodge, S. M., Brozena, J. M., Behrendt, J. C. and Finn, C. A. (1993). Active volcanism beneath the West Antarctic ice sheet and implications for ice-sheet stability, *Nature* **361**: 526–529.

Borselli, L. (1999). Technical communication segmentation of soil roughness profiles, *Earth Surface Processes and Landforms* **24**: 71–90.

Boscher, N. D., Vaché, V., Carminati, P., Grysan, P. and Choquet, P. (2014). A simple and scalable approach towards the preparation of superhydrophobic surfaces – importance of the surface roughness skewness, *Journal of Materials Chemistry A* **2**: 5744.

Boston, C. M., Evans, D. J. A. and Ó Cofaigh, C. (2010). Styles of till deposition at the margin of the Last Glacial Maximum North Sea lobe of the British-Irish Ice Sheet: An assessment based on geochemical properties of glacigenic deposits in eastern England, *Quaternary Science Reviews* **29**: 3184–3211.

Boulton, G. and Hagdorn, M. (2006). Glaciology of the British Isles Ice Sheet during the last glacial cycle: form, flow, streams and lobes, *Quaternary Science Reviews* **25**: 3359–3390.

Boulton, G. S., Smith, G. D., Jones, A. S. and Newsome, J. (1985). Glacial geology and glaciology of the last mid-latitude ice sheets, *Journal of the Geological Society* **142**: 447–474.

Bradwell, T. (2005). Bedrock megagrooves in Assynt, NW Scotland, *Geomorphology* **65**: 195–204.

Bradwell, T. (2013). Identifying palaeo-ice-stream tributaries on hard beds: Mapping glacial bedforms and erosion zones in NW Scotland, *Geomorphology* **201**: 397–414.

Bradwell, T., Small, D., Fabel, D., Dove, D., Ó Cofaigh, C. and Clark, C. (2016). Rate and style of ice stream retreat constrained by new surface-exposure ages : The Minch , NW Scotland, *Geophysical Research Abstracts, EGU* **18**: 10447.

Bradwell, T., Stoker, M. and Krabbendam, M. (2008). Megagrooves and streamlined bedrock in NW Scotland: The role of ice streams in landscape evolution, *Geomorphology* **97**: 135–156.

Bradwell, T., Stoker, M. and Larter, R. (2007). Geomorphological signature and flow dynamics of The Minch palaeo-ice stream, northwest Scotland, *Journal of Quaternary Science* **22**: 609–617.

Bradwell, T. and Stoker, M. S. (2015). Submarine sediment and landform record of a palaeo-ice stream within the British - Irish Ice Sheet, *Boreas* **44**: 255–276.

Bradwell, T. and Stoker, M. S. (2016). Glacial sediment and landform record offshore NW Scotland : a fjord – shelf – slope transect through a Late Quaternary mid-latitude ice-stream system, *in* J. A. Dowdeswell, M. Canals, M. Jakobsson, B. J. Todd, E. K. Dowdeswell and K. A. Hogan (eds), *Atlas of Submarine Glacial Landforms: Modern, Quaternary and Ancient*, The Geological Society of London, London, pp. 421–428.

Bradwell, T., Stoker, M. S., Golledge, N. R., Wilson, C. K., Merritt, J. W., Long, D., Everest, J. D., Hestvik, O. B., Stevenson, A. G., Hubbard, A. L., Finlayson, A. G. and Mathers, H. E. (2008). The northern sector of the last British Ice Sheet: Maximum extent and demise, *Earth-Science Reviews* **88**: 207–226.

Brasington, J., Vericat, D. and Rychkov, I. (2012). Modeling river bed morphology, roughness, and surface sedimentology using high resolution terrestrial laser scanning, *Water Resources Research* **48**: 1–18.

Brisbourne, A. M., Smith, A. M., Vaughan, D., King, E., Davies, D., Bingham, R. G., Smith, E., Nias, I. J. and Rosier, S. (2017). Bed conditions of Pine Island Glacier, West Antarctica, *Journal of Geophysical Research* **122**: 419–433.

Bryant, R., Moran, M. S., Thoma, D. P., Holifield Collins, C. D., Skirvin, S., Rahman, M., Slocum, K., Starks, P., Bosch, D. and González Dugo, M. P. (2007). Measuring surface roughness height to parameterize radar backscatter models for retrieval of surface soil moisture, *IEEE Geoscience and Remote Sensing Letters* **4**: 137–141.

Callard, S. L., Ó Cofaigh, C., Bennetti, S., Chiverrell, R. C., Van Landeghem, K. J. J., Sahar, M. M., Gales, J. A., Small, D., Clark, C. D., Livingstone, S. J., Fabel, D. D. and Moreton, S. G. (2018). Early deglaciation of the British Irish Ice Sheet from the Malin Sea continental shelf : west of Scotland, *Geophysical Research Abstracts* **20**: 14398.

Callens, D., Matsuoka, K., Steinhage, D., Smith, B., Witrant, E. and Pattyn, F. (2014). Transition of flow regime along a marine-terminating outlet glacier in East Antarctica, *The Cryosphere* **8**: 867–875.

Charlesworth, J. K. (1924). The glacial geology of the north-west of Ireland, *Proceedings of the Royal Irish Academy. Section B: Biological, Geological, and Chemical Science* **36**: 174–314.

Chiverrell, R. C., Burke, M. J. and Thomas, G. S. P. (2016). Morphological and sedimentary responses to ice mass interaction during the last deglaciation, *Journal of Quaternary Science* **31**: 265–280.

Chiverrell, R. C. and Thomas, G. S. P. (2010). Extent and timing of the Last Glacial Maximum (LGM) in Britain and Ireland: a review, *Journal of Quaternary Science* **25**: 535–549.

Clapperton, C. (1971). The location and origin of glacial meltwater phenomena in the eastern Cheviot Hills, *Proceedings of the Yorkshire Geological Society* **38**: 361–380.

Clark, C. D. (1993). Mega scale lineations and cross-cutting ice-flow landforms, *Earth Surface Processes and Landforms* **18**: 1–29.

Clark, C. D. (2010). Emergent drumlins and their clones: From till dilatancy to flow instabilities, *Journal of Glaciology* **56**: 1011–1025.

Clark, C. D. (2017). The BRITICE Glacial Mapping Project: version two release (2017). **URL:** *https://www.sheffield.ac.uk/geography/staff/clark_chris/britice_v2/index*

Clark, C. D., Ely, J. C., Greenwood, S. L., Hughes, A. L. C., Meehan, R., Barr, I. D., Bateman, M. D., Bradwell, T., Doole, J., Evans, D. J. A., Jordan, C. J., Monteys, X., Pellicer, X. M. and Sheehy, M. (2018). BRITICE Glacial Map, version 2: a map and GIS database of glacial landforms of the last British–Irish Ice Sheet, *Boreas* **47**: 11—-27.

Clark, C. D., Hughes, A. L. C., Greenwood, S. L., Jordan, C. and Sejrup, H. P. (2012). Pattern and timing of retreat of the last British-Irish Ice Sheet, *Quaternary Science Reviews* **44**: 112–146.

Clark, C. and Stokes, C. (2003). Palaeo-ice stream landsystem, *in* D. Evans (ed.), *Glacial Landsystems*, Arnold, London, pp. 204–227.

Clark, P. U. (1994). Unstable behavior of the Laurentide Ice Sheet over deforming sediment and its implications for climate change, *Quaternary Research* **41**: 19–25.

Clark, P. U., Dyke, A. S., Shakun, J. D., Carlson, A. E., Clark, J., Wohlfarth, B., Mitrovica, J. X., Hostetler, S. W. and McCabe, a. M. (2009). The Last Glacial Maximum., *Science* **325**: 710–714.

Cochran, W., Cooley, J., Favin, D., Helms, H., Kaenel, R., Lang, W., Maling, G., Nelson, D. E., Rader, C. and Welch, P. (1967). What is the Fast Fourier Transform?, *Proceedings of the IEEE* **55**: 1664–1674.

Conway, H., Catania, G., Raymond, C. F., Gades, A. M., Scambos, T. A. and Engelhardt, H. (2002). Switch of flow direction in an Antarctic ice stream, *Nature* **419**: 465–467.

Cooper, M. A., Jordan, T. M., Schroeder, D. M., Siegert, M. J., Williams, C. N. and Bamber, J. L. (2019). Subglacial roughness of the Greenland Ice Sheet: relationship with contemporary ice velocity and geology, *The Cryosphere Discussions* pp. 1–38.

Cowan, W. (1956). Estimating hydraulic roughness coefficients, *Agricultural Engineering* **7**: 473–475.

Crawley, M. J. (2007). *The R book*, 1st edn, Wiley, Chichester.

Dai, C. and Howat, I. M. (2017). Measuring lava flows with ArcticDEM: application to the 2012–2013 eruption of Tolbachik, Kamchatka, *Geophysical Research Letters* **44**: 12,133–12,140.

Davies, D. (2018). *The nature and dynamics of ice-stream beds : assessing their role in ice-sheet stability*, PhD thesis, Edinburgh University.

De Angelis, H. and Kleman, J. (2005). Palaeo-ice streams in the Foxe/Baffin sector of the Laurentide Ice Sheet, *Annals of Glaciology* **42**: 135–144.

De Reu, J., Bourgeois, J., Bats, M., Zwertvaegher, A., Gelorini, V., De Smedt, P., Chu, W., Antrop, M., De Maeyer, P., Finke, P., Van Meirvenne, M., Verniers, J. and Crombé, P. (2013). Application of the topographic position index to heterogeneous landscapes, *Geomorphology* **186**: 39–49.

DeConto, R. M. and Pollard, D. (2016). Contribution of Antarctica to past and future sea-level rise, *Nature* **531**: 591–597.

Deligianni, D. D., Katsala, N. D., Koutsoukos, P. G. and Missirlis, Y. F. (2001). Effect of surface roughness of hydroxyapatite on human bone marrow cell adhesion, proliferation, differentiation and detachment strength., *Biomaterials* **22**: 87–96.

Diez, A., Matsuoka, K., Ferraccioli, F., Jordan, T. A., Corr, H. F., Kohler, J., Olesen, A. V. and Forsberg, R. (2018). Basal settings control fast fce flow in the Recovery/Slessor/Bailey region, east Antarctica, *Geophysical Research Letters* **45**: 2706–2715.

Doake, C. S. M., Corr, H. F. J., Jenkins, A., Makinson, K., Nicholls, K. W., Nath, C., Smith, A. M. and Vaughan, D. G. (2013). Rutford Ice Stream, Antarctica, *in* R. B. Alley and R. A. Bindschadler (eds), *The West Antarctic Ice Sheet: Behavior and Environment*, American Geophysical Union, Washington D.C., pp. 221–235.

Dongarra, J., Sterling, T., Simon, H. and Strohmaier, E. (2005). High-performance computing: Clusters, constellations, MPPs, and future directions, *Computing in Science and Engineering* **7**: 51–59.

Dove, D., Arosio, R., Finlayson, A., Bradwell, T. and Howe, J. a. (2015). Submarine glacial landforms record Late Pleistocene ice-sheet dynamics, Inner Hebrides, Scotland, *Quaternary Science Reviews* **123**: 76–90.

Dowling, T. P. F., Spagnolo, M. and Möller, P. (2015). Morphometry and core type of streamlined bedforms in southern Sweden from high resolution LiDAR, *Geomorphology* **236**: 4–63.

Durand, G., Gagliardini, O., Favier, L., Zwinger, T. and Le Meur, E. (2011). Impact of bedrock description on modeling ice sheet dynamics, *Geophysical Research Letters* **38**: L20501.

Dutton, A., Carlson, A. E., Long, A. J., Milne, G. A., Clark, P. U., DeConto, R., Horton, B. P., Rahmstorf, S. and Raymo, M. E. (2015). Sea-level rise due to polar ice-sheet mass loss during past warm periods, *Science* **349**: 153–164.

Ebert, K. (2015). GIS analyses of ice-sheet erosional impacts on the exposed shield of Baffin Island , eastern Canadian Arctic, *Canadian Journal of Earth Sciences* **14**: 966–979.

Eitel, J. U. H., Williams, C. J., Vierling, L. A., Al-Hamdan, O. Z. and Pierson, F. B. (2011). Suitability of terrestrial laser scanning for studying surface roughness effects on concentrated flow erosion processes in rangelands, *Catena* **87**: 398–407.

Ely, J. C., Clark, C. D., Spagnolo, M., Stokes, C. R., Greenwood, S. L., Hughes, A. L., Dunlop, P. and Hess, D. (2016). Do subglacial bedforms comprise a size and shape continuum?, *Geomorphology* **257**: 108–119.

Engelhardt, H., Humphrey, N., Kamb, B. and Fahnestock, M. (1990). Physical conditions at the base of a fast moving glacier, *Science* **248**: 57–59.

Engelhardt, H. and Kamb, B. (1998). Basal sliding of Ice Stream B, West Antarctica, *Journal of Glaciology* **44**: 223–230.

Evans, D. J. A., Clark, C. D. and Mitchell, W. A. (2005). The last British Ice Sheet: A review of the evidence utilised in the compilation of the Glacial Map of Britain, *Earth-Science Reviews* **70**: 253–312.

Evans, D. J. A., Livingstone, S. J., Vieli, A. and Ó Cofaigh, C. (2009). The palaeoglaciology of the central sector of the British and Irish Ice Sheet: reconciling glacial geomorphology and preliminary ice sheet modelling, *Quaternary Science Reviews* **28**: 739–757.

Evans, D. J. A. and Thomson, S. A. (2010). Glacial sediments and landforms of Holderness, eastern England: A glacial depositional model for the North Sea Lobe of the British-Irish Ice Sheet, *Earth-Science Reviews* **101**: 147–189.

Evans, D. J. A., Young, N. J. P. and Ó Cofaigh, C. (2014). Glacial geomorphology of terrestrial-terminating fast flow lobes/ice stream margins in the southwest Laurentide Ice Sheet, *Geomorphology* **204**: 86–113.

Everest, J., Bradwell, T. and Golledge, N. (2005). Subglacial landforms of the Tweed palaeo-ice stream, *Scottish Geographical Journal* **121**: 163–173.

Eyles, N. (2012). Rock drumlins and megaflutes of the Niagara Escarpment, Ontario, Canada: a hard bed landform assemblage cut by the Saginaw-Huron Ice Stream, *Quaternary Science Reviews* **55**: 34–49.

Fabel, D., Ballantyne, C. K. and Xu, S. (2012). Trimlines, blockfields, mountain-top erratics and the vertical dimensions of the last British-Irish Ice Sheet in NW Scotland, *Quaternary Science Reviews* **55**: 91–102.

Falcini, F. A., Rippin, D. M., Krabbendam, M. and Selby, K. A. (2018). Quantifying bed roughness beneath contemporary and palaeo-ice streams, *Journal of Glaciology* **64**: 822–834.

Feng, C.-X. J., Wang, X. D. and Yu, Z. S. (2003). Neural networks modeling of honing surface roughness parameters defined by IS0 13565, *Journal of Manufacturing Systems* **21**: 395–408.

Finlayson, A. and Bradwell, T. (2007). Evidence for Loch Lomond Stadial ice cap glaciation of the Beinn Dearg massif, northern Scotland, *Quaternary Newsletter* **113**: 10–17.

Finlayson, A., Golledge, N., Bradwell, T. and Fabel, D. (2011). Evolution of a Lateglacial mountain icecap in northern Scotland, *Boreas* **40**: 536–554.

Frankel, K. L. and Dolan, J. F. (2007). Characterizing arid region alluvial fan surface roughness with airborne laser swath mapping digital topographic data, *Journal of Geophysical Research: Earth Surface* **112**: F02025.

Fretwell, P., Pritchard, H. D., Vaughan, D. G., Bamber, J. L., Barrand, N. E., Bell, R., Bianchi, C., Bingham, R. G., Blankenship, D. D., Casassa, G., Catania, G., Callens, D., Conway, H., Cook, A. J., Corr, H. F. J., Damaske, D., Damm, V., and 44, O. (2013). Bedmap2: Improved ice bed, surface and thickness datasets for Antarctica, *The Cryosphere* **7**: 375–393.

Fyfe, J. A., Long, D. and Evans, D. (1993). The geology of the Malin-Hebrides sea area, *United Kingdom Offshore Regional Report* pp. 1–91.

Gadelmawla, E. S., Koura, M. M., Maksoud, T. M. A., Elewa, I. M. and Soliman, H. H. (2002). Roughness parameters, *Journal of Materials Processing Technology* **123**: 133–145.

Gandy, N., Gregoire, L. J., Ely, J. C., Clark, C. D., Hodgson, D. M., Lee, V., Bradwell, T. and Ivanovic, R. F. (2018). Marine ice sheet instability and ice shelf buttressing influenced deglaciation of the Minch Ice Stream, northwest Scotland, *The Cryosphere* **12**: 3635–3651.

Glenn, N. F., Streutker, D. R., Chadwick, D. J., Thackray, G. D. and Dorsch, S. J. (2006). Analysis of LiDAR-derived topographic information for characterizing and differentiating landslide morphology and activity, *Geomorphology* **73**: 131–148.

Glückert, G. (1973). Two large drumlin fields in central Finland, *Fennia* **120**: 37.

Golledge, N. and Stoker, M. (2006). A palaeo-ice stream of the British Ice Sheet in eastern Scotland, *Boreas* **35**: 231–243.

Graham, A., Lonergan, L. and Stoker, M. (2007). Evidence for Late Pleistocene ice stream activity in the Witch Ground Basin, central North Sea, from 3D seismic reflection data, *Quaternary Science Reviews* **26**: 627–643.

Greenwood, S. L. and Clark, C. D. (2009). Reconstructing the last Irish Ice Sheet 1: changing flow geometries and ice flow dynamics deciphered from the glacial landform record, *Quaternary Science Reviews* **28**: 3085–3100.

Grohmann, C. H., Smith, M. J. and Riccomini, C. (2011). Multiscale analysis of topographic surface roughness in the Midland Valley, Scotland, *IEEE Transactions on Geoscience and Remote Sensing* **49**: 1200–1213.

Gudlaugsson, E., Humbert, A., Winsborrow, M. and Andreassen, K. (2013). Subglacial roughness of the former Barents Sea ice sheet, *Journal of Geophysical Research* **118**: 2546–2556.

Hall, A. M., Merritt, J. W., Connell, E. R. and Hubbard, A. (2018). Early and Middle Pleistocene environments, landforms and sediments in Scotland, *Earth and Environmental Science Transactions of the Royal Society of Edinburgh* **110**: 39–91.

Hall, R. M., Siney, P., Unsworth, A. and Wroblewski, B. M. (1997). The effect of surface topography of retrieved femoral heads on the wear of UHMWPE sockets, *Medical Engineering and Physics* **19**: 711–719.

Hanna, E., Navarro, F. J., Pattyn, F., Domingues, C. M., Fettweis, X., Ivins, E. R., Nicholls, R. J., Ritz, C., Smith, B., Tulaczyk, S., Whitehouse, P. L. and Jay Zwally, H. (2013). Ice-sheet mass balance and climate change, *Nature* **498**: 51–59.

Haubrock, S.-N., Kuhnert, M., Chabrillat, S., Güntner, A. and Kaufmann, H. (2009). Spatiotemporal variations of soil surface roughness from in-situ laser scanning, *Catena* **79**: 128–139.

Helming, K., Roth, C., Wolf, R. and Diestel, H. (1993). Characterization of rainfall - microrelief interactions with runoff using parameters derived from digital elevation models (DEMs), *Soil Technology* **6**: 273–286.

Hiemstra, J. F., Evans, D. J. A., Scourse, J. D., McCarroll, D., Furze, M. F. A. and Rhodes, E. (2006). New evidence for a grounded Irish Sea glaciation of the Isles of Scilly, UK, *Quaternary Science Reviews* **25**: 299–309.

Hillier, J. K., Kougioumtzoglou, I. A., Stokes, C. R., Smith, M. J., Clark, C. D. and Spagnolo, M. S. (2016). Exploring explanations of subglacial bedform sizes using statistical models, *PLoS ONE* **11**: 1–29.

Hillier, J. K., Smith, M. J., Clark, C. D., Stokes, C. R. and Spagnolo, M. (2013). Subglacial bedforms reveal an exponential size-frequency distribution, *Geomorphology* **190**: 82–91.

Hillier, J. and Smith, M. (2008). Residual relief separation:digital elevation model enhancement for geomorphological mapping, *Earth Surface Processes and Landforms* **33**: 2266–2276.

Hobson, R. (1967). FORTRAN IV programs to determine the surface roughness in topography for the CDC 3400 computer, *Kansas Computer Contribution* **14**: 1–28.

Howe, J. A., Dove, D., Bradwell, T. and Gafeira, J. (2012). Submarine geomorphology and glacial history of the Sea of the Hebrides, UK, *Marine Geology* **315-318**: 64–76.

Hubbard, A., Bradwell, T., Golledge, N., Hall, A., Patton, H., Sugden, D., Cooper, R. and Stoker, M. (2009). Dynamic cycles, ice streams and their impact on the extent, chronology and deglaciation of the British-Irish ice sheet, *Quaternary Science Reviews* **28**: 758–776.

Hubbard, B. and Hubbard, A. (1998). Bedrock surface roughness and the distribution of subglacially precipitated carbonate deposits: implications for formation at Glacier de Tsanfleuron, Switzerland, *Earth Surface Processes and Landforms* **23**: 261–270.

Hubbard, B., Siegert, M. J. and McCarroll, D. (2000). Spectral roughness of glaciated bedrock geomorphic surfaces: implications for glacier sliding, *Journal of Geophysical Research* **105**: 21295–21303.

Hughes, A. L. C., Clark, C. D. and Jordan, C. J. (2014). Flow-pattern evolution of the last British Ice Sheet, *Quaternary Science Reviews* **89**: 148–168.

Hughes, A. L., Clark, C. D. and Jordan, C. J. (2010). Subglacial bedforms of the last British Ice Sheet, *Journal of Maps* **6**: 543–563.

Intermap Technologies (2009). NEXTMap British Orthorectified Radar Image (ORI) Data by Intermap.
URL: *http://catalogue.ceda.ac.uk/uuid/90de599e45a84d36a16cf01904048705*

IPCC (2013). *Climate Change 2013: The Physical Science Basis*, Cambridge University Press, Cambridge.

Jansen, E., Fronval, T., Rack, F. and Channell, J. E. T. (2000). Pliocene-Pleistocene ice rafting history and cyclicity in the Nordic seas during the last 3.5 myr, *Paleoceanography* **15**: 709–721.

Jansson, K. N. and Glasser, N. F. (2005). Palaeoglaciology of the Welsh sector of the British-Irish Ice Sheet, *Journal of the Geological Society* **162**: 25–37.

Jenness, J. S. (2004). Calculating landscape surface area from digital elevation models, *Wildlife Society Bulletin* **32**: 829–839.

Jerolmack, D. J., Ewing, R. C., Falcini, F., Martin, R. L., Masteller, C., Phillips, C., Reitz, M. D. and Buynevich, I. (2012). Internal boundary layer model for the evolution of desert dune fields, *Nature Geoscience* **5**: 206–209.

Jezek, K., Wu, X., Gogineni, P., Rodríguez, E., Freeman, A., Rodriguez-Morales, F. and Clark, C. D. (2011). Radar images of the bed of the Greenland Ice Sheet, *Geophysical Research Letters* **38**: L01501.

Jordan, T. A., Ferraccioli, F., Armadillo, E. and Bozzo, E. (2013). Crustal architecture of the Wilkes Subglacial Basin in East Antarctica, as revealed from airborne gravity data, *Tectonophysics* **585**: 196–206.

Jordan, T. M., Cooper, M. A., Schroeder, D. M., Williams, C. N., Paden, J. D., Siegert, M. J. and Bamber, J. L. (2017). Self-affine subglacial roughness: consequences for radar scattering and basal thaw discrimination in northern Greenland, *The Cryosphere* **11**: 1247–1264.

Joughin, I. and MacAyeal, D. R. (2005). Calving of large tabular icebergs from ice shelf rift systems, *Geophysical Research Letters* **32**: L02501.

Joughin, I., Smith, B. E. and Medley, B. (2014). Marine ice sheet collapse potentially under way for the Thwaites Glacier basin, west Antarctica, *Science* **344**: 735–739.

Joughin, I., Tulaczyk, S., Bamber, J. L., Blankenship, D., Holt, J. W., Scambos, T. and Vaughan, D. G. (2009). Basal conditions for Pine Island and Thwaites Glaciers, West Antarctica, determined using satellite and airborne data, *Journal of Glaciology* **55**: 245–257.

Kamb, B. (1970). Sliding motion of glaciers: Theory and observation, *Reviews of Geophysics* **8**: 673–728.

Kamb, B. (2001). Basal zone of the west Antarctic ice streams and its role in lubrication of their rapid motion, *in* R. B. Alley and R. A. Bindschadler (eds), *The West Antarctic Ice Sheet: Behavior and Environment*, American Geophysical Union, pp. 157–201.

Kean, J. W. and Smith, J. D. (2006). Form drag in rivers due to small-scale natural topographic features: 1. Regular sequences, *Journal of Geophysical Research* **111**: F04009.

King, E. C., Hindmarsh, R. C. A. and Stokes, C. R. (2009). Formation of mega-scale glacial lineations observed beneath a West Antarctic ice stream, *Nature Geoscience* **2**: 585–588.

King, E. C., Pritchard, H. D. and Smith, A. M. (2016). Subglacial landforms beneath Rutford Ice Stream, Antarctica: detailed bed topography from ice-penetrating radar, *Earth System Science Data* **8**: 151–158.

King, E. C., Woodward, J. and Smith, A. M. (2007). Seismic and radar observations of subglacial bed forms beneath the onset zone of Rutford Ice Stream, Antarctica, *Journal of Glaciology* **53**: 665–672.

Kleiven, H. F., Jansen, E., Fronval, T. and Smith, T. M. (2002). Intensification of Northern Hemisphere glaciations in ice-rafted detritus evidence, *Science* **184**: 213–223.

Krabbendam, M. (2016). Sliding of temperate basal ice on a rough, hard bed: Creep mechanisms, pressure melting, and implications for ice streaming, *The Cryosphere* **10**: 1915–1932.

Krabbendam, M. and Bradwell, T. (2010). The geology and landscape of the Northwest Highlands: An introduction, *in* S. Lukas and T. Bradwell (eds), *The Quaternary of Western Sutherland and adjacent areas*, Quaternary Research Association, London, pp. 3–11.

Krabbendam, M. and Bradwell, T. (2014). Quaternary evolution of glaciated gneiss terrains: Pre-glacial weathering vs. glacial erosion, *Quaternary Science Reviews* **95**: 20–42.

Krabbendam, M., Eyles, N., Putkinen, N., Bradwell, T. and Arbelaez-Moreno, L. (2016). Streamlined hard beds formed by palaeo-ice streams: A review, *Sedimentary Geology* **338**: 24–50.

Krabbendam, M. and Glasser, N. F. (2011). Glacial erosion and bedrock properties in NW Scotland: Abrasion and plucking, hardness and joint spacing, *Geomorphology* **130**: 374–383.

Kubiak, K. J., Wilson, M. C., Mathia, T. G. and Carval, P. (2011). Wettability versus roughness of engineering surfaces, *Wear* **271**: 523–528.

Kuchar, J., Milne, G., Hubbard, A., Patton, H., Bradley, S., Shennan, I. and Edwards, R. (2012). Evaluation of a numerical model of the British-Irish ice sheet using relative sea-level data: Implications for the interpretation of trimline observations, *Journal of Quaternary Science* **27**: 597–605.

Kupko, V. S., Lukin, I. V., Risto, V. A., Kovshov, S. B. and Kosenko, O. A. (2007). A primary standard equipment for measuring roughness parameters in the range from nanometers to milimeters, *Measurement Techniques* **50**: 13–16.

Lane, S. N. (2005). Roughness - Time for a re-evaluation?, *Earth Surface Processes and Landforms* **30**: 251–253.

Lawless, M. and Robert, A. (2001). Scales of boundary resistance in coarse-graind channels: turbulent velocity profile and implication, *Geomorphology* **39**: 221–238.

Layberry, R. L. and Bamber, J. L. (2001). A new ice thickness and bed data set for the Greenland ice sheet 2. Relationship between dynamics and basal topography, *Journal of Geophysical Research* **106**: 33781–33788.

Lee, C. A., Gasster, S. D., Plaza, A., Chang, C. I., Chang, C. I. and Huang, B. (2011). Recent developments in high performance computing for remote sensing: a review, *IEEE Journal of Selected Topics in Applied Earth Observations and Remote Sensing* **4**: 508–527.

Lee, J. R., Busschers, F. S. and Sejrup, H. P. (2012). Pre-Weichselian Quaternary glaciations of the British Isles, The Netherlands, Norway and adjacent marine areas south of 68°N: implications for long-term ice sheet development in northern Europe, *Quaternary Science Reviews* **44**: 213–228.

Leuschen, C., Hale, R., Keshmiri, S., Yan, J. B., Rodriguez-Morales, F., Mahmood, A. and Gogineni, S. (2014). UAS-based radar sounding of the polar ice sheets, *IEEE Geoscience and Remote Sensing Magazine* **2**: 8–17.

Li, W., Diao, Y. P., Wang, S. Y., Fang, G. P., Wang, G. C., Dong, X. J., Long, S. C. and Qiao, G. J. (2009). New roughness parameter for the characterization of regularly textured or ordered patterned superhydrophobic surfaces, *Langmuir* **25**: 6076–6080.

Li, X., Sun, B., Siegert, M. J., Bingham, R. G., Tang, X., Zhang, D., Cui, X. and Zhang, X. (2010). Characterization of subglacial landscapes by a two-parameter roughness index, *Journal of Glaciology* **56**: 831–836.

Lindbäck, K. and Pettersson, R. (2015). Spectral roughness and glacial erosion of a land-terminating section of the Greenland Ice Sheet, *Geomorphology* **238**: 149–159.

Livingstone, S. J., Evans, D. J. A., Ó Cofaigh, C., Davies, B. J., Merritt, J. W., Huddart, D., Mitchell, W. a., Roberts, D. H. and Yorke, L. (2012). Glaciodynamics of the central sector of the last British-Irish Ice Sheet in Northern England, *Earth-Science Reviews* **111**: 25–55.

Livingstone, S. J., Ó Cofaigh, C. and Evans, D. J. (2008). Glacial geomorphology of the central sector of the last British-Irish Ice sheet, *Journal of Maps* **4**: 358–377.

Livingstone, S. J., Ó Cofaigh, C. and Evans, D. J. A. (2010). A major ice drainage pathway of the last British–Irish Ice Sheet: the Tyne Gap, northern England, *Journal of Quaternary Science* **25**: 354–370.

Livingstone, S. J., Roberts, D. H., Davies, B. J., Evans, D. J. A., Ó Cofaigh, C. and Gheorghiu, D. M. (2015). Late Devensian deglaciation of the Tyne Gap Palaeo-Ice Stream, northern England, *Journal of Quaternary Science* **30**: 790–804.

Macgregor, J. A., Catania, G. A., Conway, H., Schroeder, D. M., Joughin, I., Young, D. A., Kempf, S. D. and Blankenship, D. D. (2013). Weak bed control of the eastern shear margin of Thwaites Glacier, West Antarctica, *Journal of Glaciology* **59**: 900–912.

Maclachlan, J. C. and Eyles, C. H. (2013). Quantitative geomorphological analysis of drumlins in the Peterborough drumlin field, Ontario, Canada, *Geografiska Annaler, Series A: Physical Geography* **95**: 125–144.

Margold, M., Stokes, C. R. and Clark, C. D. (2015). Ice streams in the Laurentide Ice Sheet: Identification, characteristics and comparison to modern ice sheets, *Earth-Science Reviews* **143**: 117–146.

McCarroll, D. (2016). Trimline trauma : the wider implications of a paradigm shift in recognising and interpreting glacial limits, *Sottish Geographical Journal* **2541**: 1–11.

McCarroll, D. and Nesje, A. (1996). Rock surface roughness as an indicator of degree of rock surface weathering, *Earth Surface Processes and Landforms* **21**: 963–977.

McClean, C. J. and Evans, I. S. (2000). Apparent fractal dimensions from continental scale digital elevation models using variogram methods, *Transactions in GIS* **4**: 361–378.

Mendeleev, V. (2003). Empirical relations for height and spacing parameters of surface roughness, *Measurement Techniques* **46**: 662–666.

Menezes, P. L., Kishore and Kailas, S. V. (2009). Influence of roughness parameters and surface texture on friction during sliding of pure lead over 080 M40 steel, *International Journal of Advanced Manufacturing Technology* **43**: 731–743.

Menzies, J. (1979). A review of the literature on the formation and location of drumlins, *Journal of Glaciology* **22**: 373–384.

Mercer, B. (2007). National and regional scale DEMs created from airborne INSAR, *Proceedings of PIA07 - Photogrammetric Image Analysis* **36**: 113–118.

Merritt, J. O. N. W., Auton, C. A. and Firth, C. R. (1995). Ice-proximal glaciomarine sedimentation and sea-level change in the inverness area, scotland: a review of the deglaciation of a major ice stream of the British Late Devensian Ice Sheet, *Quaternary Science Reviews* **14**: 289–329.

Merritt, J. W., Connell, E. R. and Hall, A. M. (2017). Middle to Late Devensian glaciation of north-east Scotland: implications for the north-eastern quadrant of the last British–Irish ice sheet, *Journal of Quaternary Science* **32**: 276–294.

Mitchell, W. A. (1994). Drumlins in ice sheet reconstructions, with reference to the western Pennines, northern England, *Sedimentary Geology* **91**: 313–332.

Mitchell, W. A., Bridgland, D. R. and Innes, J. B. (2010). Late Quaternary evolution of the Tees-Swale interfluve east of the Pennines: the role of glaciation in the development of river systems in northern England, *Proceedings of the Geologists' Association* **121**: 410–422.

Morin, P., Porter, C., Cloutier, M., Howat, I., Noh, M.-J., Willis, M., Bates, B., Willamson, C. and Peterman, K. (2016). ArcticDEM; a publically available, high resolution elevation model of the Arctic, *Geophysical Research Abstracts, EGU* **18**: 8396.

Moser, K., Ahn, C. and Noe, G. (2007). Characterization of microtopography and its influence on vegetation patterns in created wetlands, *Wetlands* **27**: 1081–1097.

Muto, A., Anandakrishnan, S., Alley, R. B., Horgan, H. J., Parizek, B. R., Koellner, S., Christianson, K. and Holschuh, N. (2019). Relating bed character and subglacial morphology using seismic data from Thwaites Glacier , West Antarctica, *Earth and Planetary Science Letters* **507**: 199–206.

Najjar, D., Bigerelle, M. and Iost, A. (2003). The computer-based bootstrap method as a tool to select a relevant surface roughness parameter, *Wear* **254**: 450–460.

Newton, M., Evans, D. J. A., Roberts, D. H. and Stokes, C. R. (2018). Bedrock mega-grooves in glaciated terrain: A review, *Earth-Science Reviews* **185**: 57–79.

Ng, F. and Conway, H. (2004). Fast-flow signature in the stagnated Kamb Ice Stream, West Antarctica, *Geology* **32**: 481–484.

Nye, J. F. (1970). Glacier sliding without cavitation in a linear viscous approximation, *Proceedings of the Royal Society* **315**: 381–403.

Ó Cofaigh, C., Weilbach, K., Lloyd, J. M., Benetti, S., Callard, S. L., Chiverrell, R. C., Dunlop, P., Saher, M., Livingstone, S. J. and Katrien, J. J. (2019). Early deglaciation of the British-Irish Ice Sheet on the Atlantic shelf northwest of Ireland driven by glacioisostatic depression and high relative sea level, *Quaternary Science Reviews* **208**: 1–50.

Perkins, A. J. and Brennand, T. A. (2014). Refining the pattern and style of Cordilleran Ice Sheet retreat: Palaeogeography, evolution and implications of lateglacial ice-dammed lake systems on the southern Fraser Plateau, British Columbia, Canada, *Boreas* **44**: 319–342.

Peters, J. L., Benetti, S., Dunlop, P. and Ó Cofaigh, C. (2015). Maximum extent and dynamic behaviour of the last British-Irish Ice Sheet west of Ireland, *Quaternary Science Reviews* **128**: 48–68.

Peters, J. L., Benetti, S., Dunlop, P., Ó Cofaigh, C., Moreton, S. G., Wheeler, A. J. and Clark, C. D. (2016). Sedimentology and chronology of the advance and retreat of the last British-Irish Ice Sheet on the continental shelf west of Ireland, *Quaternary Science Reviews* **140**: 101–124.

Peters, L. E., Anandakrishnan, S., Alley, R. B., Winberry, J. P., Voigt, D. E., Smith, A. M. and Morse, D. L. (2006). Subglacial sediments as a control on the onset and location of two Siple Coast ice streams, West Antarctica, *Journal of Geophysical Research* **111**: B01302.

Plewes, L. A. and Hubbard, B. (2001). A review of the use of radio-echo sounding in glaciology, *Progress in Physical Geography* **25**: 203–236.

Pollard, D. and DeConto, R. M. (2009). Modelling West Antarctic ice sheet growth and collapse through the past five million years., *Nature* **458**: 329–332.

Pollard, D. and Deconto, R. M. (2012). A simple inverse method for the distribution of basal sliding coefficients under ice sheets, applied to Antarctica, *The Cryosphere* **6**: 953–971.

Potter, K. N., Zobeck, T. M. and Hagan, L. (1990). A microrelief index to estimate soil erodibility by wind, *Transactions of the ASAE* **33**: 151–155.

Praeg, D., McCarron, S., Dove, D., Ó Cofaigh, C., Scott, G., Monteys, X., Facchin, L., Romeo, R. and Coxon, P. (2015). Ice sheet extension to the Celtic Sea shelf edge at the Last Glacial Maximum, *Quaternary Science Reviews* **111**: 107–112.

Prescott, P. W. (2013). *Quantifying subglacial roughness and its link to glacial geomorphology and ice speed*, PhD thesis, Durham University.

Putkinen, N., Eyles, N., Putkinen, S., Ojala, A. E. K., Palmu, J. P., Sarala, P., Väänänen, T., Räisänen, J., Saarelainen, J., Ahtonen, N., Rönty, H., Kiiskinen, A., Rauhaniemi, T.

and Tervo, T. (2017). High-resolution LiDAR mapping of glacial landforms and ice stream lobes in Finland, *Bulletin of the Geological Society of Finland* **89**: 64–81.

Rea, B. R. and Evans, D. J. A. (1996). Landscapes of areal scouring in N.W. Scotland, *Scottish Geographical Magazine* **112**: 47–50.

Rignot, E. (2004). Accelerated ice discharge from the Antarctic Peninsula following the collapse of Larsen B ice shelf, *Geophysical Research Letters* **31**: L18401.

Rignot, E., Mouginot, J. and Scheuchl, B. (2011). Ice flow of the Antarctic Ice Sheet, *Science* **333**: 1427–1430.

Riley, S. J., DeGloria, S. D. and Elliot, R. (1999). A terrain ruggedness index that qauntifies topographic heterogeneity, *Intermountain Journal of Sciences* **5**: 23–27.

Rinterknecht, V., Jomelli, V., Brunstein, D., Favier, V., Masson-Delmotte, V., Bourlès, D., Leanni, L. and Schläppy, R. (2014). Unstable ice stream in Greenland during the Younger Dryas cold event, *Geology* **42**: 759–762.

Rippin, D. M. (2013). Bed roughness beneath the Greenland ice sheet, *Journal of Glaciology* **59**: 724–732.

Rippin, D. M., Bamber, J. L., Siegert, M. J., Vaughan, D. G. and Corr, H. F. J. (2006). Basal conditions beneath enhanced-flow tributaries of Slessor Glacier, East Antarctica, *Journal of Glaciology* **52**: 481–490.

Rippin, D. M., Bingham, R. G., Jordan, T. A., Wright, A. P., Ross, N., Corr, H. F. J., Ferraccioli, F., Le Brocq, A. M., Rose, K. C. and Siegert, M. J. (2014). Basal roughness of the Institute and Möller Ice Streams, West Antarctica: Process determination and landscape interpretation, *Geomorphology* **214**: 139–147.

Rippin, D. M., Vaughan, D. G. and Corr, H. F. J. (2011). The basal roughness of Pine Island Glacier, West Antarctica, *Journal of Glaciology* **57**: 67–76.

Ritz, C., Edwards, T. L., Durand, G., Payne, A. J., Peyaud, V. and Hindmarsh, R. C. (2015). Potential sea-level rise from Antarctic ice-sheet instability constrained by observations, *Nature* **528**: 115–118.

Roberts, D. H., Dackombe, R. V. and Thomas, G. S. P. (2007). Palaeo ice streaming in the central sector of the British-Irish Ice Sheet during the Last Glacial Maximum : evidence from the northern Irish Sea Basin., *Boreas* **36**: 115–129.

Roberts, D. H., Evans, D. J. A., Lodwick, J. and Cox, N. J. (2013). The subglacial and ice-marginal signature of the North Sea Lobe of the British-Irish Ice Sheet during the Last Glacial Maximum at Upgang, North Yorkshire, UK, *Proceedings of the Geologists' Association* **124**: 503–519.

Roberts, D. H., Evans, D. J., Callard, S. L., Clark, C. D., Bateman, M. D., Medialdea, A., Dove, D., Cotterill, C. J., Saher, M., Ó Cofaigh, C., Chiverrell, R. C., Moreton, S. G., Fabel, D. and Bradwell, T. (2018). Ice marginal dynamics of the last British-Irish Ice Sheet in the southern North Sea: Ice limits, timing and the influence of the Dogger Bank, *Quaternary Science Reviews* **198**: 181–207.

Rodríguez-Caballero, E., Cantón, Y., Chamizo, S., Afana, A. and Solé-Benet, A. (2012). Effects of biological soil crusts on surface roughness and implications for runoff and erosion, *Geomorphology* **145-146**: 81–89.

Rose, K. C., Ross, N., Jordan, T. A., Bingham, R. G., Corr, H. F. J., Ferraccioli, F., Le Brocq, A. M., Rippin, D. M. and Siegert, M. J. (2015). Ancient pre-glacial erosion surfaces preserved beneath the West Antarctic Ice Sheet, *Earth Surface Dynamics* **3**: 139–152.

Ross, N., Bingham, R., Corr, H. F. J., Ferraccioli, F., Jordan, T., Le Brocq, A., Rippin, D., Young, D., Blankenship, D. and Siegert, M. J. (2012). Steep reverse bed slope at the grounding line of the Weddell Sea sector in West Antarctica, *Nature Geoscience* **5**: 393–396.

Ross, N., Jordan, T. A., Bingham, R. G., Corr, H. F. J., Ferraccioli, F., Le Brocq, A., Rippin, D. M., Wright, A. P. and Siegert, M. J. (2014). The Ellsworth subglacial highlands: Inception and retreat of the West Antarctic Ice Sheet, *Bulletin of the Geological Society of America* **126**: 3–15.

Salcher, B. C., Hinsch, R. and Wagreich, M. (2010). High-resolution mapping of glacial landforms in the North Alpine Foreland, Austria, *Geomorphology* **122**: 283–293.

Sankey, J. B., Glenn, N. F., Germino, M. J., Gironella, A. I. N. and Thackray, G. D. (2010).

Relationships of aeolian erosion and deposition with LiDAR-derived landscape surface roughness following wildfire, *Geomorphology* **119**: 135–145.

Schoof, C. (2002). Basal perturbations under ice streams: Form drag and surface expression, *Journal of Glaciology* **48**: 407–416.

Schroeder, D. M., Blankenship, D. D., Young, D. A., Witus, A. E. and Anderson, J. B. (2014). Airborne radar sounding evidence for deformable sediments and outcropping bedrock beneath Thwaites Glacier, West Antarctica, *Geophysical Research Letters* **41**: 7200–7208.

Scourse, J. D., Haapaniemi, A. I., Colmenero-Hidalgo, E., Peck, V. L., Hall, I. R., Austin, W. E., Knutz, P. C. and Zahn, R. (2009). Growth, dynamics and deglaciation of the last British–Irish ice sheet: the deep-sea ice-rafted detritus record, *Quaternary Science Reviews* **28**: 3066–3084.

Sedlaček, M., Podgornik, B. and Vižintin, J. (2009). Influence of surface preparation on roughness parameters, friction and wear, *Wear* **266**: 482–487.

Sejrup, H. P., Hjelstuen, B. O., Torbjørn Dahlgren, K., Haflidason, H., Kuijpers, A., Nygård, A., Praeg, D., Stoker, M. S. and Vorren, T. O. (2005). Pleistocene glacial history of the NW European continental margin, *Marine and Petroleum Geology* **22**: 1111–1129.

Shabtaie, S. and Bentley, C. (1987). West Antarctic Ice Streams draining into the Ross Ice Shelf: configuration and mass balance, *Journal of Geophysical Research* **92**: 1311–1336.

Shaw, R. (2007). An examination of novel roughness parameters to be used in conjunction with the HSE slips assessment tool (SAT), *Technical report*, Health and Safety Executive, RR549.

Shepard, M. K. and Campbell, B. A. (1999). Radar scattering from a self-affine fractal surface: near-nadir regime, *Icarus* **141**: 156–171.

Shepard, M. K., Campbell, B. A., Bulmer, M. H., Farr, T. G., Gaddis, L. R. and Plaut, J. J. (2001). The roughness of natural terrain: a planetary and remote sensing perspective, *Journal of Geophysical Research* **106**: 32,777–32,795.

Shepherd, A. and Wingham, D. (2007). Recent sea-level contributions of the Antarctic and Greenland ice sheets., *Science* **315**: 1529–1532.

Shepherd, A., Wingham, D. J., Mansley, J. A. and Corr, H. F. (2001). Inland thinning of Pine Island Glacier, West Antarctica., *Science* **291**: 862–4.

Siegert, M. J., Ross, N., Li, J., Schroeder, D. M., Rippin, D., Ashmore, D., Bingham, R. and Gogineni, P. (2016). Subglacial controls on the flow of Institute Ice Stream, West Antarctica, *Annals of Glaciology* **57**: 19–24.

Siegert, M. J., Taylor, J. and Payne, A. J. (2005). Spectral roughness of subglacial topography and implications for former ice-sheet dynamics in East Antarctica, *Global and Planetary Change* **45**: 249–263.

Siegert, M. J., Taylor, J., Payne, A. J. and Hubbard, B. (2004). Macro-scale bed roughness of the Siple Coast ice streams in west Antartica, *Earth Surface Processes and Landforms* **29**: 1591–1596.

Skidmore, E. and Saleh, A. (1997). Comment on chain method for measuring soil roughness, *Soil Science Society of America* **61**: 1532–1535.

Small, D., Smedley, R. K., Chiverrell, R. C., Scourse, J. D., Ó Cofaigh, C., Duller, G. A., McCarron, S., Burke, M. J., Evans, D. J., Fabel, D., Gheorghiu, D. M., Thomas, G. S., Xu, S. and Clark, C. D. (2018). Trough geometry was a greater influence than climate-ocean forcing in regulating retreat of the marine-based Irish-Sea Ice Stream, *Bulletin of the Geological Society of America* **130**: 1981–1999.

Smedley, R. K., Scourse, J. D., Small, D., Hiemstra, J. F., Duller, G. A., Bateman, M. D., Burke, M. J., Chiverrell, R. C., Clark, C. D., Davies, S. M., Fabel, D., Gheorghiu, D. M., McCarroll, D., Medialdea, A. and Xu, S. (2017). New age constraints for the limit of the British–Irish Ice Sheet on the Isles of Scilly, *Journal of Quaternary Science* **32**: 48–62.

Smith, A. M. (1997). Variations in basal conditions on Rutford Ice Stream, West Antarctica, *Journal of Glaciology* **43**: 245–255.

Smith, A. M., Murray, T., Nicholls, K. W., Makinson, K., Adalgeirsdottir, G., Behar, A. E. and Vaughan, D. G. (2007). Rapid erosion, drumlin formation, and changing hydrology beneath an Antarctic ice stream, *Geology* **35**: 127–130.

Smith, B. E., Raymond, C. F. and Scambos, T. (2006). Anisotropic texture of ice sheet surfaces, *Journal of Geophysical Research* **111**: 1–8.

Smith, M. W. (2014). Roughness in the earth sciences, *Earth-Science Reviews* **136**: 202–225.

Smith, M. W., Cox, N. J. and Bracken, L. J. (2011). Terrestrial laser scanning soil surfaces: A field methodology to examine soil surface roughness and overland flow hydraulics, *Hydrological Processes* **25**: 842–860.

Sofia, G., Pirotti, F. and Tarolli, P. (2013). Variations in multiscale curvature distribution and signatures of LiDAR DTM errors, *Earth Surface Processes and Landforms* **38**: 1116–1134.

Spagnolo, M., Bartholomaus, T. C., Clark, C. D., Stokes, C. R., Atkinson, N., Dowdeswell, J. A., Ely, J. C., Graham, A. G. C., Hogan, K. A., King, E. C., Larter, R. D., Livingstone, S. J. and Pritchard, H. D. (2017). The periodic topography of ice stream beds: insights from the Fourier spectra of mega-scale glacial lineations, *Journal of Geophysical Research* **122**: 1355–1373.

Spagnolo, M., Clark, C. D., Ely, J. C., Stokes, C. R., Anderson, J. B., Andreassen, K., Graham, A. G. C. and King, E. C. (2014). Size, shape and spatial arrangement of mega-scale glacial lineations from a large and diverse dataset, *Earth Surface Processes and Landforms* **39**: 1432–1448.

Spagnolo, M., Clark, C. D. and Hughes, A. L. C. (2012). Drumlin relief, *Geomorphology* **153-154**: 179–191.

Stokes, C. R. (2018). Geomorphology under ice streams: Moving from form to process, *Earth Surface Processes and Landforms* **43**: 85–123.

Stokes, C. R. and Clark, C. D. (1999). Geomorphological criteria for identifying Pleistocene ice streams, *Annals of Glaciology* **28**: 67–74.

Stokes, C. R. and Clark, C. D. (2001). Palaeo-ice streams, *Quaternary Science Reviews* **20**: 1437–1457.

Stokes, C. R. and Clark, C. D. (2003). The Dubawnt Lake palaeo-ice stream: Evidence for dynamic ice sheet behaviour on the Canadian Shield and insights regarding the controls on ice-stream location and vigour, *Boreas* **32**: 263–279.

Stone, R. and Dugundji, J. (1965). A study of microrelief - its mapping, classification, and quantification by means of a Fourier analysis, *Engineering Geology* **1**: 89–187.

Studinger, M., Bell, R. E., Blankenship, D. D., Finn, C. A., Arko, R. A., Morse, D. L. and Joughin, I. (2001). Subglacial sediments: A regional geological template for ice flow in West Antarctica, *Geophysical Research Letters* **28**: 3493–3496.

Suh, A. Y. and Polycarpou, A. A. (2003). Effect of molecularly thin lubricant on roughness and adhesion of magnetic disks intended for extremely high-density recording, *Tribology Letters* **15**: 365–376.

Suh, A. Y., Polycarpou, A. A. and Conry, T. F. (2003). Detailed surface roughness characterization of engineering surfaces undergoing tribological testing leading to scuffing, *Wear* **255**: 556–568.

Suresh, P. V. S., Rao, P. V. and Deshmukh, S. G. (2002). A genetic algorithmic approach for optimization of surface roughness prediction model, *International Journal of Machine Tools & Manufacture* **42**: 675–680.

Survey, O. (2017). Ordnance Survey Meridian 2.
URL: *https://digimap.edina.ac.uk/webhelp/os/data_information/os_products/meridian_2.htm*

Tagil, S. and Jenness, J. S. (2008). GIS-based automated classification and topographic, landcover and geologic attributes of landforms around the Yazoren Polje, Turkey, *Journal of Applied Sciences* **8**: 910–921.

Taylor, J., Siegert, M. J., Payne, A. J. and Hubbard, B. (2004). Regional-scale bed roughness beneath ice masses: Measurement and analysis, *Computers and Geosciences* **30**: 899–908.

Tegowski, J., Trzcinska, K., Kasprzak, M. and Nowak, J. (2016). Statistical and spectral features of corrugated seafloor shaped by the Hans Glacier in Svalbard, *Remote Sensing* **8**: doi:10.3390/rs8090744.

Telfer, M., Wilson, P., Lord, T. and Vincent, P. (2009). New constraints on the age of the last ice sheet glaciation in NW England using optically stimulated luminescence dating, *Journal of Quaternary Science* **24**: 906–915.

Thierens, M., Pirlet, H., Colin, C., Latruwe, K., Vanhaecke, F., Lee, J., Stuut, J.-B., Titschack, J., Huvenne, V., Dorschel, B., Wheeler, A. and Henriet, J.-P. (2012). Ice-rafting from the British–Irish ice sheet since the earliest Pleistocene (2.6 million years

ago): implications for long-term mid-latitudinal ice-sheet growth in the North Atlantic region, *Quaternary Science Reviews* **44**: 229–240.

Tulaczyk, S., Kamb, B., Scherer, R. P. and Engelhardt, H. F. (1998). Sedimentary processes at the base of a West Antarctic ice stream; constraints from textural and compositional properties of subglacial debris, *Journal of Sedimentary Research* **68**: 487–496.

Van der Veen, C. J., Leftwich, T., von Frese, R., Csatho, B. M. and Li, J. (2007). Subglacial topography and geothermal heat flux: Potential interactions with drainage of the Greenland ice sheet, *Geophysical Research Letters* **34**: L12501.

Vaughan, D. G., Corr, H. F. J., Ferraccioli, F., Frearson, N., O'Hare, A., Mach, D., Holt, J. W., Blankenship, D. D., Morse, D. L. and Young, D. A. (2006). New boundary conditions for the West Antarctic ice sheet: Subglacial topography beneath Pine Island Glacier, *Geophysical Research Letters* **33**: L12501.

Washtell, J., Carver, S. and Arrell, K. (2009). A viewshed based classification of landscapes using geomorphometrics, *Proceedings of Geomorphometry Conference* pp. 44–49.

Weertman, J. (1957). On the sliding of glaciers, *Journal of Glaciology* **3**: 33–38.

Welch, B. C., Pfeffer, W. T., Harper, J. T. and Humphrey, N. F. (1998). Mapping subglacial surfaces of temperate valley glaciers by two-pass migration of a radio-echo sounding survey, *Journal of Glaciology* **44**: 164–170.

Wilson, M. F. J., O'Connell, B., Brown, C., Guinan, J. C. and Grehan, A. J. (2007). Multiscale terrain analysis of multibeam bathymetry data for habitat mapping on the continental slope, *Marine Geodesy* **30**: 3–35.

Winsborrow, M. (2007). *Exploring controls on the location of Laurentide palaeo-ice streams*, PhD thesis, University of Sheffield.

Winsborrow, M. C. M., Clark, C. D. and Stokes, C. R. (2010). What controls the location of ice streams?, *Earth-Science Reviews* **103**: 45–59.

Winter, K., Ross, N., Ferraccioli, F., Jordan, T. A., Corr, H. F., Forsberg, R., Matsuoka, K., Olesen, A. V. and Casal, T. G. (2018). Topographic steering of enhanced ice flow at the bottleneck between East and West Antarctica, *Geophysical Research Letters* **45**: 4899–4907.

Wolf, K. L., Ahn, C. and Noe, G. B. (2011). Microtopography enhances nitrogen cycling and removal in created mitigation wetlands, *Ecological Engineering* **37**: 1398–1406.

Wright, A. P., Young, D. A., Roberts, J. L., Schroeder, D. M., Bamber, J. L., Dowdeswell, J. A., Young, N. W., Le Brocq, A. M., Warner, R. C., Payne, A. J., Blankenship, D. D., Van Ommen, T. D. and Siegert, M. J. (2012). Evidence of a hydrological connection between the ice divide and ice sheet margin in the Aurora Subglacial Basin, East Antarctica, *Journal of Geophysical Research* **117**: F01033.

Yorke, L., Rumsby, B. T. and Chiverrell, R. C. (2012). Depositional history of the Tyne valley associated with retreat and stagnation of Late Devensian Ice Streams, *Proceedings of the Geologists' Association* **123**: 608–625.

Zhang, J. Z., Chen, J. C. and Kirby, E. D. (2007). Surface roughness optimization in an end-milling operation using the Taguchi design method, *Journal of Materials Processing Technology* **184**: 233–239.

Zou, Y., Li, Y., Kaestner, M. and Reithmeier, E. (2016). Low-coherence interferometry based roughness measurement on turbine blade surfaces using wavelet analysis, *Optics and Lasers in Engineering* **82**: 113–121.